Effects of Molecular Weight and Solution Concentration on Electrospinning of PVA

By

Jing Tao

A Thesis

Submitted to the Faculty

of the

Worcester Polytechnic Institute

In partial fulfillment of the requirements for the

Degree of Master of Science

in

Materials Science and Engineering

By

June 12, 2003

APPROVED:

Dr. Satya Y. Shivkumar, Major advisor

Dr. Richard D. Sisson, Jr., Materials Science and Engineering Program Head

----
Dr. Gretar Tryggvason, Mechanical Engineering Department Head

ABSTRACT

The effects of molecular weight (M_w) and concentration (c) on the structure of electrospun PVA have been studied. Experiments have been conducted for M_w values ranging from 9000 g/mol to 124,000 g/mol. The concentration was varied from 5 to 35 wt %. Data were acquired for several solvents including water, Dimethyl Sulfoxide, Ethylene Glycol and N-Methyl Pyrrolidone. The transient phenomena occurring during jet breakdown were examined by high speed digital photography. The structure in the electrospun polymer was analyzed by scanning electron microscopy. The fiber diameter distribution for various conditions was characterized by optical image analysis. The effects of additives such as NaCl and Poly Ethylene Glycol on the structure have been studied. The results indicate that a minimum M_w and c corresponding to $[\eta]c \sim 5$ or Capillary number, $Ca \sim 0.5$ is necessary for forming a fibrous structure. As M_w or c increase, the fiber diameter becomes larger and a broader distribution of fibers may be obtained. The average diameter of the fiber, D, follows a Power law relationship: $D\ (nm) = 18.6([\eta]c)^{1.11}$. Round fibers may be obtained at low M_w and c, while flat fibers are observed at high M_w and c. The transition from round to flat fibers appears to begin at $[\eta]c \sim 12$. At any $[\eta]c$, there is a minimum Capillary and Ohnesorge numbers at which fibers are stabilized and a maximum at which viscous effects become dominant. The addition of NaCl lowers the average fiber diameter in PVA samples with a high molecular weight. Electrospinning can be used to produce nanofibers of PVA with various architectures.

ACKNOWLEDGEMENTS

TABLE OF CONTENTS

LIST OF FIGURES

LIST OF TABLES

1. INTRODUCTION

Porous polymeric structures are used in a wide range of applications including wound dressings, vascular grafts, tissue engineering scaffolds, and controlled drug delivery systems. A primary requirement for most of these applications is the ability to control the macroscopic structure in the base polymer (*e.g.* fibrous, woven, non-woven etc.). In addition, it is also necessary to control the amount, size, and the degree of interconnectivity in the pores. In tissue engineering scaffolds, for example, a porous structure with a large amount of interconnected pores of proper size is a key requirement for cell attachment and growth.

A variety of techniques have been developed to produce polymeric structures with a high degree of porosity and interconnectivity. The common processes that have been used are fiber bonding, phase separation, 3-D printing, and solvent casting with particulate leaching. However all these processes have several drawbacks including long or complicated procedures for preparation, high processing temperature and residual organic solvent in the final polymer. In addition, the control over pore amount, size and interconnectivity is not adequate. In most cases, the size of the base polymer and the pore are on the order of several μm to hundreds of μm.

In order to circumvent some of these problems, a process called electrospinning has been developed and has attracted much attention recently. Electrospinning can be used to produce fibrous structures with fiber sizes on the order of 100 *nm* to 100 *μm*. In order to

produce the porous structure by electrospinning, the polymer is dissolved in a suitable solvent. The solution is placed in a capillary and is subjected to a high voltage (typically between 5 to 30 kV). A jet with some electrical charge is ejected from the capillary when the mutual repulsion of electrical force overcomes the surface tension of the droplet of polymer solution. Thereafter the jet travels towards the grounded collector. During its transit, it undergoes splitting, splaying and branching, thereby reducing the effective diameter of the jet significantly. In addition, the solvent evaporates from the jet before reaching the collector until finally sub-micron fibers are collected as a non-woven mat. By manipulating the process parameters like the intensity and shape of the applied electrical field, surface tension and viscosity of the polymer solution, electrospinning can be used to produce highly interconnected porous structures of a wide range of pore sizes. Polymers with diverse micro and macro structures can be produced with relative ease.

Electrospinning can be applied to most of the polymers in the form of solutions or melts. Polymers that have been electrospun include: polyurethane (PU), polypropylene (PP), polylactic acid (PLA), polyglycolic acid (PGA), poly ε-caprolactone (PCL), polyethylene oxide (PEO), polyvinyl alcohol (PVA) and collagen, etc. The objective of this work is to produce porous polymeric structures with PVA. This hydrophilic polymer is water soluble and is the largest volume synthetic resin produced in the world. The excellent chemical resistance, physical properties and biodegradability of PVA have led to the development of many commercial products based on this polymer. The physical and solution properties of PVA that are important in electrospinning such as viscosity, electrical conductivity and surface tension show strong dependence on molecular weight.

Hence, the effects of molecular weight and solution concentration on the electrospinning

characteristics and on the structure in the electrospun polymer have been studied.

2. LITERATURE REVIEW

In recent years, advances in polymer engineering have enabled the production of new porous matrices from a variety of polymers for many biomedical applications [1,2]. The development of such macromolecular networks has led to major advancements in tissue engineering, drug delivery, orthopedics, wound healing, and medical textiles. Many of these polymers degrade by hydrolysis and have a range of mechanical and physical properties. Their degradation characteristics may depend on several parameters including their molecular structure, crystallinity, microgeometry and pore structure. Basic information on some of the typical biomedical polymers is presented in the following sections.

2.1 Polymeric biomaterials

Polymers are the most commonly used group of materials for biomedical applications [3]. Polymers are used in products ranging from low risk, noninvasive devices such as blood bags and surgical gloves through to high risk applications for cardiovascular and orthopedic implants. The advantages of biopolymers, both synthetic and natural, over other biomaterials lie in their outstanding physical and chemical properties [4]. The polymers can be manipulated by a variety of fabrication techniques to exhibit fairly good tensile strength and excellent ductility. A list of typical biopolymers is given in Table I [5]. The polymers used in medical applications can be classified as degradable and non-degradable polymers. The typical examples of non-degradable polymers include

polyvinyl chloride (PVC), polyethylene (PE), polyurethane, Nylon, and Teflon etc. These polymers are important in many clinical applications including hip implants, artificial lenses, large diameter vascular grafts, and catheters, etc. [6].

Table I   List of biopolymers used in tissue engineering and drug deliveryapplications [5].

Classification	Polymer
Natural polymers	
Protein-based polymers	Collagen, albumin, gelatin
Polysaccharides	Agarose, alginate, carrageenan, hyaluronic acid, dextran, chitosan, cyclodextrins
Synthetic polymers	
Biodegradable	
Polyesters	Poly(lactic acid), poly(glycolic acid), poly(hydroxy butyrate), poly(ε-caprolactone), poly(β-malic acid), poly(dioxanones)
Polyanhydrides	Poly(sebacic acid), poly(adipic acid), poly(terphthalic acid) and various copolymers
Polyamides	Poly(imino carbonates), polyamino acids
Phosphorous-based polymers	Polyphosphates, polyphosphonates, polyphosphazenes
Others	Poly(cyano acrylates), polyurethanes, polyortho esters, polydihydropyrans, polyacetals
Non-biodegradable	
Cellulose derivatives	Carboxymethyl cellulose, ethyl cellulose, cellulose acetate, cellulose acetate propionate, hydroxypropyl methyl cellulose
Silicones	Polydimethylsiloxane, colloidal silica
Acrylic polymers	Polymethacrylates, poly(methyl methacrylate), poly hydro(ethyl-methacrylate)
Others	Polyvinyl pyrrolidone, ethyl vinyl acetate, poloxamers, poloxamines

Biodegradable polymers are designed to undergo extensive chain scission to form small soluble oligomers or monomers. Degradation may proceed by a biologically active process or by passive hydrolytic cleavage [7]. Biodegradable polymers can be manipulated to exhibit different degradation rate and mechanical properties for various

5

applications. In drug delivery, the polymer could degrade and release the incorporated drug at a controlled rate over certain duration, while in tissue engineering it is often required to have certain micro and macro morphologies and appropriate mechanical strength for the best incorporating of the implanted structure with the local tissue. Typical properties of biodegradable polymers are shown in the Table II [4]. It can be seen from Table II that biodegradable polymers exhibit great diversity in their mechanical properties.

Table II   Typical Properties of common Biodegradable Polymers [4]

Polymer	Melting point (°C)	Glass transition temperature (°C)	Modulus^a (Gpa)	Elongation
PGA	225–230	35–40	7.0	15–20
LPLA	173–178	60–65	2.7	5–10
DLPLA	Amorphous	55–60	1.9	3–10
PCl	58–63	−65––60	0.4	300–500
PDO	N/A	−10–0	1.5	N/A
PGA–TMC	N/A	N/A	2.4	N/A
85/15 DLPLG	Amorphous	50–55	2.0	3–10
75/25 DLPLG	Amorphous	50–55	2.0	3–10
65/35 DLPLG	Amorphous	45–50	2.0	3–10
50/50 DLPLG	Amorphous	45–50	2.0	3–10
Bone			10–20	
Steel			210	

Synthetic aliphatic polyesters such as polylactic acid (PLA), poly glycolic acid (PGA) and their copolymers have been used widely in many applications [8]. In addition, other polyesters such as polycaprolactone (PCL) have been used in applications requiring a lower rate of degradation than PLA or PGA. Hydrophilic polymers have attracted as much interest due to their distinctive water-solubility [9,10]. The most commonly used ones include: poly ethylene glycol (PEG), poly ethylene oxide (PEO), PVA and poly

acrylic/mechacrylic acid (PAA/PMAA). The mer structures for these polymers are shown in the Fig. 1.

PEG and PEO have the same monomer unit, while PEO repeats this unit in the whole molecular chain; PEG has a hydroxyl group at one end and a hydrogen atom at the other. Also, the monomer of PVA is isomeric with that of PEO. The difference between them and the special characteristics will be discussed in detail in the following sections.
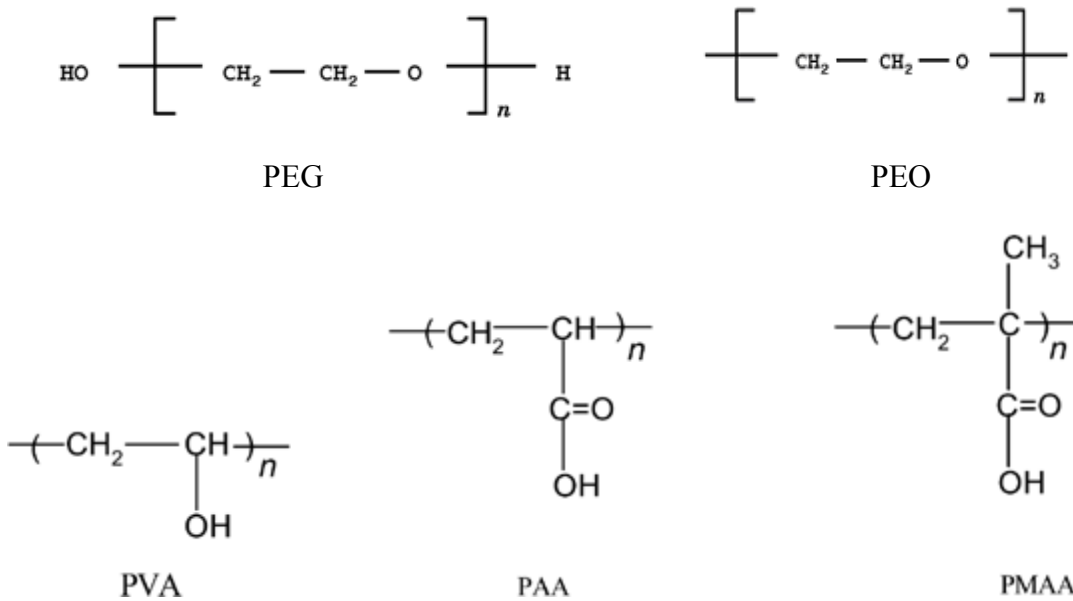
Fig. 1   mer structures of PEG, PEO, PVA, PAA and PMAA [11]

2.2 Polyvinyl alcohol (PVA)

PVA as a hydrophilic polymer is water soluble and is the largest volume synthetic resin produced in the world [12]. The excellent chemical resistance, physical properties and

biodegradability of PVA have led to the development of many commercial products based on this polymer. PVA is used as an emulsifier and as a stabilizer for colloid suspensions, as a sizing agent and coating in the textile and paper industries, and as an adhesive [12]. PVA is a truly biodegradable polymer with the degradation products being water and carbon dioxide. Hence, it is used in many biomedical and pharmaceutical applications, due to its advantages such as: nontoxic, noncarcinogenic, and bioadhesive characteristics with the ease of processing [11].

2.2.1 Molecular structure and physical properties of PVA

Commercial PVA is typically made by the hydrolysis of poly (vinyl acetate) or PVAC in the reaction as shown in Fig. 2 [13].
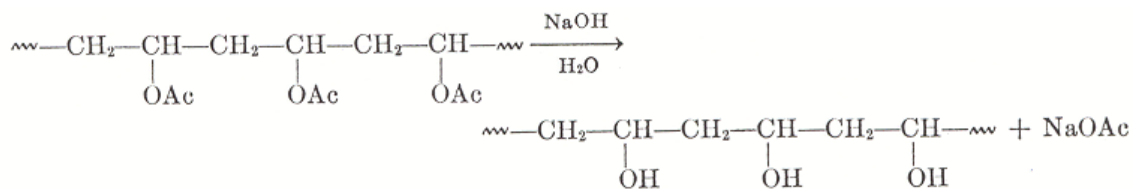
Fig. 2   Hydrolysis of PVAC to produce PVA [13]

As seen from Fig. 2, its monomer unit is isomeric with that of PEO. However, while oxygen forms etheric bonds with two neighboring carbons (C-O-C) in the backbone of PEO, it is located in -OH side groups in PVA. The hydroxyl groups could be a source of hydrogen bonding (-H), which readily formed between PVA chains in aqueous solutions [14]. The percentage of acetate groups converted to alcohol groups determines the hydrolysis level of PVA, which affects the degree of polymer crystallinity [15]. For high

hydrolysis PVAs, the hydroxyl groups on one polymer chain can form hydrogen bonding with hydroxyl groups of another chain as illustrated in Fig. 3 (a). Consequently, the polymers will line up with each other and produce orientation. The acetyl groups in PVA with partial hydrolysis PVA act as spacers, which limit the crystallinity by preventing molecular chains from close approach as illustrated in Fig. 3 (b) [14].

(a)
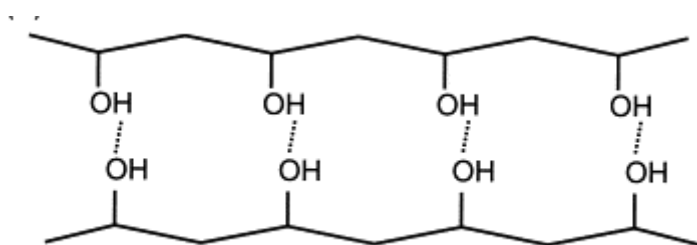
(b)
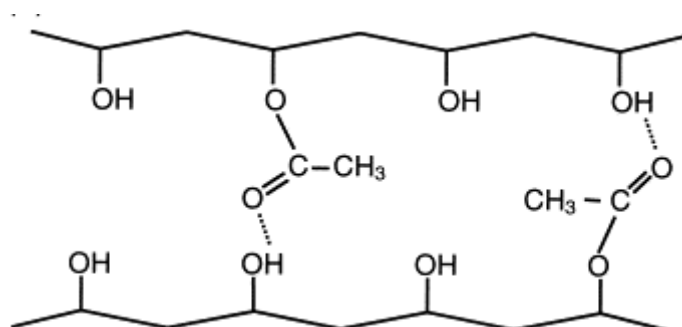
Fig. 3   *Hydrogen bonding in commercial PVA (a) at high hydrolysis many secondary hydrogen bonds can be established. (b) at low hydrolysis, acetate groups act as spacers and restrict the level of hydrogen bonding. [14]*

Due to the difficulty of carrying the reaction to completion without more drastic treatment, there is always an appreciable proportion (commonly, 2 mol % or less) of residual acetate groups from the parent poly (vinyl acetate) [17].

The percentage hydrolysis of PVA refers to the amount of the acetate groups replaced by the hydroxyl groups in the reaction and can be calculated according to the following equation [12]:

$$\text{Degree of hydrolysis} = \frac{x}{x+y} \times 100\%$$ (1)

, where x and y are the molar fractions of the hydroxyl and the acetate groups, respectively, specified in the following stoichiometric formula:

$$-[CH_2\text{-}CH]_x -[CH_2\text{-}CH]_y$$
$$\quad\;\; OH \qquad\qquad OCOCH_3$$
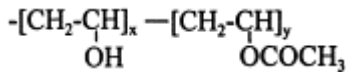
The higher the degree of hydrolysis, the fewer the acetate groups that remain in the molecules. In contrast, O atoms in the backbone of PEO increase the stiffness of the chain, and hence make the melting point and glass transition temperature significantly lower compared to that of pure PVA of comparable chain length [16,17]. Accordingly the tensile strength achievable (typically, 13-16 MPa) is much lower than that of PVA (typically, 67-100 MPa) [16,17].

The degree of hydrolysis influences the polymer behavior in the solution. In aqueous PVA solutions, a part of the inter-chain hydrogen bonding remains, in addition to the hydrogen bonding between the PVA chains and the water molecules formed newly upon dissolution [12]. The extent of both inter and intra chain hydrogen bonding and solute–solvent hydrogen bonding is mainly determined by the degree of hydrolysis in the PVA chains. Thus viscosity, surface tension and other solution properties can be related to the degree of hydrolysis. The effect of the degree of hydrolysis on solution viscosity and solubility are schematically illustrated in Fig. 4 [12]. The physical and mechanical properties of PVA are shown in Appendix I.
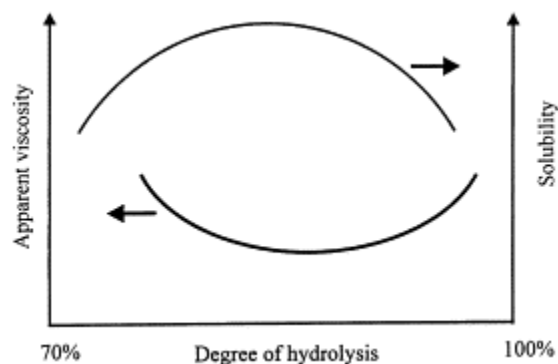
Fig. 4   Schematic diagram of the interrelationship between apparent viscosity and degree of hydrolysis, and between solubility and degree of hydrolysis for aqueous PVA solution [12].

2.2.2   Crystallinity and specific gravity

Despite the fact that by and large, samples of common PVA are found to be essentially atactic, due to the small size of the hydroxyl group, the molecular chains of PVA can fold up easily in an organized manner [15]. PVA is then one of the few polymers that can achieve high *crystallinity*, which is mostly within the narrow range of 20% to 55% as shown in Fig. 6. The *crystalline structure* of PVA is found to be monoclinic with β angle (see Fig. 5(a)) equals $92.2 \pm (0.3)$ ° or hexagonal, and is orthorhombic for quenched samples [18]. The *density* of PVA varies from 1.19 g/cm^3 for completely amorphous sample to 1.31 g/cm^3 for completely crystalline sample while generally it will be found to lie within the limits of 1.28 to 1.31 g/cm^3 [17,18]. The crystallinity of PVA tends to decrease with increasing molecular weight and decreasing hydrolysis. Long molecular chains involve impeded segmental motion and thus make it more difficult for the molecules to fold up into crystalline structures. Hydrolysis decreased with increasing the number of residual acetate group in the molecules. The bulky size of the pendent acetate group prevents the molecular chains to closely fold up to form crystalline.
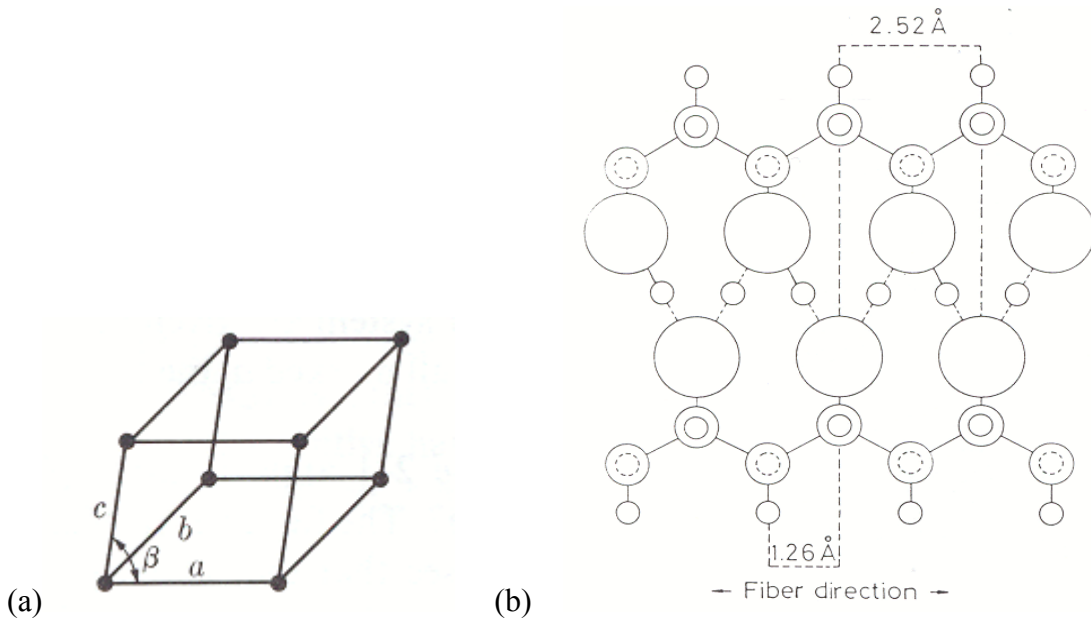
Fig. 5 *(a) Schematic illustration of the structure of monoclinic lattice; (b) Crystal structure of PVA. PVA chains are projected on the (101) plane. The circles in descending order of size represent oxygen, carbon and hydrogen atoms, respectively. The dashed and solid circles distinguish between hydrogen atoms on opposite sides of the chains [19].*
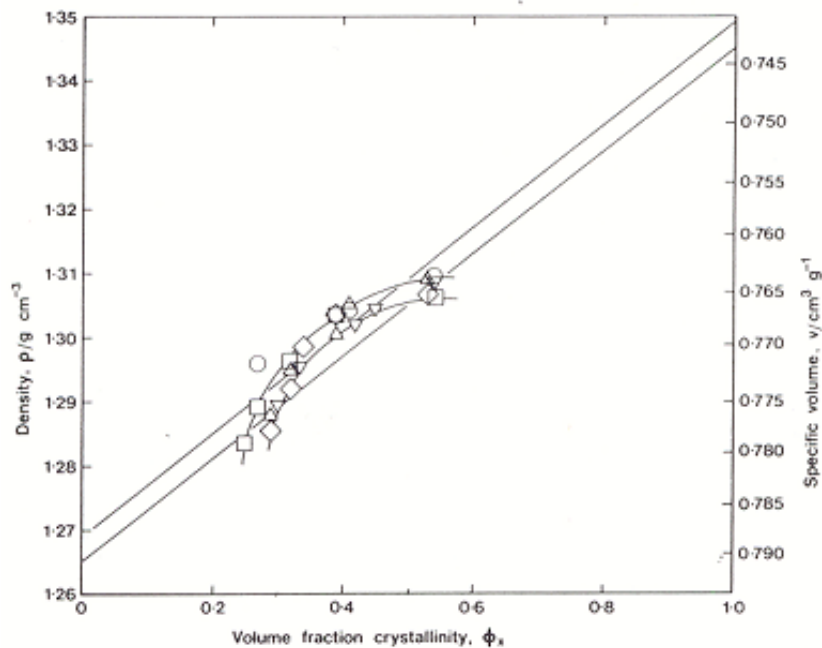
Fig. 6 *Density of PVA as a function of crystallinity. Data are shown for M_w =14000, 31000, 57000, 10000, and 20000 g/mol. [15]*

2.2.3 Solution behavior of PVA

The solubility, viscosity, and surface tension of PVA depend on temperature, concentration, % hydrolysis and molecular weight of the material. PVA is soluble in highly polar and hydrophilic solvents, such as water, Dimethyl Sulfoxide (DMSO), Ethylene Glycol (EG), and N-Methyl Pyrrolidone (NMP) [17,20]. Water is the most important solvent for PVA and the aqueous properties of PVA solutions will be reviewed in the following sections. The solubility of PVA in water depends on the degree of polymerization (DP), hydrolysis, and solution temperature [13]. Any change in these three factors affects the degree and character of hydrogen bonding in the aqueous solutions, and hence the solubility of PVA and other solution properties.

The intra and inter molecular hydrogen bonding in aqueous PVA solutions was discussed previously. Due to the existence of the hydrogen bonding, it is always difficult to achieve molecularly dispersed PVA solutions, especially for PVA of large molecular weight. In such cases, stirring and/or heating could help the dissolution. The effect of temperature on the solubility of PVA is shown in Fig. 7 [17] for various values of DP. At low DP and low degree of hydrolysis, complete solubility can be achieved even at low temperatures (B) [17]. As the DP increases at high degree of hydrolysis, the temperature needs to be increased to improve the solubility (C and D). Temperatures as high as 80 to 90 °C may be required to obtain complete solubility. At very high DP and low degree of hydrolysis, the polymer starts to gel at room temperature and the solubility decreases rapidly (A).
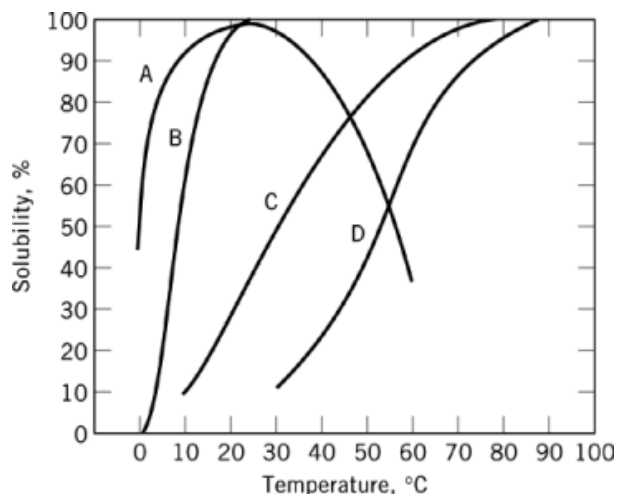
Fig. 7   Solubility of PVA in water as a function of temperature. Data for various grades of PVA are shown. A, 78–81 mol% hydrolyzed, DP = 2000–2100; B, 87–89 mol% hydrolyzed, DP = 500–600; C, 98–99 mol% hydrolyzed, DP = 500–600; D, 98–99 mol% hydrolyzed, DP = 1700–1800 [17].

For PVA of a certain molecular weight, the extent of both inter and intra chain hydrogen bonding, and the solute-solvent hydrogen bonding are mainly determined by the degree of hydrolysis of PVA and the solution temperature [17]. For PVA of low % hydrolysis, due to the bulky size and hydrophobic character of the remaining acetate groups in the molecules, OH groups on neighboring chains are prevented from getting close enough to form inter chain hydrogen bonds [12,17]. The solubility of partially-hydrolyzed PVA is thus high at room temperature while fully-hydrolyzed PVA is essentially insoluble in water at the same situation.

On the other hand, in the solution of higher temperature, the extent of inter and intra chain hydrogen bonding is disrupted by the higher mobility of the molecules and the ones between PVA and water are thus enhanced. As a result, the solubility of highly-hydrolyzed PVA increases dramatically as seen in the Fig. 7. The hydrophobic nature of

the acetate groups results in a negative heat of solution, which increases as the number of acetate groups is increased [17]. This means that the solubility decreases as the temperature increases and/or the percentage of hydrolysis decreases (curve A).

Tacx et al [20] have identified 4 regions during the dissolution of PVA as shown in Fig. 8 [20]. As the polymer dissolves, η_{sp}/c increases (Region I). After a certain time, η_{sp}/c reaches a peak value and starts to decrease. This decrease may be caused by the dissolution of some entangled molecules (Region II). Subsequently, η_{sp}/c is constant (Region III) indicating that dissolution is essentially complete. At large time, η_{sp}/c may decrease due to oxidation or hydrolysis (Region 4).
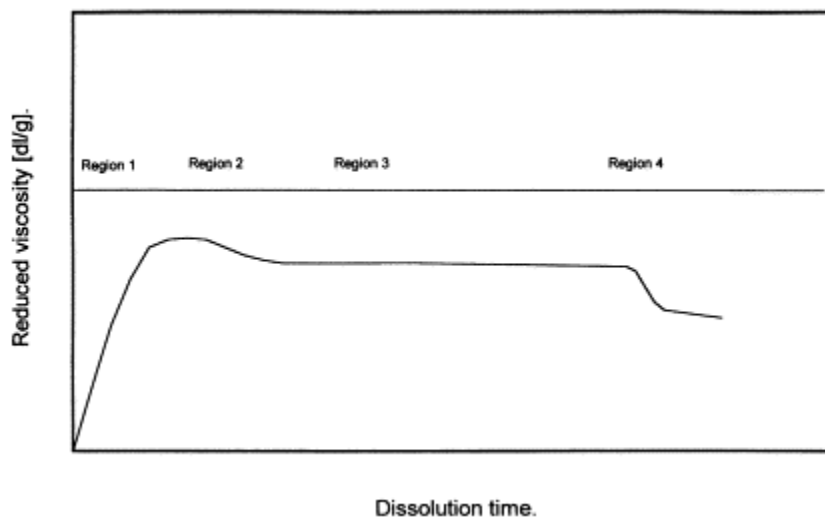
Fig. 8   Schematic illustration of the dissolution of PVA as a function of time [20].

2.2.4   Viscosity of PVA solutions

PVA solutions are generally shear thinning and may exhibit significant thixotropy [21]. The viscosity of aqueous PVA solutions increases with the molecular weight and

concentration. The dependence of solution viscosity on DP, concentration, hydrolysis, and temperature is as shown in Figs. 9 and 10 [17,13]. Clearly, the viscosity decreases with increasing temperature and is directly proportional to DP (Fig. 9). The activation energy, Q, based on the Arhenius equation:

$$\eta = \eta_0 \, \exp\!\left(\frac{Q}{RT}\right) \tag{2}$$

can be calculated to be on the order of 20 kJ/mol.
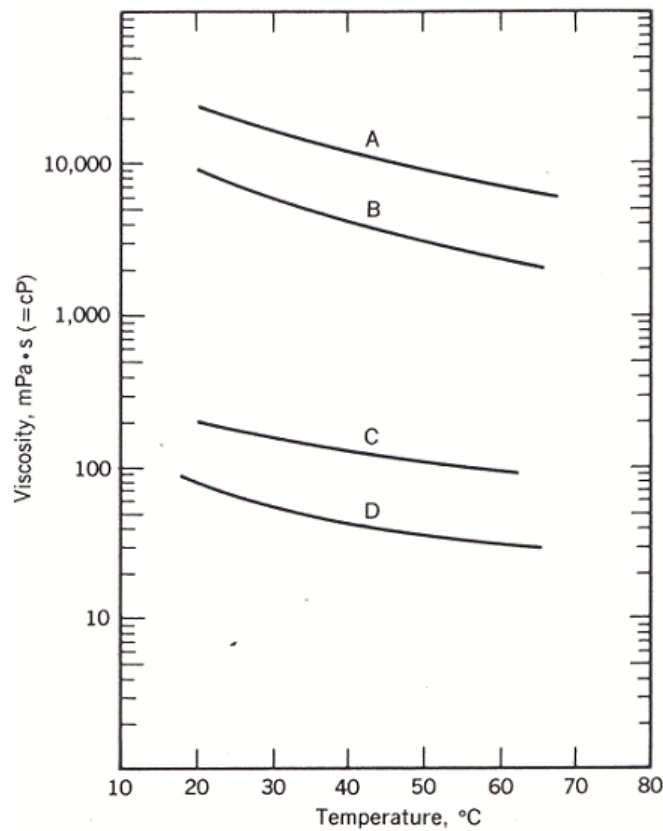
Fig. 9   *Solution viscosity of PVA as a function of temperature. A, DP=2200; B, DP=1500; C, DP=550; D, DP= 220. (Concentration = 16 wt %, 87-89% hydrolyzed)[17].*

The DP and concentration have a stronger effect on viscosity than temperature and the degree of hydrolysis (Fig. 9,10). This result indicates that the degree of hydrogen bonding is affected more by DP and concentration. The viscosity of the solution is increased because the existence of longer chains or higher molecular weight, and/or more chains or higher concentration enhances the formation of inter and intra molecular hydrogen bonding. As a result, water becomes a poorer solvent and hence the viscosity of the solution increases. The temperature and % hydrolysis have a weaker effect on the solution viscosity because the amount of residual acetic groups or more active molecular mobility does not help as much as molecular weight or concentration on reducing the hydrogen bonding within and between chains [13].
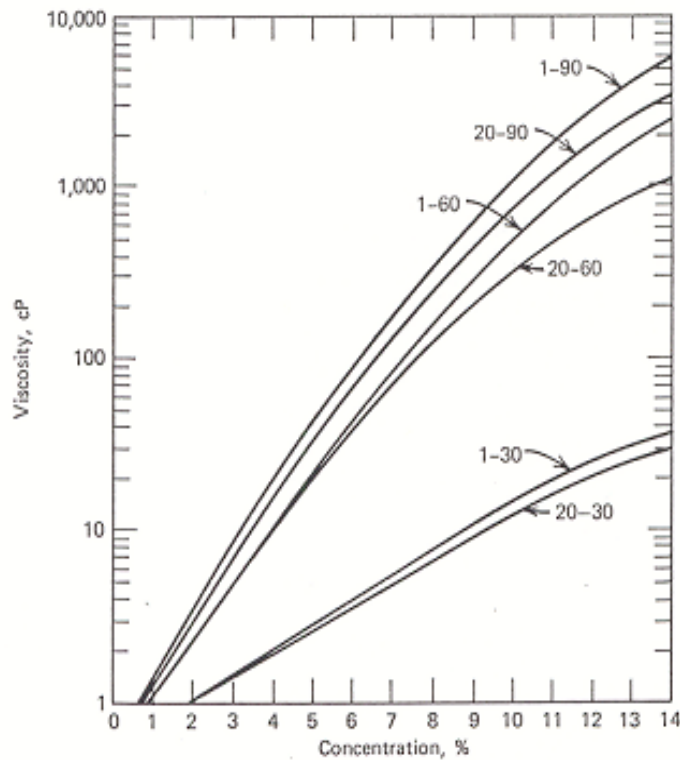
Fig. 10   Solution viscosity at 60°C as a function of concentration. Data for various grades of PVA are shown. Information on the different grades of PVA used in this investigation are given in III [13].

17

Table III   DP and %hydrolysis for the various grades of PVA in Fig. 10.

Grade of PVA	Degree of polymerization	% hydrolysis
1-90	2400-2500	99%
20-90		87-89 %
1-60	1700-1800	99%
20-60		87-89 %
1-30	500-600	99%
20-30		87-89 %

For most polymers, the dependence of intrinsic viscosity [η] on M_w can be described by the Mark-Houwink equation:

$$[\eta] = KM_w^a \qquad (3)$$

where K and a are constants for a given polymer solution. The relationship between [η] and M_w for a PVA solution is shown in Fig. 11 [22]. It can be seen that the rheology of PVA solutions can be described by the Mark-Houwink equation. Tacx et al [20] obtained

a: P120 solution
b: 0.041 Mrad
c: 0.082 Mrad
d: 0.123 Mrad
e: 0.191 Mrad
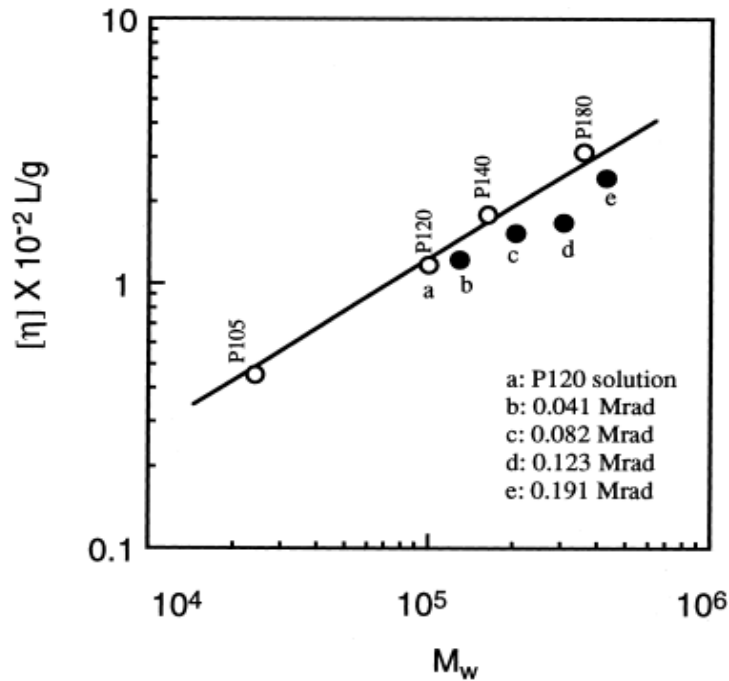
Fig. 11   Typical plot of the Mark-Houwink equation for an aqueous PVA solution [22].

18

the following constants in the Mark-Houwink equation for dissolution in water at 30°C:

$$[\eta] = 6.51x10^{-4} M_w^{0.628}$$ (4)

In dilute aqueous PVA solutions, the Huggins equation can be used to describe the specific viscosity, η_{sp}, as a product of $[\eta]c$:

$$\eta_{sp} = [\eta]c + k_H [\eta]^2 c^2 + k_2 [\eta]^3 c^3 + ...$$ (5)

where κ_H is the Huggins viscosity coefficient, which reflects both hydrodynamic and thermodynamic interactions of polymer molecules [23]. The Huggins viscosity coefficient is generally between 0.35 and 0.45, although higher values have been measured in PVA due to the existence of hydrogen bonding [23].

2.2.5 Surface tension

The addition of PVA to water effectively lowers the surface tension, γ, of water as shown in Table IV [17]. The surface tension of the solution drops further as the concentration of PVA is increased.

Table IV   Surface tension of solutions containing various amounts of PVA [17].

Solution	γ (mN/m)
Water	72
1 g of PVA in 100 g of water	48.6
2 g of PVA in 100 g of water	46.1
4 g of PVA in 100 g of water	45.4
8 g of PVA in 100 g of water	44.6

The surface tension of aqueous solution of PVA varies with molecular weight or DP, % hydrolysis and concentration [17]. The data in Fig. 12 show that at constant DP, the surface tension increases with increasing level of hydrolysis. Similarly at constant level of hydrolysis, the surface tension increases with DP (Fig. 13). For all DP and hydrolysis, between 0% to around 0.1% concentration, the surface tension drops quickly from about 73 mN/m to 48 mN/m and decreases slightly after that. The surface tension decreases throughout the range of polymer concentration considered. The decrease in the surface tension is due to the increased adsorption of the available polymer molecules at the air-aqueous solution interface as the polymer concentration increases [24,25].
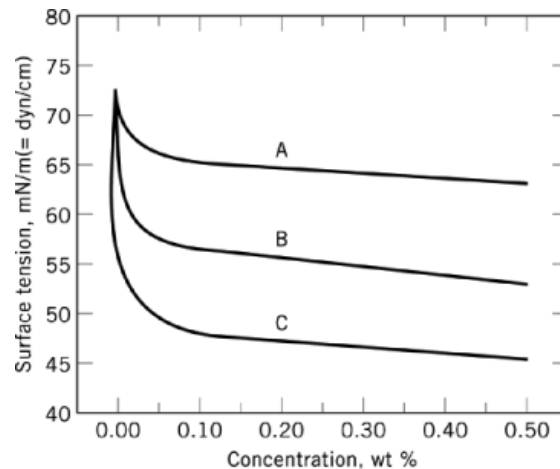
Fig. 12   Surface tension of aqueous PVA solutions 20°C as a function of concentration. The degree of polymerization in the PVA was 1700. A, 98-99% hydrolyzed; B, 87-89% hydrolyzed; C, 78-81% hydrolyzed [17].

Additives to the solution may change the surface tension values. It has been shown that adding NaCl to the polymer solution increases its surface activity [25]. The data shown in Fig. 14 [25] show that the surface tension of the aqueous PVA solution decreases
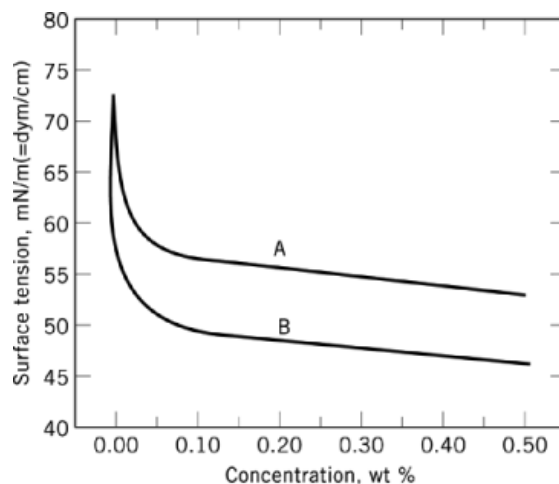
Fig. 13   Surface tension of aqueous PVA solutions 20°C as a function of concentration. The degree of hydrolysis in the polymer was 87-89 mol%. A, DP = 1700; B, DP = 550. [17].

significantly with increasing NaCl concentration up to 7.0 wt %. This behavior has been attributed to the increased adsorption of the polymer molecules at the air-aqueous solution interface as the NaCl is added. In other words, NaCl is making the aqueous phase less favorable for the polymer molecules, causing more molecules to go to the interface and consequently reducing the surface tension [25]. Note, however, that the addition of NaCl increases the viscosity of the solution indicating that water becomes less favorable as a solvent (Fig. 15) [12]. The addition of 1.2 Molar NaCl almost doubles the apparent viscosity of the solution. The maximum value of viscosity is observed at about 1.2 wt % NaCl. Increasing the NaCl concentration beyond 1.2% lowers the apparent viscosity. The addition of electrolytes disrupts the hydrogen bonding and causes a decrease in viscosity for both water and the corresponding aqueous polymer solution. It can be expected that the electrical conductivity of the solution will also be affected by the addition of NaCl. It has been reported that ionic additions to polymer solutions may improve conductivity of polymer solutions [26]. Further, additions of NaCl to the

solution may also improve crystallinity in the polymer [27]. It should be noted that all these parameters may be significant in electrospinning as will be discussed in the following sections.
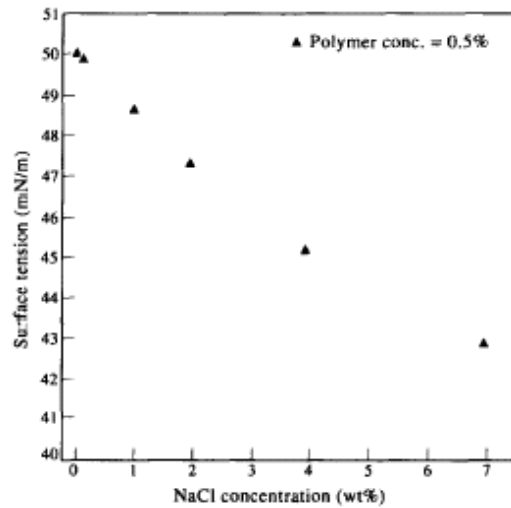
Fig. 14   Effect of NaCl additions to aqueous PVA (M_w=72,000 g/mol) on the surface tension of the solution at 30℃ [25].
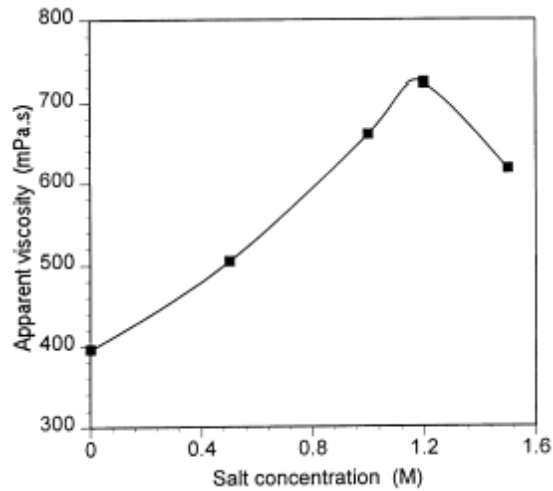
Fig. 15   Effect of salt concentration upon apparent viscosity for a 10% PVA, Mw=100000, 88% hydrolyzed aqueous solution, T=25℃, shear rate=46/s [12].

2.2.6 Physical Properties

PVA is a polymer with good hydrogen bonding and a high degree of crystallinity. The *melting point* of PVA depends on M_w, degree of hydrolysis, %crystallinity and tacticity of the polymer. Typical melting points are on the order of 228 to 240°C for *atactic*, 212 to 235°C for *isotactic* and 230 to 267°C for *syndiotactic* structures [15]. The glass transition temperature is 85°C for highly hydrolyzed PVA and 58°C for 87%-89% hydrolyzation [17]. PVA is usually crosslinked for several applications, especially for biomedical and pharmaceutical applications such as blood contact, artificial kidney, and drug delivery. PVA is used extensively as a membrane material in soft tissue replacements, articular cartilage, artificial organs and membranes because of its high water content, tissue-like elasticity, adequate mechanical strength, and relative biocompatibility [11]. PVA has an excellent ability to form hydrogels. PVA gels can be made by cross-linking chemically by a difunctional agent and physically by UV light with photo-initiators, electron-beam or gamma radiation. The physical methods have advantages over the chemical cross-linking as they do not leave behind toxic agents. [11]

The polymer can exhibit a high tensile strength as shown in Appendix I. The mechanical properties are a strong function of molecular weight and the relative humidity as shown in Fig. 16 [11]. It can been seen from the Fig. 16 that the tensile strength of PVA varies from 30 MPa to 110 MPa, depending on M_w and relative humidity. The ability to obtain such a wide range of tensile strength values makes the polymer appropriate for diverse applications. The dielectric behavior of the polymer is determined by the charge distribution and also by statistical thermal motion of its polar group. Since dielectric

properties of polar materials will depend on whether or not the dipoles are attached to the main chain [28], as the structure of PVA is, dipole polarization will depend on segmental
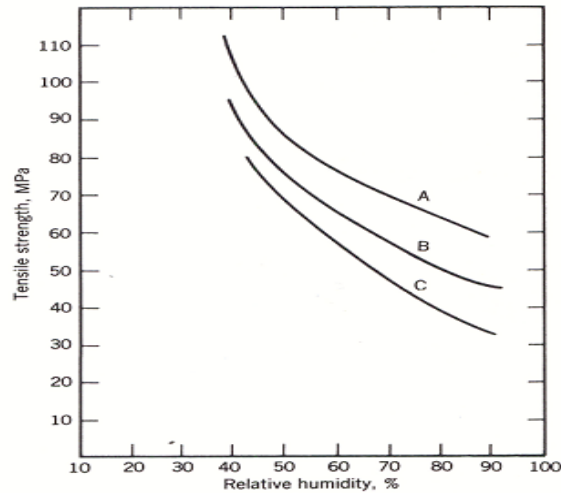
Fig. 16   Tensile strength as a function of relative humidity for fully hydrolyzed poly(vinyl alcohol) films. A, Degree of polymerization=2400; B, 1700; C, 500 [11].

mobility and is thus low at temperatures below the glass transition temperature. Polar molecules have high electric constant. The value of dielectric constant is dependent on temperature and frequency.

2.3 Porous Structure

Polymeric fibers, particles, membranes and porous scaffolds have attracted great interest in the recent research of biomedical engineering [1,2]. The practical applications of these structures of biopolymers vary from wound dressing, drug delivery, vascular grafts to tissue engineering scaffolds. An example of a porous polymeric structure used in tissue

24

engineering is shown in Fig. 17 [1]. A majority of these, although not all, involve the use of three-dimensional polymeric scaffolds implanted at a tissue defect site to both replace the function of the tissue temporarily and help the body to regenerate or repair it. The scaffolds must therefore provide a suitable substrate for cell attachment, proliferation, differentiated functions and, in certain cases, cell migration [1,2]. Such applications place strict requirements on the physical and chemical properties of the specific polymeric scaffolds. The porous structure must provide space for cell to grow in and facilitate the transport of cells and nutrients to maintain normal cellular activities. The loss in mechanical properties of the resorbable polymer should match the temporal development of the strength in the native tissue. The polymer scaffolds can also serve as carriers for cells, growth factors, and/or other bio-molecular signals in order to obtain targeted and controlled release of these active ingredients [2]
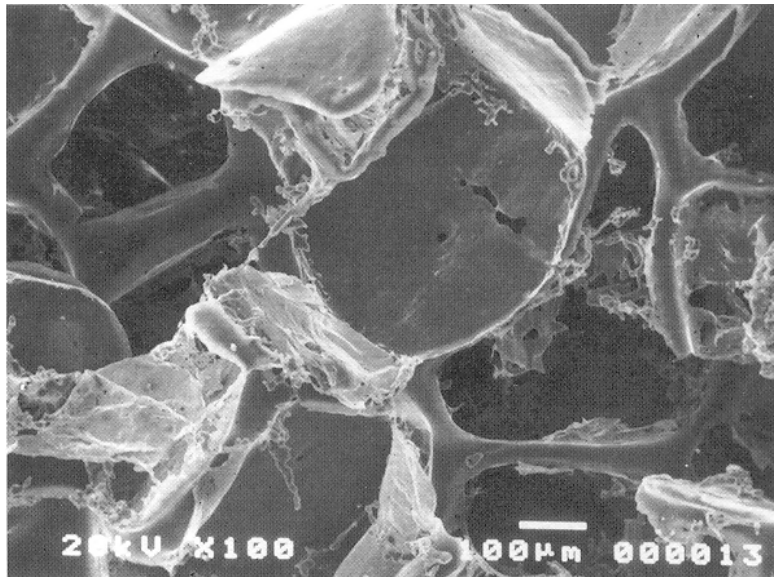
Fig. 17   *Photograph of a porous PLGA scaffold used for tissue engineering. The porosity was induced by a porogen, sodium chloride of size range 300-500 μm [1].*

The key characteristics of the scaffolds include high porosity and surface area, structural strength, and specific three-dimensional shapes, which are determined by the scaffold fabrication techniques and the polymeric materials used [1]. Many techniques have been developed to produce porous structures with high interconnected porosity. The characteristics differentiating various techniques include the use of solvents, heat, pressure, or pore creating additives. The majors processing techniques to produce porous structures include: *Fiber bonding, Solvent casting and particulate leaching, Gel casting, Phase separation and Three-dimensional printing [1, 2].* They differ from one another in the means to produce the porous microstructures. Fiber bonding achieves highly interconnected pores by adding and later removing an insoluble nonwoven mesh of some polymer to the primary polymer solution, leaving voids where was previously occupied by the nonwoven mesh. Solvent casting and particulate leaching can achieve the same results by adding to (and later removing) the polymer solution small insoluble particles as porogens. Sodium Chloride particles between 300-500 μm are typically used as porogens. Gel casting is similar to solvent casting, but it produces micro-porous structure by processing the initial gel through several stages of solvent exchanges in mixtures of acetone, ethanol, and water. Phase separation is a process primarily to address the problem of drug delivery by avoiding harsh chemical or thermal environments in the process. The solution of the polymer and the bioactive molecules with liquid-liquid phase separation is quenched to produce a solid and the solvent component is removed by sublimation, leaving behind a porous structure. Three-dimensional printing is a solid free-form fabrication process that produces components by inkjet printing a binder onto sequential powder layers. Other processes to produce porous structures are *Extrusion,*

Membrane Lamination, gas foaming, etc. The advantages and disadvantages of some of the principal techniques to produce porous polymers are summarized in Table V [29].

2.4 Electrospinning

Recently, the process of electrospinning has attracted much attention because it can consistently produce polymer fibers that range from 5 to 500 *nm* in diameter [30]. This process is a variation of the better known electrospray process, which produces small particles using electrical force [31]. In this process, a polymer solution or melt held by its surface tension at the end of a capillary tube is subject to an electrical field. Initially the polymer solution forms a droplet at the end of the capillary tube. As the voltage increases, charge is induced on the fluid surface, and the droplet is distorted to form a conical shape known as Taylor cone. When a critical voltage is reached a jet is ejected from the apex of the cone. As the jet accelerates and thins in the electric fields, radical charge repulsion results in splitting of the primary jet into multiple filaments by *splaying* [31-33]. By comparison, in the electrospray process, the jet is broken into small droplets and sub-micron beads are obtained (Fig. 18). For high viscosity liquids (~1 to 10 Pa.s), the jet does not break up, but travels as a jet to the grounded target. It undergoes thinning, splaying and bending as it travels, and the solvent evaporates leaving behind a charged fiber deposited on a grounded collector to form a nonwoven mesh [31]. The electrospun fibers may have a sizable static charge making it possible to manipulate them into three-dimensional (3-D) structures during their deposition with the help of electrical field.

Table V   Advantages and Disadvantages of various processes currently used to produce porous polymers [29]

Process	Advantages	Disadvantages
Fiber bonding	Easy process High porosity High surface area to volume ratio	High processing temperature for non-amorphous polymer Limit range of polymers Lack of mechanical strength Problems with residual solvent Lack of control over micro-architecture
Phase separation	Allows incorporation of bioactive agents Highly porous structures	Lack of control over micro-architecture Problems with residual solvent Limited range of pore sizes
Solvent casting and particulate leaching	Highly porous structures Large range of pore sizes Independent control of porosity and pore size Crystallinity can be tailored	Limited membrane thickness Lack of mechanical strength Problems with residual solvent Residual porogens
Membrane lamination	Macro shape control Independent control of porosity and pore size	Lack of mechanical strength Problems with residual solvent Tedious and time-consuming Limited interconnected pores
Melt moulding	Independent control of porosity and pore size Macro shape control	High processing temperature for non-amorphous polymer Residual porogens
Polymer/ceramic fiber composite-foam	Good compressive strength Independent control of porosity and pore size	Problems with residual solvent Residual porogens
High-pressure processing	Organic solvent free Allows incorporation of bioactive agents	Nonporous external surface Closed pore structure
High-pressure processing and particulate leaching	Organic solvent free Allows incorporation of bioactive agents Highly porous structures Large range of pore sizes Independent control of porosity and pore size	Limited interconnected pores Lack of mechanical strength Residual porogens
Freeze drying	Highly porous structures High pore interconnectivity	Limited to small pore sizes
Hydrocarbon templating	No thickness limitation Independent control of porosity and pore size	Problems with residual solvent Residual porogens

Depending on the solution viscosity, electrical field strength and other process parameters, porous structures of varying morphologies can be obtained. The process can be conducted vertically and horizontally as in Figs. 18 and 19 [31,34]. The viscoelastic behavior of the polymer solution keeps the elongated jet from breaking into beads and helps to maintain fibers with relatively uniform diameters.
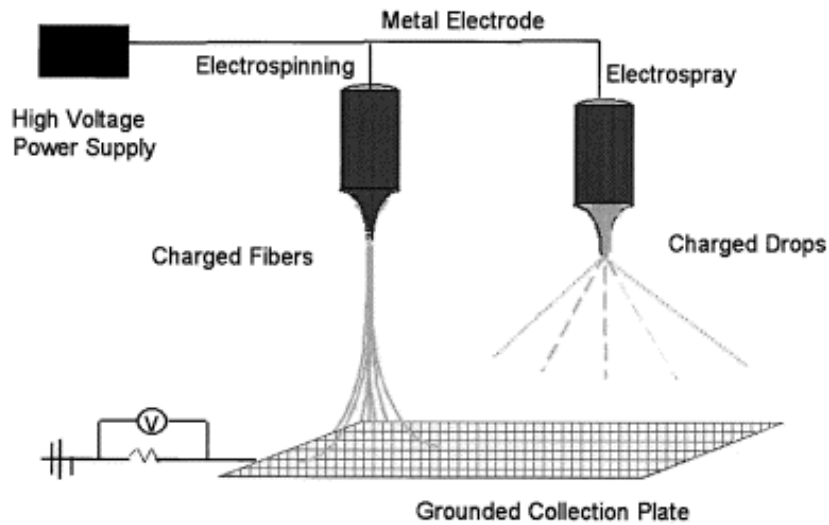
Fig. 18   Schematic illustration of electrospinning and electrospray processes [31]
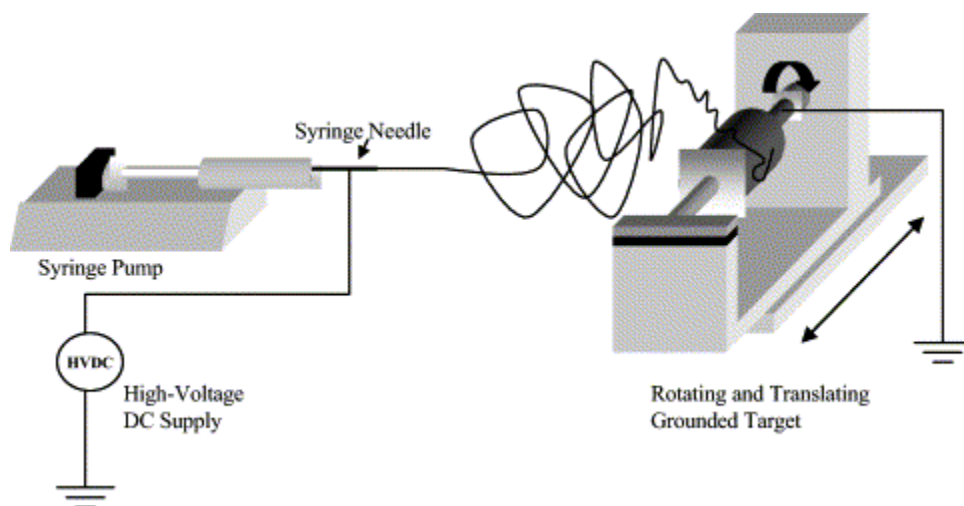
Fig. 19   Schematic illustration of the set-up for producing 3-D structures [34].

29

Electrospinning or electrospraying can have several advantages. Sub-micron particles or fibers can be produced with very high surface areas as shown in Fig. 20 [35]. Electrospun 3-D structures may have small pore sizes and very high surface areas, highly suitable for tissue engineering. The degree of crystallinity and orientation in the polymer can be controlled. Drugs, growth factors and/or other biomolecules can easily be added to the solution and be incorporated in the fiber or particle. Multiple solutions can be used to produce graded or layered structures. Organic and inorganic solutions can be used produce polymer ceramic nano-composites.
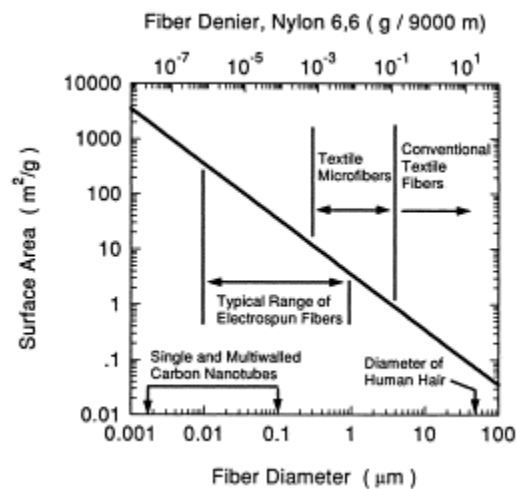
Fig. 20   *Surface area in the porous structure as a function of fiber diameter for various processing techniques [35].*

The fibers produced by electrospinning belong to non-woven fabrics. More than 40 different types of polymer fibers have been generated by electrospinning including Collagen [36], poly (ethylene-co-vinyl alcohol0 [34], SLPF[37], nylon 66 [38] and PCL [39]

2.4.1 Basic Operating Mechanisms

Electrospinning is a process in which the solution jet is broken down into smaller jets by an appropriate balance between surface tension forces which hold it together and electrical forces which try to break it apart. Initially the polymer solution is held by its surface tension in the form of a droplet at the end of the capillary tube. As the voltage is increased, charge is induced on the fluid surface, sessile and pendant droplets of the polymer solution acquire stale shapes, known as Taylor cone, at equilibrium of the electric forces and surface tension. When the intensity of the electrical fields rises beyond a critical point, a single jet is ejected from the apex of the cone. This occurs because the surface tension is overcome by electrical repulsion between the mutual charges on the surface of the drop [37]. Taylor identified a critical voltage at which this breakdown would occur [40]:

$$V_C^2 = 4\frac{H^2}{L^2}\left(\ln\frac{2L}{R} - \frac{3}{2}\right)(0.117\pi\gamma R) \qquad (6)$$

where Vc is the critical voltage, H, the separation between the capillary and the ground, L, the length of the capillary, R, the radius of the capillary, and γ is the surface tension of the liquid. A similar relationship was developed by Hendricks et al. [41] for the potential required for the electrostatic spraying from a hemispherical drop pendant from a capillary tube:

$$V = 300\sqrt{20\pi\gamma r} \qquad (7)$$

where r is the radius of the pendant drop [41]. In his seminal work on the behavior of an isolated charged drop of a range of fluids, Taylor determined that at an half angle of 49.3° of the apex of the droplet, surface tension balances electrostatic forces[40, 42]. Taylor

cones are the critical points of the equilibrium between these two forces, above which, i.e., when $V > Vc$, non-equilibrated electrical forces on the droplet causes a thin jet of solution to eject from the surface of the cone and travel toward the nearest electrode of opposite polarity, or electrical ground. A schematic illustration of the various physical phenomena occurring during electrospinning is shown in Fig. 21 [43].

At a relatively low concentration of the polymer solution and/or a low applied electrical field, three different operation modes for electrospray have been classified [44-46] as (a) *dripping* mode, (b) *spindle* mode, (c) *oscillating jet* mode, which describe the shape and motion of the droplet forming and disintegration; (d) the *precession* mode, in which a rapidly whipping jet is emitted from the nozzle, before it breaks into droplets. The last two modes are qualitatively close to the whipping mode in electrospinning in the existence of a twisted or rapidly whipping jet.

Typically in the electrospinning of a polymer solution, as the voltage increases above the critical value, initially a straight jet was formed from the Taylor cone. The electrically charged jet travels towards the grounded collector in a straight line for few centimeters and at the end of this segment a conical shape can be observed, which is believed to be the complicated path taken by the jet. Electrospinning process is quite rapid. After an elapsed time of 1ms, only the conical envelopes of splaying subfilaments from the jet have been observed due to the extremely fast whipping of the jet [46].

The electrospinning jet can be characterized by 4 regions [43]: (a) Base, a region where the jet emerges from the polymer solution, typically the Taylor cone (Fig. 21) (b) Jet, the region beyond the base, where the electrical force stretches the jet and accelerates the polymer liquid. The diameter of the jet decreases and the length increases as the jet

Reservoir

Capillary

Taylor's Cone

Low → unoriented molecules

Elongational Flow

High → High orientation

Stress Relaxation

Spinodal

Splitting

Solvent
Evaporation

Splaying

Nucleation +
Growth

Electrospun
Polymer

Amorphous, oriented,
fibrillar, spherulitic
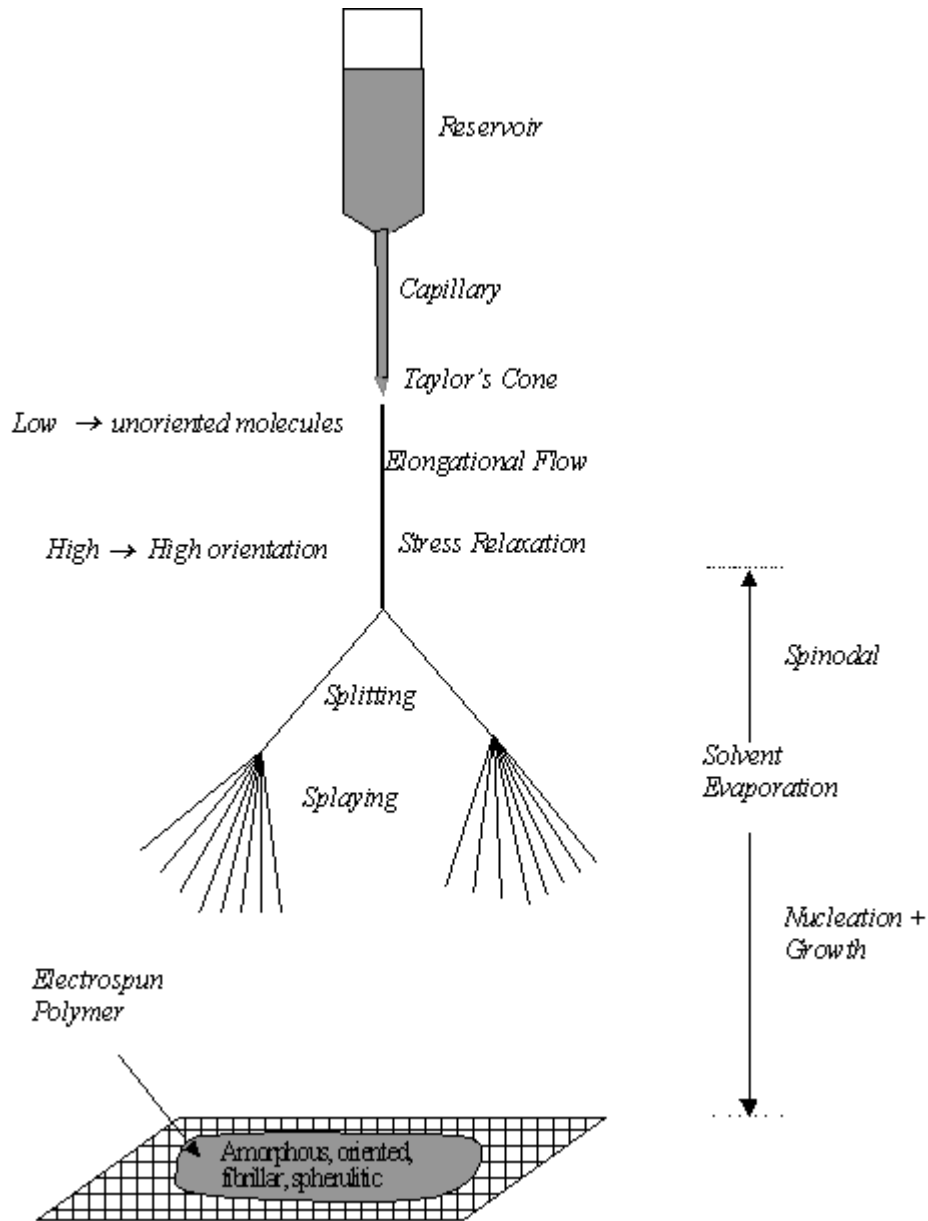
Fig. 21   A schematic illustration of the various physical phenomena occurred during electrospinning a viscoelastic polymer [43].

33

moves towards the collector. (c) Splitting and Splaying region: Splitting refers to the breakup of the jet into two equal parts, while splaying occurs when a single jet divides into many charged jets with approximately equal diameters and charge per unit length.
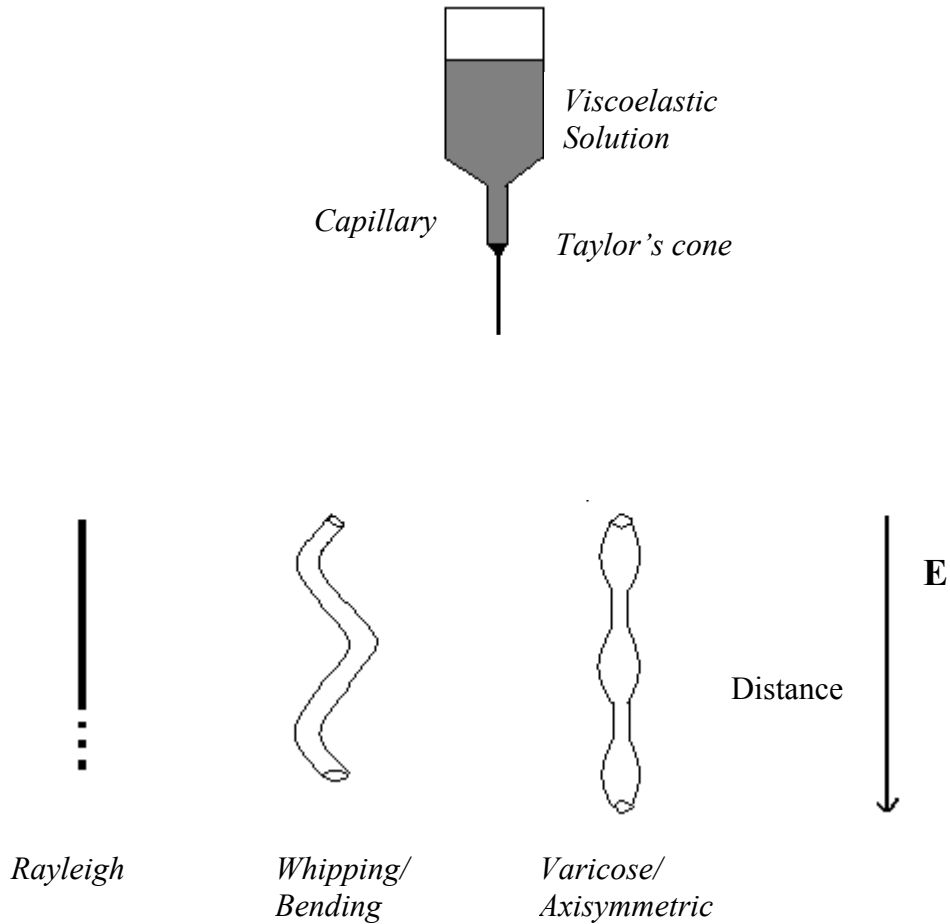
Fig. 22   Various instabilities that may be induced in the viscoelastic jet that is ejected from the Taylor's cone [43].

Various instabilities that may lead to the breakdown of a viscoelastic jet are summarized in Fig. 22 [43].   The bending and the varicose instabilities play a major role in the electrospinning process.   Hohman et al [45,46] predicted the growth rate of *varicose instability*, in which radius of the jet varies continuously while the centerline of the jet

remains straight, and a *whipping or bending instability*, in which the centerline of the jet is constant and the diameter of the jet is modulated. Also demonstrated are three different unstable modes: (1) the Rayleigh mode is driven by the electrical counterpart of the surface tension and is the axisymmetric extension of the classical Rayleigh instability; (2) the axisymmetric conducting mode and (3) the whipping conducting mode may occur when the conductivity of the solution is finite. The last two conducting modes are enhanced when increased electrical fields or surface charge density suppressed the classical Rayleigh instability. Bending instability plays a central role in the electrospinning process. When the electrical conductivity of the fluid is finite, the whipping or the axisymmetric mode of the jet becomes unstable. The instability is caused by an imbalance in the tangential stress on the interface, caused by the interaction of the induced surface charge density and the tangential electric field.

Table VI Various factors associated with electrospinning of polymers from solution [43].

Polymer	Solution	Process
Molecular weight	Type of solvent	Applied field strength
Polydispersity Index	Concentration	Deposition distance
T_g	Viscosity	Flow rate
isomeric structure	Electrical conductivity	Deposition time
crosslinking	Dielectric strength	Solvent evaporation rate
	Surface tension	Size of capillary
	Additives	Collection technique
	Temperature	Relative Humidity

2.4.2 Morphologies produced by electrospinning

In the process of electrospinning different morphologies of fibers and/or beads can be produced due to specific combinations of solution properties and experimental settings. The list of variables that can be controlled to produce various structures is shown in Table VI [43]. Flat or round fibers can be produced by controlling the processing conditions (Fig. 23). Round fibers are typically produced when the solvent evaporates completely before the splayed jet reaches the collector. Ribbon-shaped flat fibers, shown in Fig. 23 (b), are obtained when the solvent evaporation rate is low and the wet fibers reaching the collector are flattened upon impact. [47] Hollow fibers can be produced by forming a skin rapidly. The remaining solvent has to escape by diffusion through the skin [47]. The hardened skin prevents the shrinkage of the jet as the solvent gradually evaporates and thereby results in hollow fibers. Significant branching and splitting can also be observed in many structures (Fig. 24) [47].

| (a) | (b) |
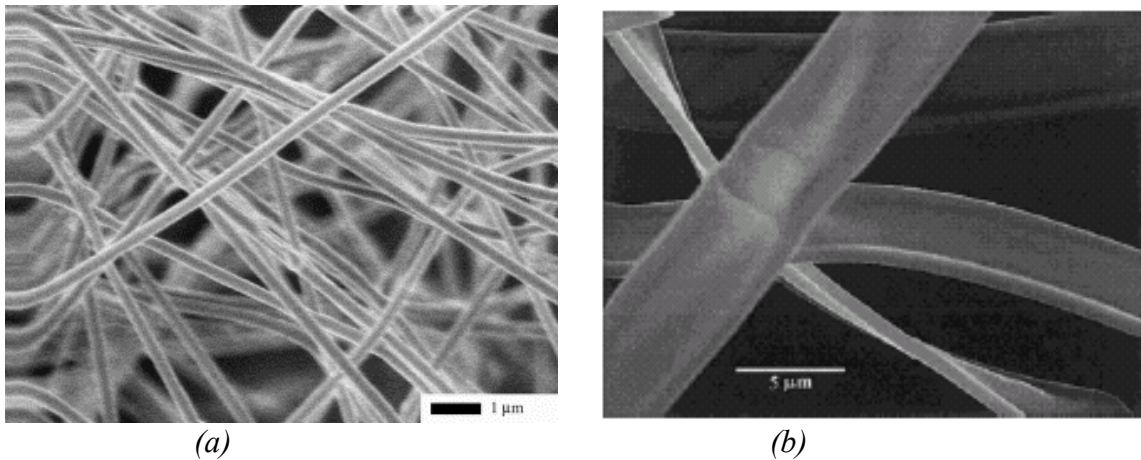
Fig. 23 Photographs showing round (a) and flat (b) fibers in electrospun PEO [44,47].

36

(a)   (b)
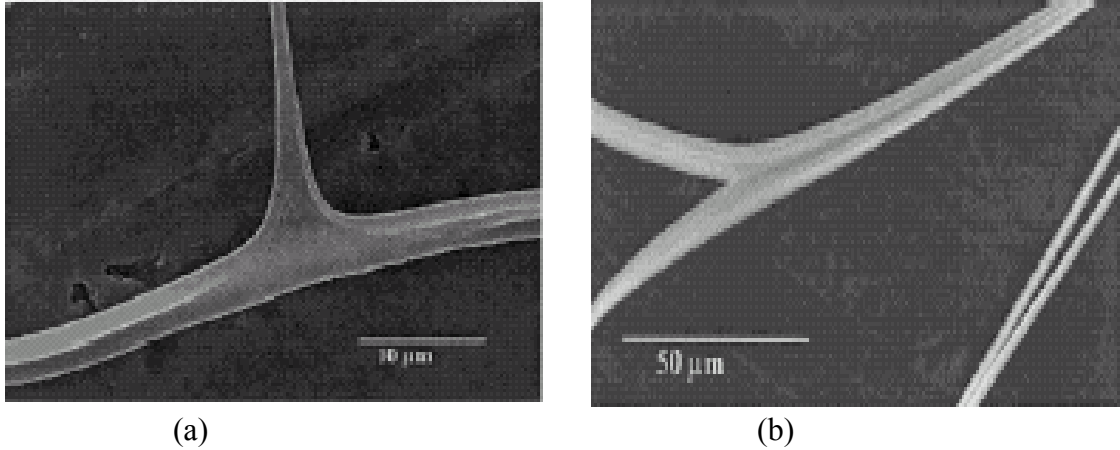
Fig. 24   Photographs showing branching (a) and splitting in electrospun HEMA [47].
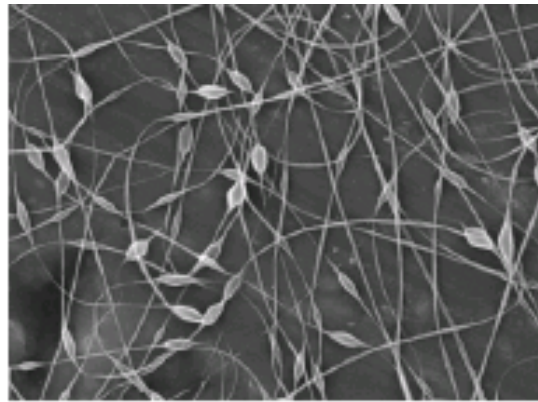
Fig. 25 Photographs showing bead-on-string morphology in the electrospun polymer [48].

In some cases, a so-called 'bead on fiber' structure is produced, mostly with solutions of low concentration as shown in Fig. 25 [48]. A probable reason for the formation of beads on the fiber is that if the surface tension of the solution is large and not negligible compared to the tangential electrical force for some poorly conducting solutions, it tends to resist the stretching force of electrical repulsion and form beads. At higher viscosity, smooth and thick fibers are produced as a result of extensive entanglement between the macromolecules. Mesh-like structures with the right pore characteristics can be produced by adjusting the collection technique as shown in Fig. 26 [48]. When the solvent is not

completely evaporated from the fibers, the intersections of two fibers will merge together by nucleation and growth and form a mesh-like microstructure with each fibers bonded with many other at their intersection points.

Many parameters can influence the structure and properties of the electrospun polymer as shown in Table VI. These variables can be related to the base polymer, the solution and the operating conditions. Among these, the effects of applied field strength, solution concentration and deposition rate have been studied extensively in the literature. The effects of various parameters on the morphology in the electrospun polymer are summarized in Fig. 27 [37]. In general, the diameter of the fiber decreases as the applied field strength is increased. The solution
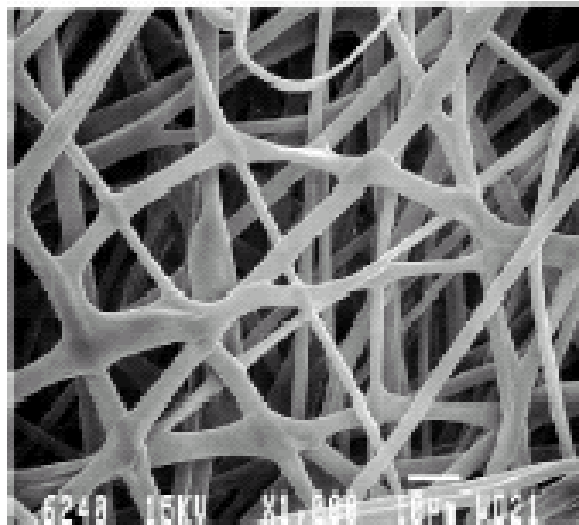
Fig. 26   Mesh-like structure in electrospun EVOH [34].

concentration has a major effect on the structural morphology and fineness of the electrospun polymer. The concentration may affect the viscosity and surface tension

significantly as described previously. There is a minimum concentration needed to stabilize the fibrous jet. There is also a maximum concentration at which the solution viscosity is too high for jet splaying to be effective. Between this minimum and maximum, the fiber diameter increases with concentration. The effects of viscosity of the solution on the electrospun structures are extensive. Higher solution viscosity generally results in smooth fibers as discussed above. Due to the evaporation and solidification in its path, the jet becomes more viscous with time and its elastic modulus increases. This increase in viscosity increases the shear stress for splaying and hence, may gradually make bending instability more difficult. Low deposition distances can lead to collapse, flattening and coalescence of the fibers. At high deposition distance, in contrast, the

Fig. 27   Schematic illustration of the effects of process parameters on the the structure of the electrospun product [37].

solvent may evaporate completely and consequently round fibers with a highly open structure may be obtained. However, as the deposition distance increases, the electrical field strength/unit length can be reduced and this may affect the fiber morphology.

Surface tension plays a major role in the breakdown on the jet. Surface tension always counteracts the bending instability because this instability leads to an increase of the area of the jet surface. Higher surface tension generally tends to produce more beaded structures. In order to produce thin fibers, it is desirable to have as small a value of surface tension as possible. Thinner fibers with fewer beads are produced in more conductive solutions as shown in Fig. 28 [48]. As the electrical conductivity increases, the surface charge densities are higher, which result in stronger repulsion between adjacent segments. This enhanced the elongation stress counteracting the viscous effects and leads to thinner fibers with fewer beads [48].

(a)   (b)
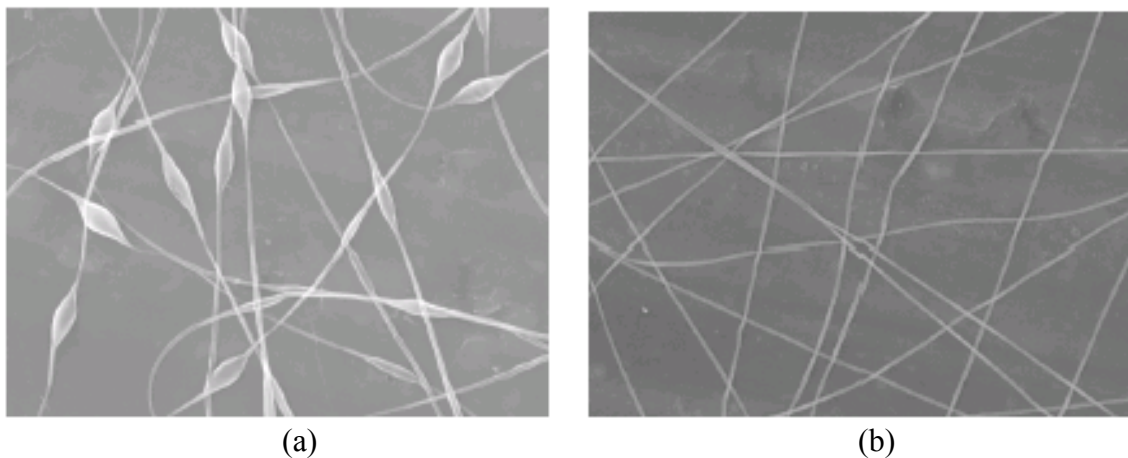
Fig. 28   Photographs showing the structure in electrospun PEO (a) solution conductivity 1.23 Coulomb/liter (b) solution conductivity 28.2 Coulomb/liter [48].

2.4.3 Structure in the Electrospun Polymer

Electrospinning can be used to produce novel fibers with the diameters in the range from 100 *nm* to 10 *μm*. As the solvent evaporates, the polymer molecules can come together by either a phase separation through a spinodal reaction or through classic nucleation and growth of the crystalline phase [49]. As a result, the structure in the polymer deposited on the collector can consist of a totally amorphous, an oriented, a spherulitic or a textured fibrillar structure. In electrospinning, jets are stretched along their axis by the external electrical field and are elongated further by the repulsive force between charges on adjacent segments. The resulted area reduction rate and the associated high longitudinal strain rate imply that the macromolecules in the fibers should be stretched and axially oriented [50]. It is generally recognized that electrospinning may lower the degree of crystallinity in the polymer [37, 51-53]. The exact reasons for this behavior are not clear. It has been suggested that the development of structure in electrospinning occurs much more rapidly than other processes and this kinetic effect may result in lower crystallinity [53]. A high degree of orientation may also be observed in the fibrils. The degree of orientation of the molecules in the amorphous regions is directly proportional to the amount of extensional flow.

In summary, electrospinning is a novel technique that can be used to produce nano-scale porous structures with a variety of morphologies. The fiber size and distribution, and inter-fiber spacing (*i.e.* porosity) and distribution can be varied significantly by controlling the process parameters. Drugs and growth factors can be incorporated easily into the structure for biomedical applications.   The porous structure produced by

electrospinning can have a very high ratio between surface area and volume and is ideally suited in applications such as drug delivery and tissue engineering. The effects of variables associated with the electrospinning process have been studied extensively in the literature. However, the variables associated with the polymer such as molecular weight, polydispersity index and crosslinking have not be investigated thoroughly. The effects of molecular weight, crosslinking and extent of hydrolysis are especially important in polymers such as PVA. Even though PVA has good mechanical properties in the dry state, its applications are limited by its poor resistance to water. The water resistance is generally improved by crosslinking. Electrospinning can be a potential technique to produce crosslinked nanofibers for many applications. In order to produce and control the structure of these nanofibers, it is imperative that various factors associated with structure formation be examined thoroughly.

3. OBJECTIVES

The overall objectives of this work are to develop a suitable processing methodology to produce porous polyvinyl alcohol structures by electrospinning. The specific goals are:

♦ to determine the processing conditions to produce porous PVA structures

♦ to study the combined effects of molecular weight and solution concentration on the structure of the electrospun polymer

♦ to examine the effects of different solvents on electrospinning characteristics

♦ to determine potential additives to the solution to control the structure in the porous polymer

4. MATERIALS AND METHODS

PVA with various weight average molecular weights (M_w) was obtained from Aldrich Chemical Company, Milwaukee, WI. The characteristics of the polymers used in the study are shown in Table VII. Several different solvents were used to dissolve the PVA. These solvents included water, N-Methyl Pyrrolidone (NMP), Ethylene Glycol (EG) and Dimethyl Sulfoxide (DMSO). All the solvents were obtained from Aldrich Chemical Company, Milwaukee, WI. Relevant properties of these solvents are shown in Table VIII [54-56].

Table VII   *Weight average molecular weight (M_w) and % hydrolyzation of PVA used in this study.*

Sample #	M_w (g/mol)	% Hydrolyzation
A	9,000 – 10,000	98-99%
B	13,000 – 23,000	98%
C	31,000 – 50,000	98-99%
D	50,000 – 85,000	97%
E	89,000 – 98,000	98-99%
F	124,000 – 186,000	99+%

The experimental set-up consisted of a 50 ml syringe and an 18-gauge stainless steel needle that were positioned vertically on a clamp as shown in Fig. 29. The metal electrode and the collector plate were made of copper. The collector plate was covered with aluminum foil. The plate was positioned at a distance of 10 cm from the needle. About 1 to 6 g of the polymer was dissolved in the solvent (typically distilled water) at the desired temperature (80ºC for water) to produce solutions with concentration ranging from 5 to 35 wt %. The specific values of concentration used with each molecular weight

are summarized in Table IX. The solution was heated and stirred for 20 to 60 minutes to complete the dissolution. About 15 ml of the solution was added into the syringe at 80º C. In some experiments, other solvents were used to study the effects of solvents on electrospinning. The conditions used during electrospinning with solvents other than water are summarized in Table X. The effects of additives to the solution were studied in some experiments. Two types of additives were examined: (a) NaCl and (b) poly ethylene glycol. NaCl (99%) was obtained from Morton table salt. Appropriate amounts of the additive were added directly to the aqueous solutions. Experiments were conducted for NaCl additions of 0.5,1, and 3 wt %. In the case of poly ethylene glycol, the material was supplied by Aldrich with M_n = 400 g/mol and viscosity of 8.12 mPa s at 37º C. Experiments were conducted at concentrations of 5 and 10 wt %.

The syringe and the needle were enclosed in a chamber in order to control the evaporation rate of the solvent. A voltage of 30 kV was applied to the solution and the solution jet emerging from the needle was collected on the aluminum foil. The electrical field was applied for a predetermined duration. In different experiments, the voltage was applied for a time ranging from 2 min to 2 hr. Subsequently, the aluminum foil was removed from the collecting plate, and the samples were dried for at least 24 hr. Specimens for microscopic examination were obtained at the center (X) of the jet cone as shown in Fig. 29. The samples were sputter coated with gold-palladium and examined in a JSM-840 scanning electron microscope. The images from the scanning electron microscope were analyzed with *Microsun 2000/s* image analysis software to

Table VIII   Relevant properties of the solvents used in this study [54-56].

Solvent	Molecular structure	Grade	Viscosity (mPa s)	T (ºC)	Surface tension (mN/m)	T (ºC)	Dielectric constant	Tm (ºC)	Tb (ºC)	Heat of vaporization (KJ/mol)	Density (g/cm³)
Water	H_2O	100% Distilled	1.793	0	74.23	10		0	100	40.65 at 100º C	1
			0.89	25	71.99	25	80.1				
			0.547	50	67.94	50					
			0.378	75	63.57	75					
			0.282	100	58.91	100					
DMSO	$(CH_3)_2SO$	99.9%	2.47	20		10		18	189	43.1 at 189º C	1.033
			1.987	25	42.92	25	47.24				
			1.29	50	40.06	50					
				75		75					
				100		100					
EG	$HOCH_2$-CH_2OH	99.8%	26/ 21	15/ 20	47.99	25	41.4	-13	197	50.5 at 197.3º C	1.113
			16.1	25	48.4	28					
			6.554	50	45.76	50					
			3.34	75	43.54	75					
			1.975	100	41.31	100					
NMP	$HOCH_2$-CH_2OH	99+%		10		10		-24	82	52.8	1.101
			1.65	25	40.7	25	32.55				
				50		50					
				75		75					
				100		100					

obtain data on the distribution of fibers and particles in the electrospun PVA. This image analysis was conducted at magnifications of 5000 X and 1000 X. The high magnification was needed to clearly demarcate each of the thin fibers. At least three images obtained at various locations in the sample were analyzed under each condition. More than 100 fibers were examined under each condition.

High speed digital photography was used to record the transit of the polymer from the capillary to the grounded collector. A SONY video camera (DCR-TRV900) was used to record the process at a speed of 30 frames/sec. A magnification 1.5 to 2 x was used

during data collection. The *Avid* software was used to analyze the images obtained every 33.3 ms.

High Voltage Power Supply

Copper electrode

Syringe

Polymer Solution

Needle

Jet of solution

Grounded Collector

X
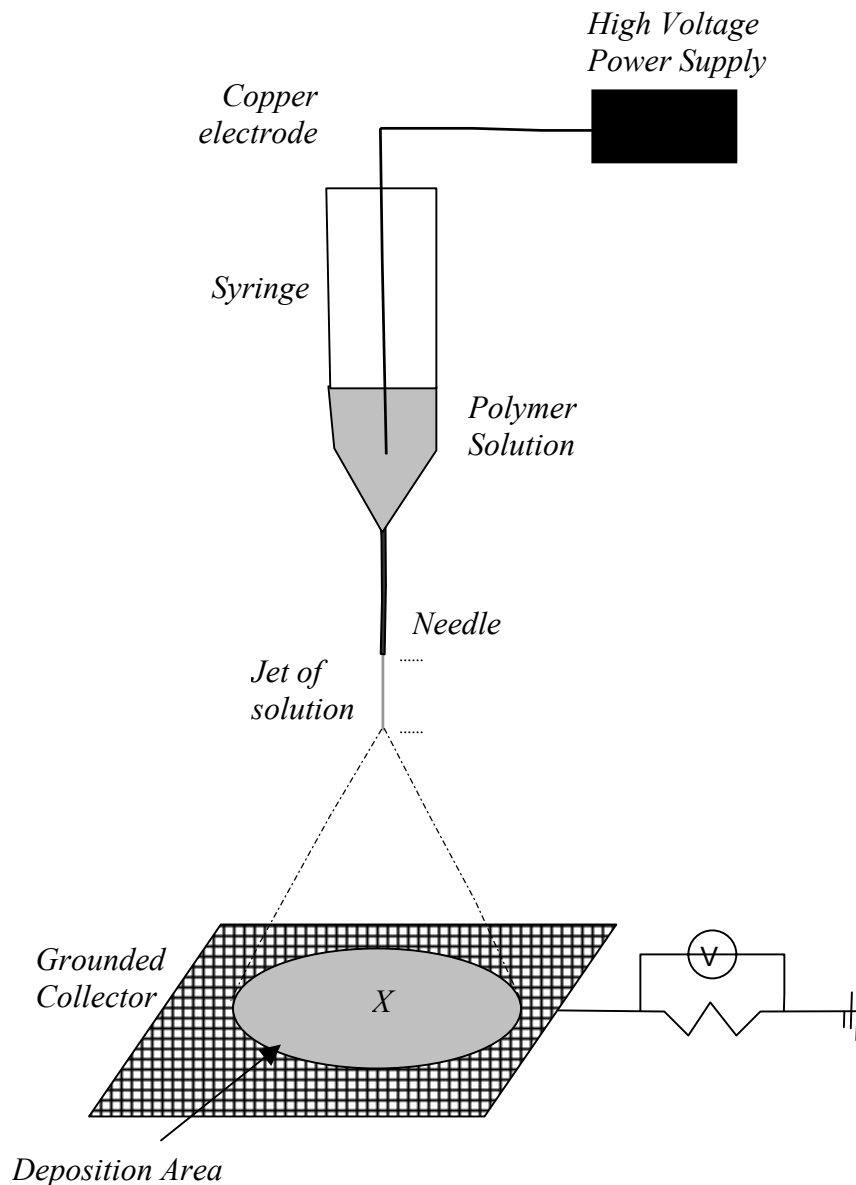
Deposition Area

Fig. 29   Schematic of the experimental set-up. Samples for microscopic examination were obtained from the center(X) of the deposition area. The diameter of the deposition area was generally on the order of 2 cm in most experiments.

Table IX   Summary of concentrations used for each molecular weight.   Only those concentrations at which a fibrous structure could be obtained was selected for each molecular weight. The solvent was distilled water at 80°C.

Solvent	T (°C)		Mw (g/mol)	Concentration (wt %)
Water	80	A	9000-10000	22%
				25%
				27%
				30%
				33%
				35%
		B	13000-23000	21%
				23%
				25%
				27%
				29%
				31%
		C	31000-50000	18%
				20%
				22%
				24%
				26%
		D	50000-85000	9%
				11%
				13%
				15%
				17%
		E	89000-98000	10%
				12%
				14%
				16%
				18%
		F	124000-186000	5%
				6%
				7%
				8%
				9%
				10%

Table X   *Summary of conditions used to produce porous polymers with solvents other than water.*

Solvent	T (ºC)	Mw (g/mol)	Concentration (wt %)
NMP	30	124000-186000	3%
			8.5%
DMSO	65	50000-85000	7.5%
			12%
		124000-186000	8%
EG	140	50000-85000	9%
			11%

5. RESULTS AND DISCUSSION

The breakup of polymer jets into droplets and fibers is strongly influenced by rheological properties of the solution. High molecular weight polymers added to solutions may suppress the breakup and atomization of the solution. In many commercial applications, macromolecules are intentionally added to control misting or suppress the formation of droplets less than 5 μm [57]. For example, high molecular weight polyisobutylene is intentionally added to machining fluids and jet fuels to prevent spray formation. It may also be added in spray paints to increase the overall drop size. Numerous studies have shown that the breakdown of solutions containing polymers is strongly influenced by the rheological properties of the solution [58]. Salient aspects of solution rheology with respect to PVA solutions are discussed in the following sections.

5.1 Viscosity of PVA solutions

The viscosity of PVA solutions (η) depends on the molecular weight (M_w), concentration (c), degree of hydrolysis and the type of solvent.   The dependence of zero shear viscosity on M_w in many polymers can be described by the following Power law equation [59]:

$$\eta = K^{'}\left(M_w\right)^{3.4} \tag{8}$$

In general, the effects of M_w and c on solution viscosity can be modeled as [59]:

$$\eta = K\left(c\rho\right)^{\alpha}\left(M_w\right)^{\beta} \tag{9}$$

The measured viscosity data for PVA solutions in water [13] has been fitted to the above

power law equation. The exponents α and β were calculated to be 4.39 and 2.90

respectively. Equation (9) was then used to generate viscosity data for the molecular

weights and concentrations used in this study as shown in Fig. 30. Note that the viscosity

of the solution depends strongly on M_w and concentration. The intrinsic viscosity $[\eta]$ for

polymer solutions can be related to M_w by the Mark-Houwink equation:

$$[\eta] = K^{''}(M_w)^a \qquad (10)$$

The Mark-Houwink constants (K" and a) for PVA reported in the literature for various

conditions are summarized in Table XI. The product of $[\eta]$ and c can be used to define
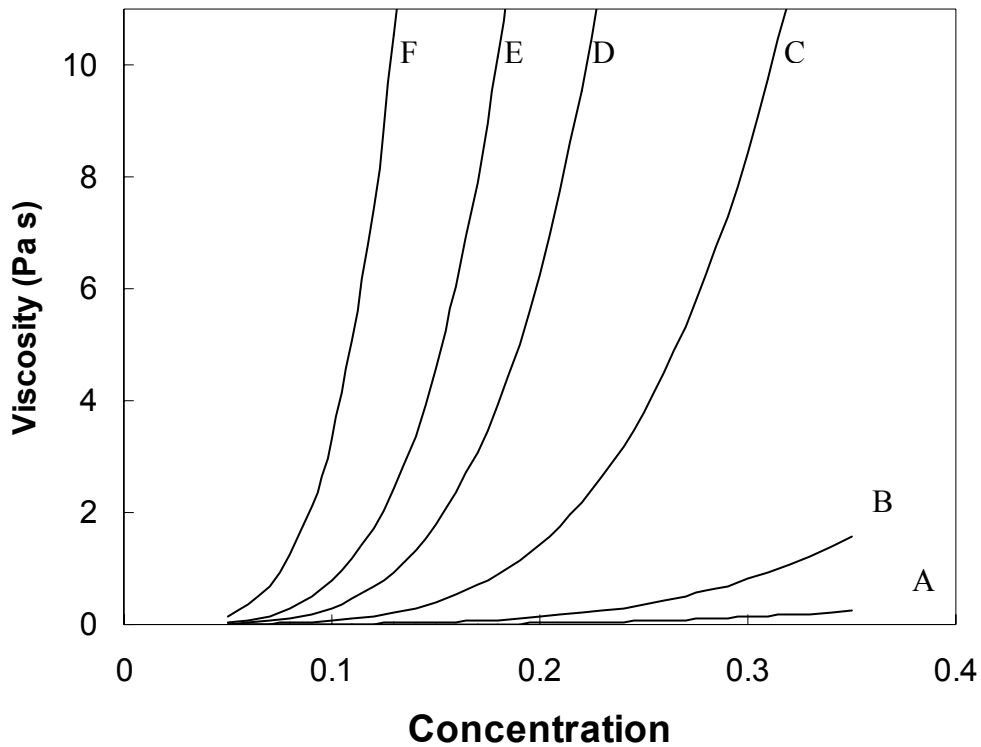
Fig. 30   *Variation of solution viscosity with molecular weight and concentration. The measured viscosity data from the literature has been fitted to equation (6) [13]. This equation was then used to predict the viscosity for molecular weights and concentrations used in this study. The letters in the legend correspond to the molecular weight information shown in Table IX.*

$[\eta]c$, a dimensionless concentration. The typical variation of $[\eta]c$ with c for the values

of M_w and c at which stable fibrous structures were obtained is plotted in Fig. 31. As can

be expected, $[\eta]c$ increases with c for various molecular weights. As M_w increases, the

slope of lines in Fig. 31 increases. This result suggests that M_w has a greater effect on the

rheological properties of the solution than the concentration. The viscoelastic behavior of

polymer solutions can be divided into various regions depending on the value of $[\eta]c$. In

dilute solutions, $[\eta]c < 1$ and the viscosity does not change much with concentration.

The entanglements become significant for $[\eta]c > 4$.   For $[\eta]c > 4$, the viscosity begins to

Table XI   Mark-Houwink constants for PVA solutions obtained from various sources in the literature.

Solvent	Mw (g/mol)	Temperature(°C)	K (10⁻⁴ dl/g)	a	Reference
Water	NA	80	9.4	0.56	[61]
Water	$6 \times 10^3 < M < 160 \times 10^3$	30	6.66	0.66	[61]
Water	$6 \bullet 10^3 < M < 21 \bullet 10^3$	25	2.0	0.76	[61]
Water	NA	30	4.53	0.64	[61]
Water	NA	20-30	5.38	0.63	[15]
Water	NA	20-30	7.31	0.616	[15]
Water	NA	20-30	4.35	0.64	[15]
Water	NA	20-30	6.7	0.64	[15]
Water	NA	20	6.25	0.65	[15]
Water	NA	80	7.4	0.61	
Water	$69 \bullet 10^3 < M < 690 \bullet 10^3$	30	6.51	0.628	[20]
Water	86.8% hydrolysis	NA	8.00	0.58	[17]
Water	93.5% hydrolysis	NA	7.40	0.6	
Water	96.4% hydrolysis	NA	6.90	0.61	
Water	100 % hydrolysis	NA	5.95	0.63	
DMSO	NA		1.6	0.84	[15]
DMSO	$69 \bullet 10^3 < M < 690 \bullet 10^3$	65	1.51	0.804	[20]
EG	$69 \bullet 10^3 < M < 690 \bullet 10^3$	140	3.54	0.692	[20]
NMP	NA	30	1.69	0.79	[61]

increase significantly and viscous effects become important. The data shown in Fig. 31 indicate that a minimum level of entanglement is necessary (or *[η]c* > 4) for stable fibrous structures to be produced. Polymer solutions can also exhibit greater resistance to elongational flow than shear flow [60]. The tensile or elongational viscosity, λ, in Troutonian fluids is almost 3 times the shear viscosity, η. Many polymer solutions exhibit non-Troutonian tensile thickening behavior. The behavior of the solution under extensional flow may have a significant effect on the breakup of the solution jet during electrospinning as will be discussed in the following sections.
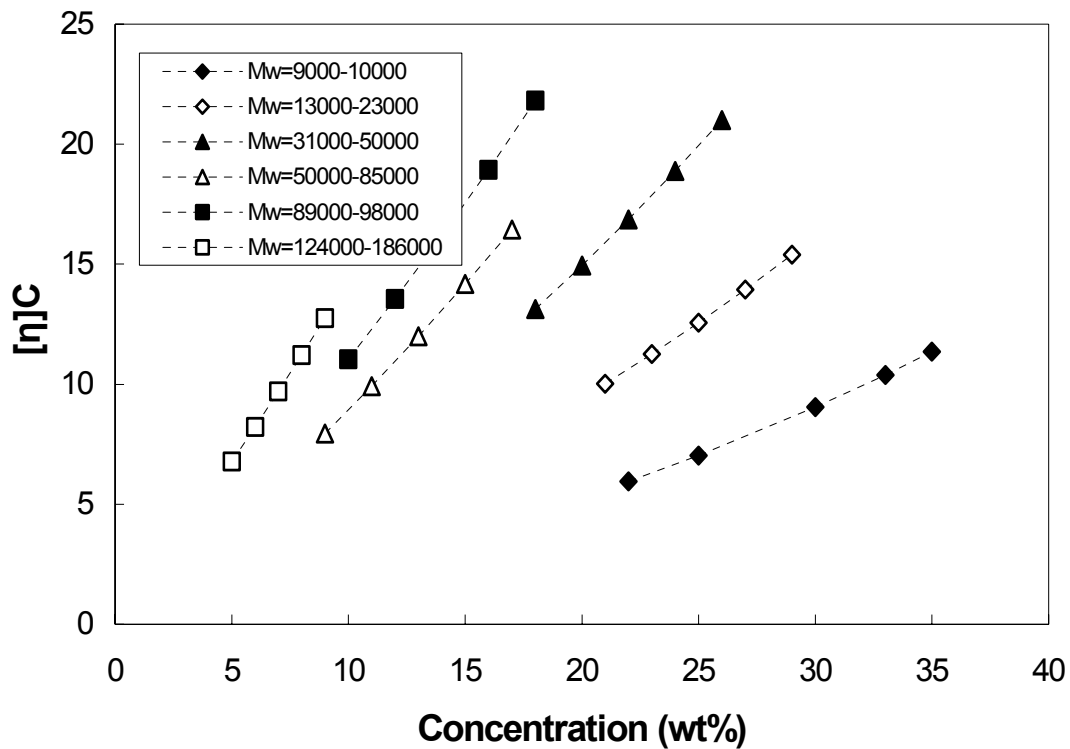
Fig. 31   Variation of dimensionless concentration [η]c with the concentration of PVA in aqueous solutions. Data have been plotted for experimental conditions under which stable fiber structures were produced. The intrinsic viscosity has been calculated from the Mark-Howink equation.

5.2 Structures in the Electrospun Polymer

The structure in the electrospun polymer may consist of beads, fibers and a combination of beads and fibers, depending on the conditions used during the experiment. Most experiments were conducted to obtain a fibrous structure in the polymer. At low concentration and M_W, many beads were observed in the structure along with fibers. This type of structure has been typically referred to as the 'bead on string' morphology in the literature. The shapes of the beads varied from spherical to spindle-like, as seen in Fig. 32. Fibrous structures were stabilized at higher M_w and concentrations as shown in Fig. 33. Fibrous structures contained a relatively broad distribution of fibers which were laid on each other due to the collection procedure. Both round and flat fibers were observed in the structure. Round fibers are obtained when the solvent evaporates completely before reaching the collector [48]. Flat fibers may be obtained when the solvent does not evaporate completely before reaching the collector. In this case, the wet fibers may flatten upon impact. Flat fibers were typically observed at high M_w and concentrations (Fig. 34 (b)). In some cases, flat and round fibers could be detected in the same structure indicating a transition from round to flat fibers at high M_w and concentration. The fibers may exhibit bending, coiling and twisting because of the various stabilites in the jet as shown in Fig. 35 (a) [33,45,46]. In addition, long straight fibers are also observed (Fig. 35 (b)). These fibers may have undergone splaying and a high degree of extensional flow.

(a)   (b)
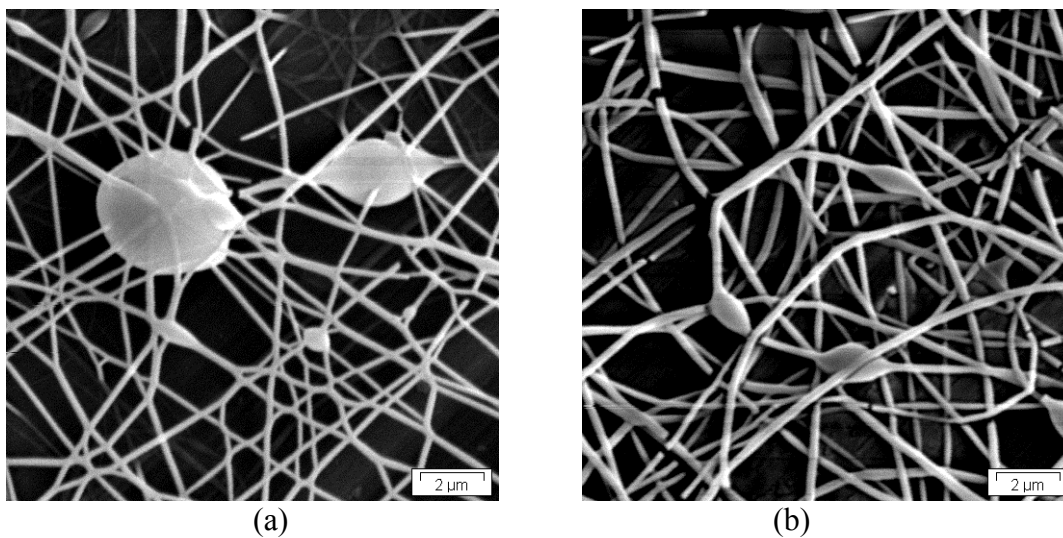
Fig. 32   Examples of bead on string structures in the electrospun polymer.   Such structures were typically observed at low M_w and concentration (a) M_w = 9000-10000, C = 22 wt % and (b) M_w =50000-85000 g/mol, C = 9 wt %.

(a)   (b)
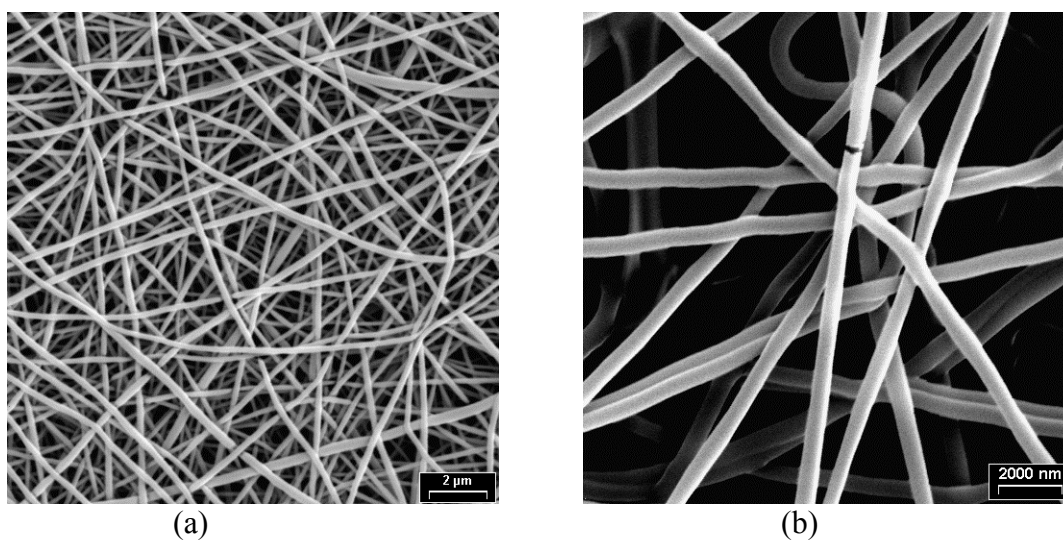
Fig. 33   Examples of fibrous structures with round fibers.   (a) M_w = 9000-10000 g/mol, C = 22 wt % and (b) M_w =50000-85000 g/mol, C = 15 wt %.

(a)   (b)
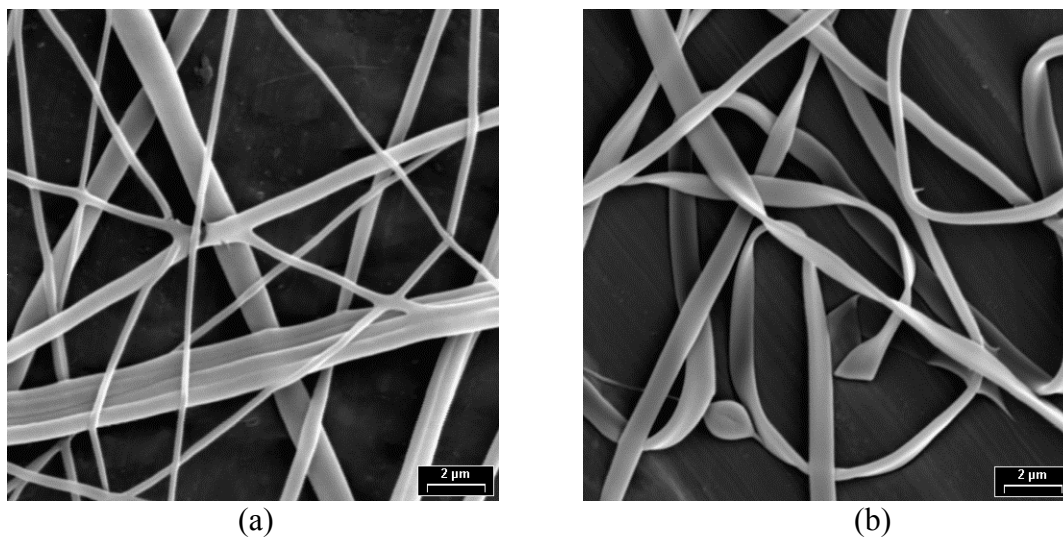
Fig. 34   Examples of fibrous structures with flat fibers.   (a) M_w = 124000-186000 g/mol, C = 8 wt % and (b) M_w =31000-50000 g/mol, C = 22 wt %.

(a)   (b)
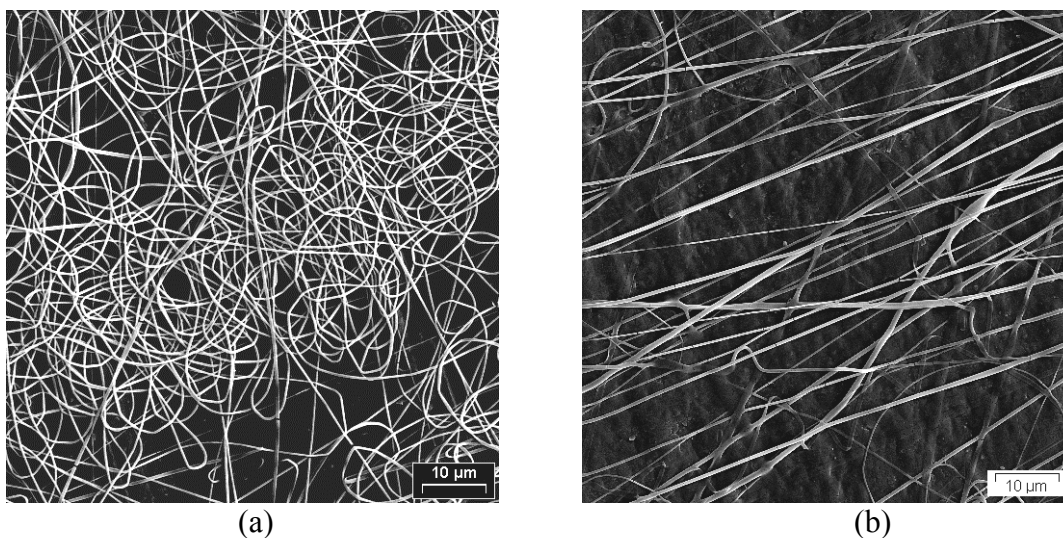
Fig. 35   Examples of coiling and bending (a) and extensive elongational flow (b) in fibers.

(a)   (b)   (c)
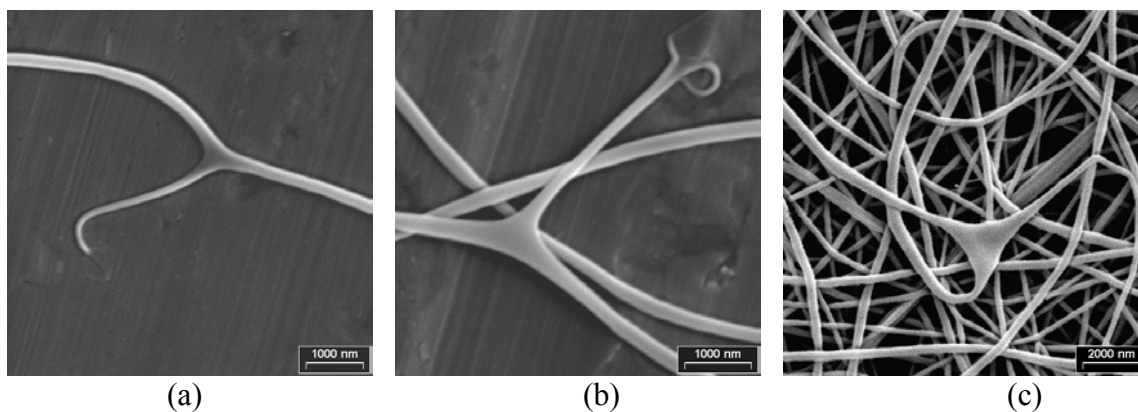
Fig. 36   Examples of branching. Note the secondary branching in (b).

56

| (a) | (b) | (c) |
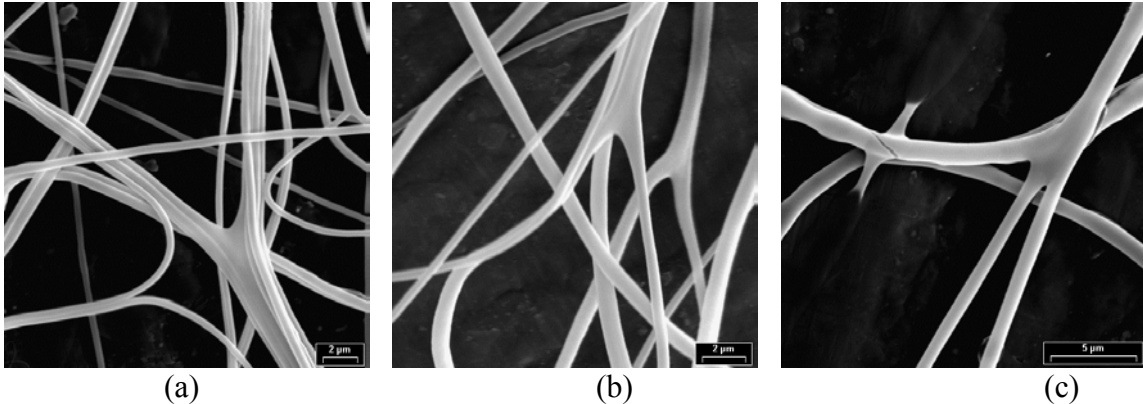
Fig. 37   Examples of fiber splitting. (a) Splitting into two sub-fibers from a bunch of merged fibers; (b) Splitting into two sub-fibers from a single fibers (c) Splitting into three sub-fibers, two of which are thinner and travel in the direction of the primary fiber, and the other one is similar in diameter with the primary fiber but travels at an angle of around 45° with the direction of the primary fiber.

The fibers may exhibit branching as shown in Fig. 36. Branched fibers ejecting almost perpendicular from the surface of the primary fiber were found for both straight and coiled fibers. The branched fibers tend to taper away within a short distance (Fig. 36 (a)) or split additional thinner fibers which taper away quickly (Fig. 36 (b)). Branches may also originate from deformed beads as shown in Fig. 36 (c). Branching is a common phenomenon in electrospinning [47]. At high Mw and/or concentrations, some fibers were found to branch along its path continuously. Splitting of the fibers was observed in many cases (Fig. 37). In contrast to branched fibers, split fibers are generally together with the primary fiber. They often take a shape of 'Y', with two branched fibers of approximately equal diameter emerging from a single fiber. Unlike branched fibers, split fibers do not exhibit a taper in their diameter (Fig. 37).

5.3 Transient Effects during jet breakdown

The physical phenomena occurring during the electrospinning process were observed with a high speed digital camera. Experiments were conducted at several values of M_w and c to highlight the jet breakdown mechanisms. In the absence of any electrical field the solution just flew through the capillary. The rate of drop formation at the tip of the needle and the rate of dripping decrease significantly with increasing M_w and c. The dimensionless concentration $[\eta]c$ will be used to describe combined effects of M_w and c. The rate of drop formation and dripping decrease with increasing $[\eta]c$. When a voltage is applied, the Taylor cone is generated and at a critical voltage a jet is ejected from the tip of the needle. This critical voltage, V_c, can be calculated from the Taylor equation [40]:

$$V_C^2 = 4\frac{H^2}{L^2}\left(\ln\frac{2L}{R} - \frac{3}{2}\right)(0.117\pi\gamma R) \tag{6}$$

The surface tension of PVA solution varies with M_w and c. Using a typical value of 50 mN/m [13], the critical voltage is on the order of 6 kV. Note that in equation (6) $V_c \propto \sqrt{\gamma}$, indicating a stable jet may form at a lower voltage as γ is reduced. Since γ decreases with increasing $[\eta]c$, V_c is inversely proportional to $[\eta]c$. The breakdown of the jet emerging from the capillary for two different values of $[\eta]c$ are shown in Fig. 38.

Sequential photographs illustrating the development of the jet and its breakdown are shown in Figs. 39 and 40. The solution from the capillary forms the Taylor's cone and gradually detaches from the capillary as the jet is formed. At low $[\eta]c$, this detachment

is almost instantaneous, while at high *[η]c*, it may take up to a second for the elongational flow to begin. Note for example, that in Fig. 40, the bead starts to detach from the tip after 0.57 s. Elongational flow is recorded at 0.60 s and at 0.63 s, splaying and splitting can be observed in the jet. After about 0.66 s, the jet undergoes extensive splaying as a result of the viscoelastic properties of the solution and the mushroom-like pattern shown in Fig. 40 (b) are obtained. The jet shows some oscillations in the

(a)   (b)
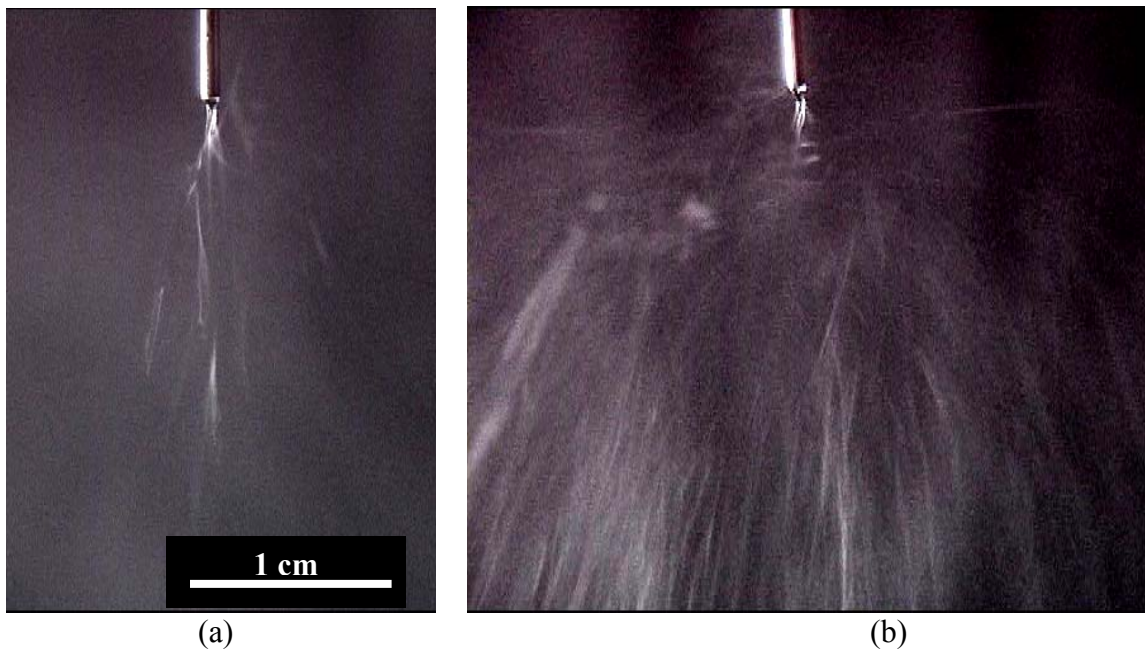
Fig. 38   Photographs showing the breakdown of a fully formed jet for two different values of [η]c. (a) 6.5 (b) 10.

breakdown pattern perhaps due to the lack of adequate solution flow rate. It should be noted that at high values of *[η]c*, the solution flow rate is small, so some of the solvent may evaporate from the tip of the needle and further reduce the flow rate. By comparison, at low *[η]c*, the jet forms almost immediately and splaying and splitting can be observed even after 0.03 s. The electrospinning continues without many changes in the jet patterns.

The position of a single mini-jet can be monitored as a function of time as shown in Fig. 41. This data can then be used to calculate the local jet velocity. The local jet velocity calculated for various mini-jets was averaged to obtain an overall value of jet velocity for a specific value of $[\eta]c$. This average velocity is plotted as a function of $[\eta]c$ in Fig. 42. The average velocity generally decreases with increasing values of $[\eta]c$. Hence, as $[\eta]c$ increases, there is a greater level of splaying and the jet breaks down into many small mini-jets because of the increased viscoelastic effect (Fig. 40). However, each of these mini-jets takes a longer time to reach the collector.
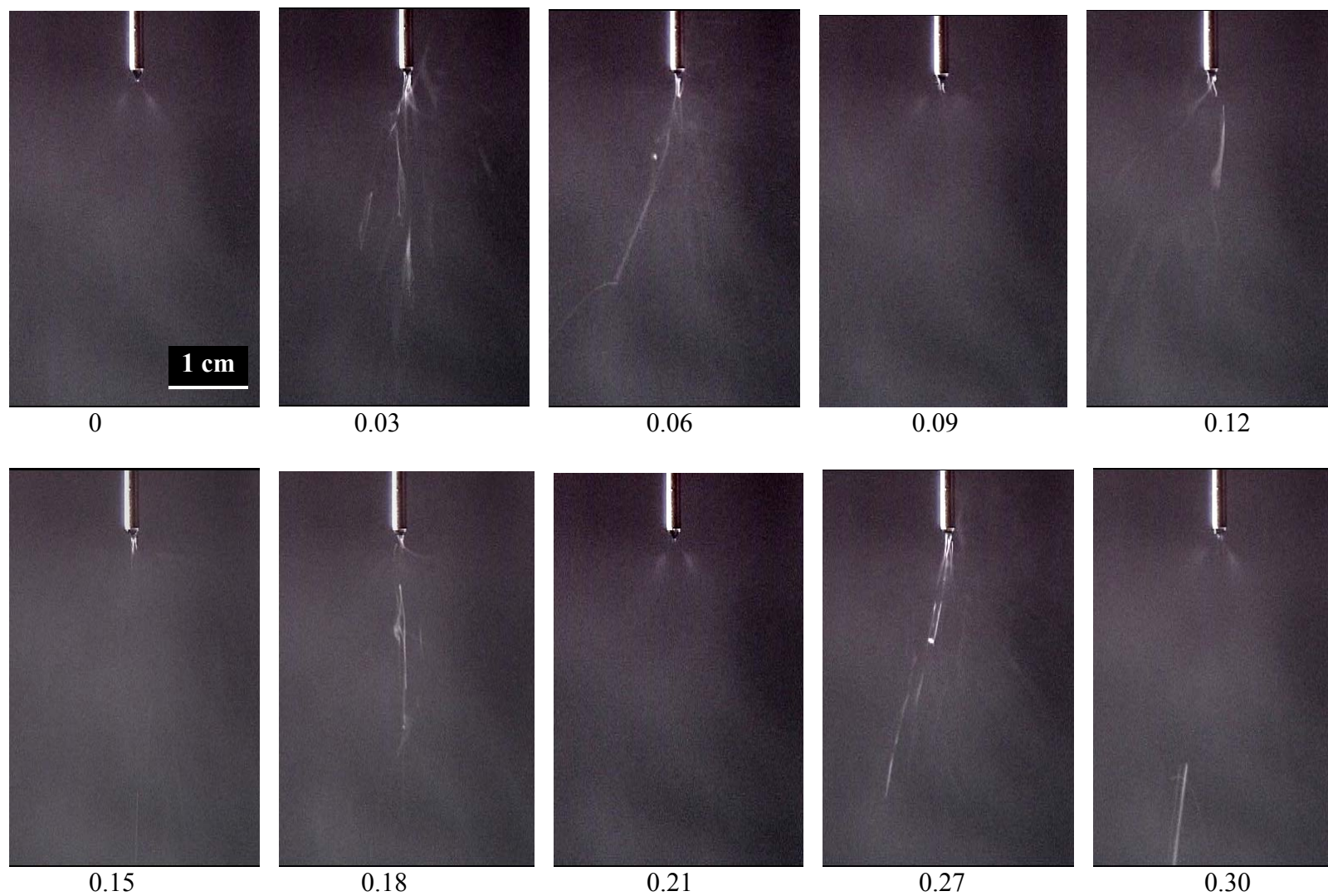
Fig. 39   Sequential photographs showing the nature of the solution jet for various times (s) after the application of the voltage. The voltage was applied at t = 0 s. ([η]c = 6.5)

61
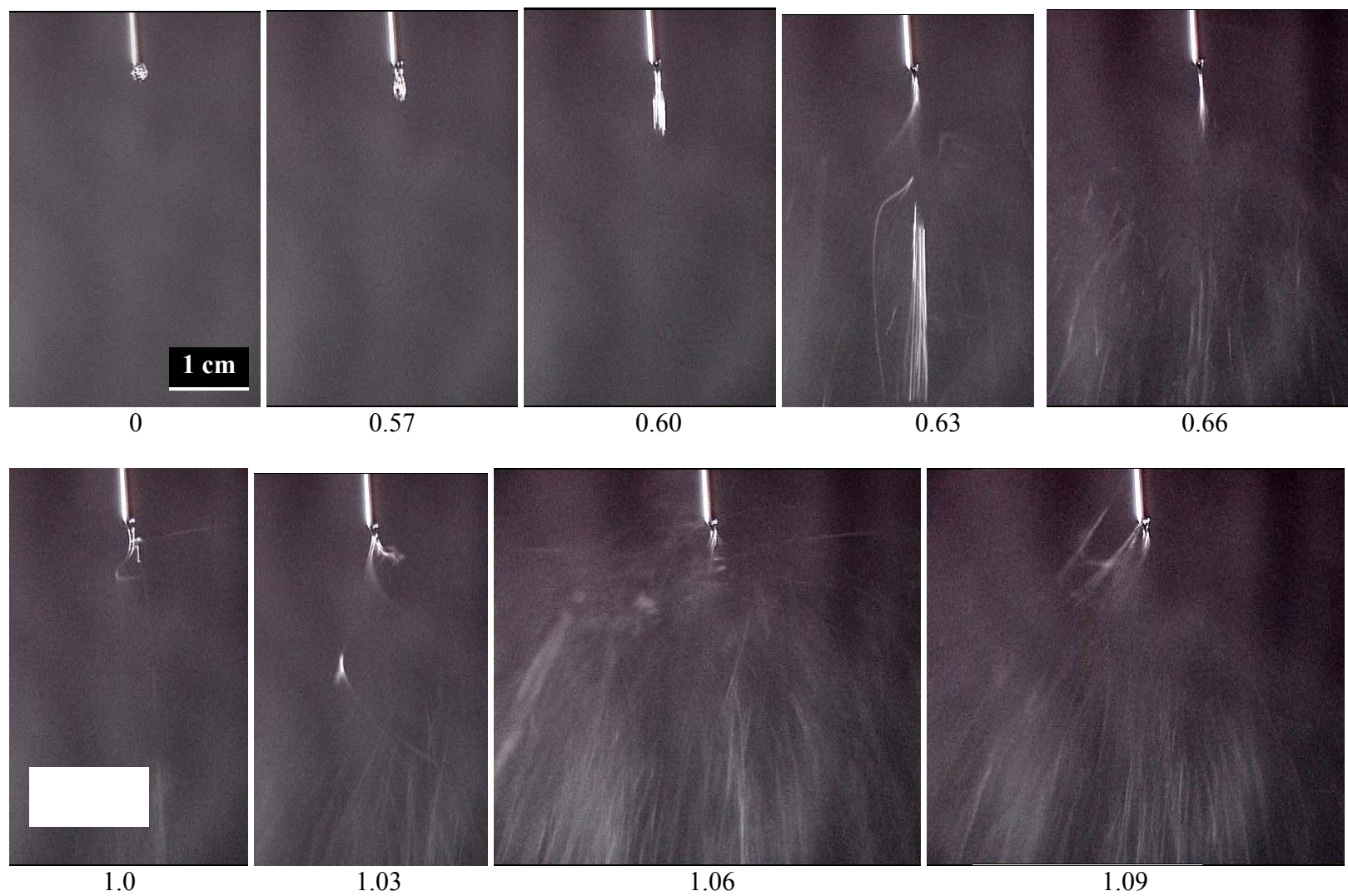
Fig. 40   *Sequential photographs showing the nature of the solution jet for various times (s) after the application of the voltage. The voltage was applied at t = 0 s. ([η]c = 10)*
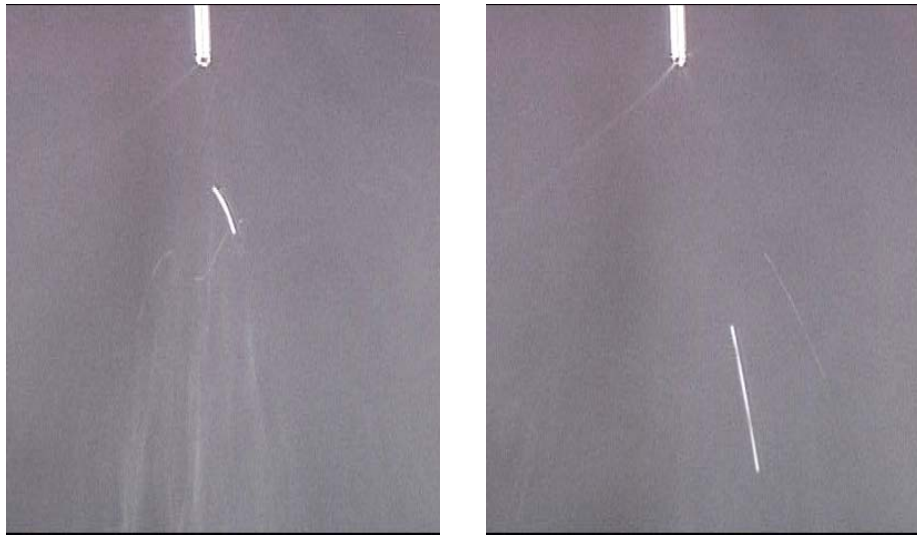
Fig. 41   Photographs illustrating the position of a minijet in successive frames.   By monitoring the position of a minijet in successive frames, the local jet velocity was calculated.
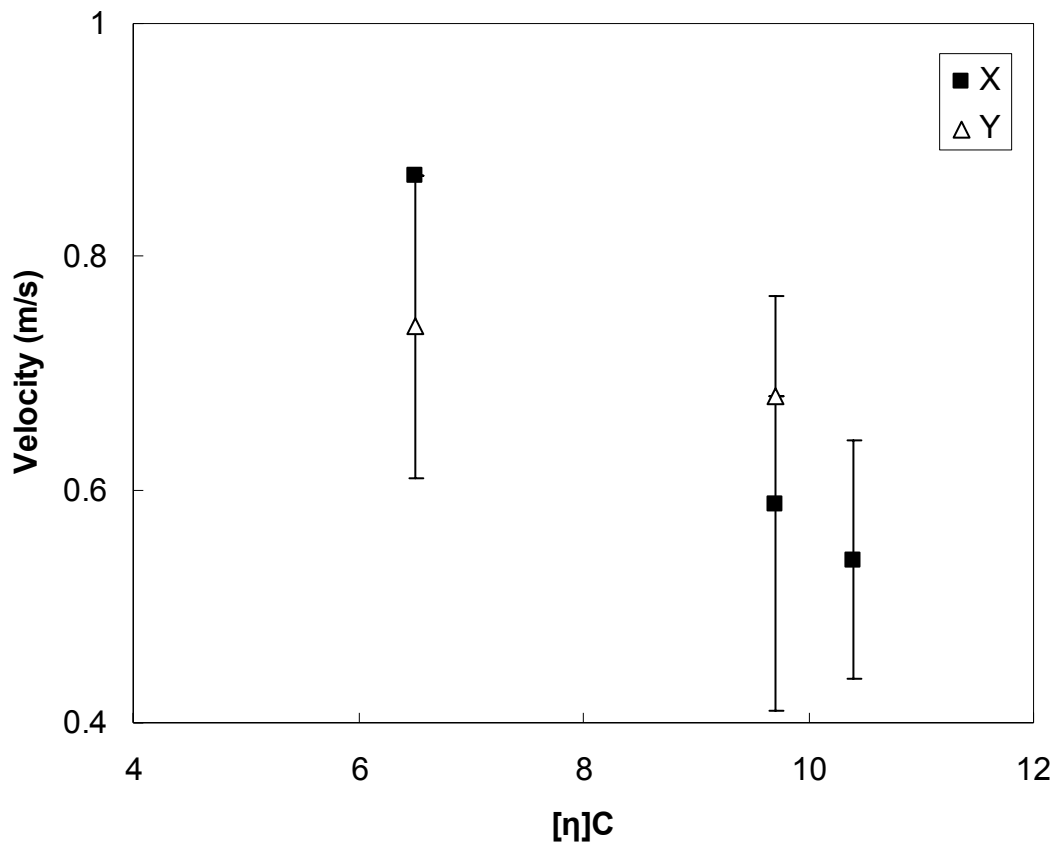
Fig. 42   Average jet velocity as a function of [η]c.   The velocity values for before (Y) and after (X) the application of the voltage are shown.

5.4 Effects of Molecular Weight and Concentration

The effect of varying concentration at a constant molecular weight is shown in Fig. 43. At low molecular weights, the fiber diameter increases slightly as the concentration is increased. However, at high M_w, the diameter increases significantly with concentration and also flat fibers are observed even at low concentrations.

The distribution of fibers also changes as the molecular weight increases as shown in Fig. 44. As M_w increases, a broader distribution of fibers may be obtained (Fig. 45).

(a) M_w = 9000 – 10,000 g/mol

| 22 | 25 | 30 | 35 |

(b) M_w = 31000 – 50,000 g/mol

| 18 | 22 | 24 | 26 |
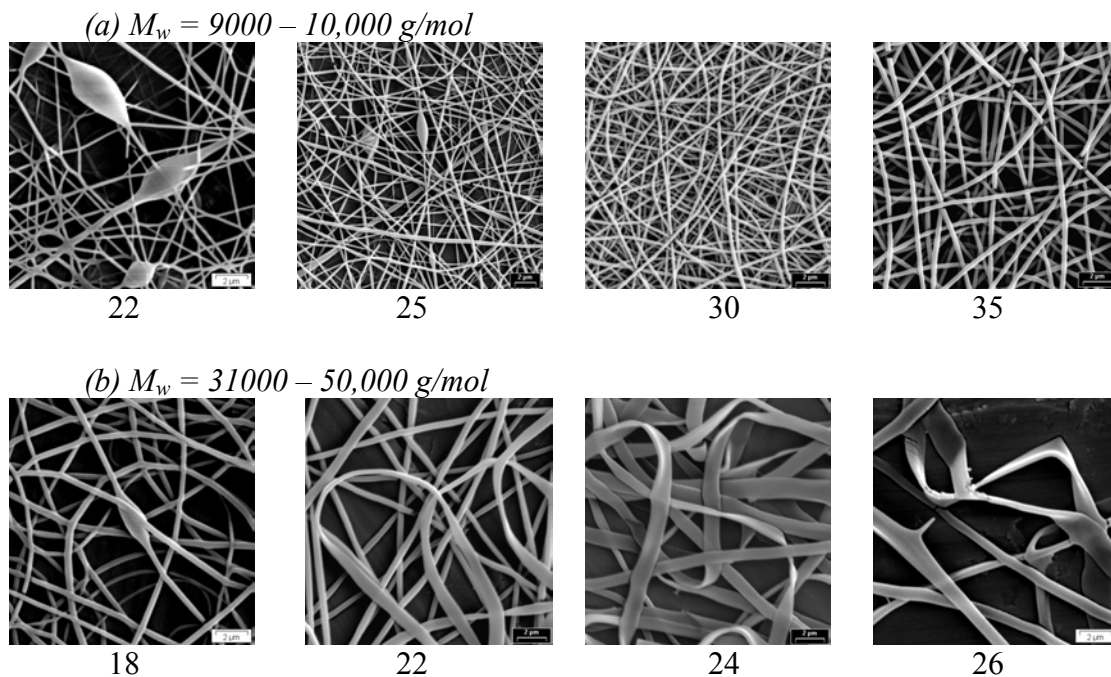
Fig. 43   Photographs showing the effect of concentration (wt %) for two different values of M_w.

The average diameters measured for various conditions used in this study are shown in Fig. 46. As indicated above, the diameter increases with increasing M_w and concentration. The data indicate that the effect of concentration is more pronounced in

samples with higher molecular weight. The dimensionless concentration will be used to analyze the effects of molecular weight and concentration on the structure. At $5 < [\eta]c < 6$, the fibrous structure is not completely stable and a bead on string structure is obtained

(a)   (b)
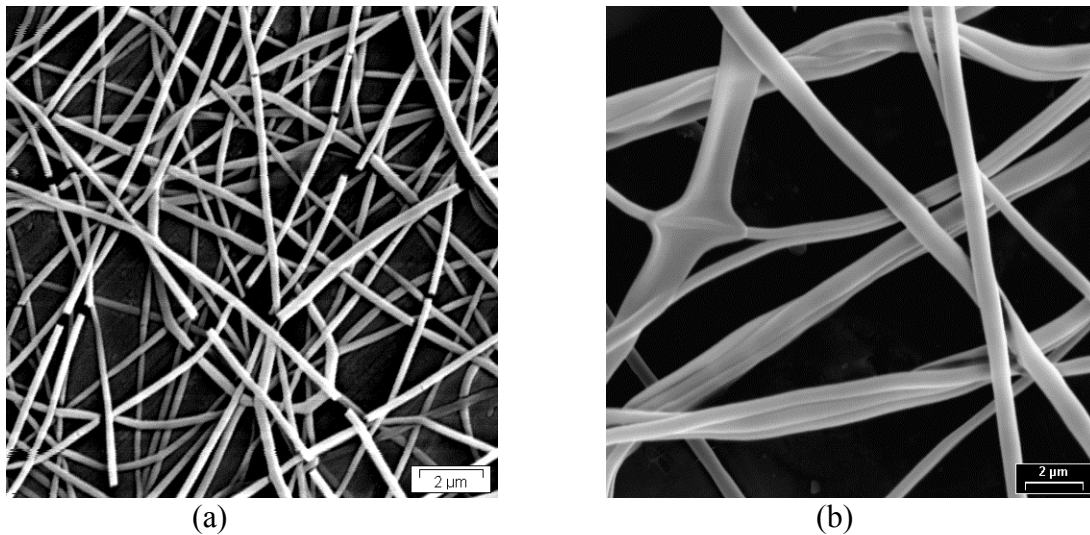
Fig. 44   Photographs showing the effect of concentration at a constant concentration (9 wt %) (a) M_w = 50000-85000 g/mol; (b) M_w = 124000-1860000 g/mol

(a)   Diameter (µm)   (b)
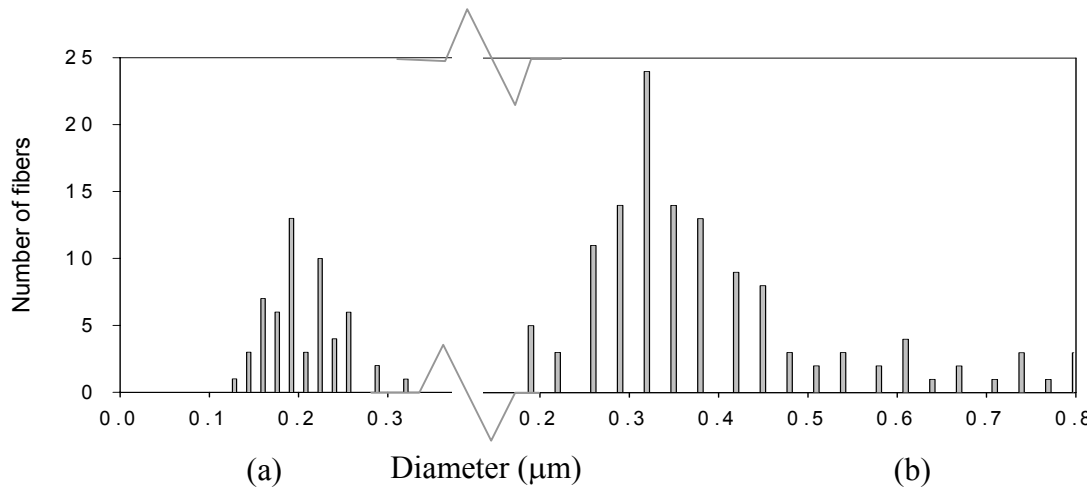
Fig. 45   Distribution of fibers at a constant concentration (9 wt %) (a) M_w = 50000-85000 g/mol (b) M_w = 124000-1860000 g/mol
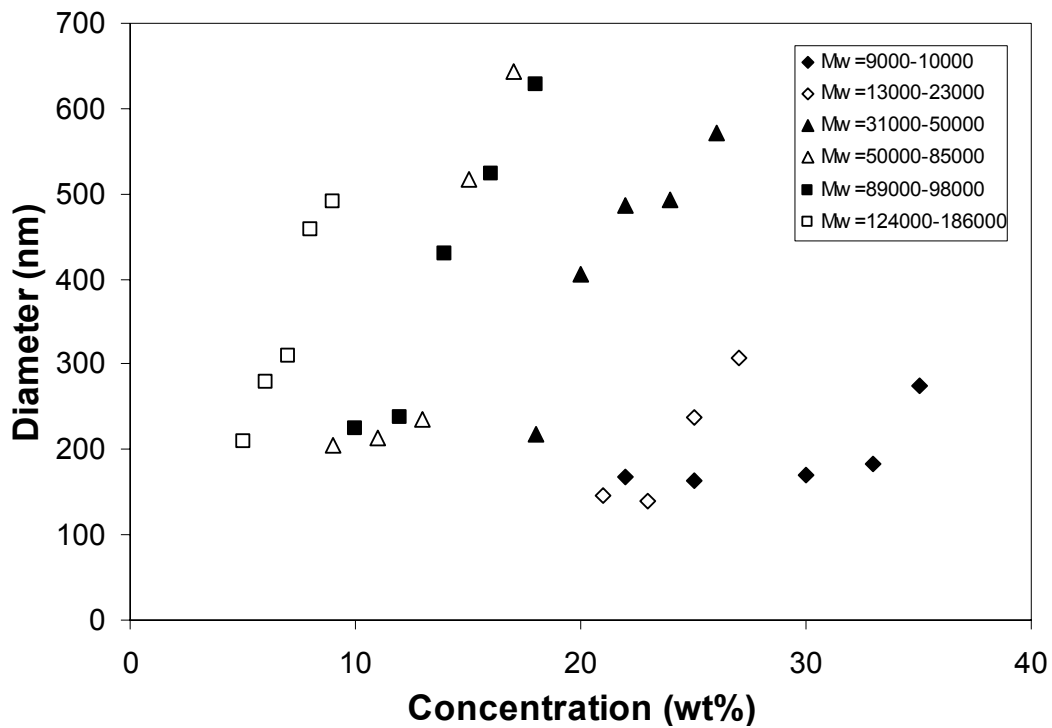
Fig. 46   Variation of average diameter with molecular weight and concentration.

6.4

12.6

16.9

21.8
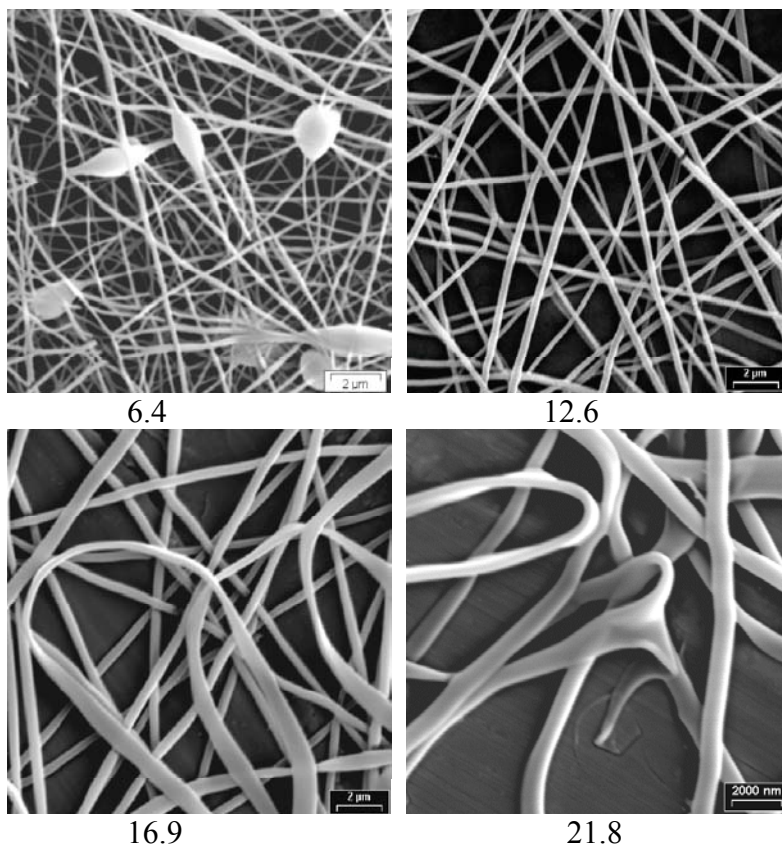
Fig. 47 Photographs showing the changes in the structure with increasing values of [η]c.

(Fig. 47). The fibrous structure becomes stable at *[η]c* > 6. As *[η]c* increases further, the fibers become thicker and start to flatten. The measured diameters of the fibers are plotted in Fig. 49 for various values of *[η]c*. It can be seen that as *[η]c* increases, the diameter increases. A power-law relationship between *D*, the average diameter of the fiber, and *[η]c* can be obtained from the data shown in Fig. 48:

$$D = 18.6 \left[[\eta]c \right]^{1.11} \tag{10}$$

The low exponent in equation (12) indicates that the average diameter increases almost linearly with *[η]c*. Further, the effect of molecular weight seems to be greater than the effect of concentration. The transition from extremely dilute to dilute regions in PVA aqueous solutions may occur at *[η]c* ≈ 4. At this point, although there may be some overlap of the hydrodynamic radius, the effects of entanglements are negligible (dilute region) [62]. Entanglements start to form between 4 < *[η]c* < 9 and begin to play an important role at *[η]c* > 9. At this point, the solution viscosity begins to increase and the viscous forces increase appreciably. Hence, the fiber diameter increases significantly at *[η]c* > 9.
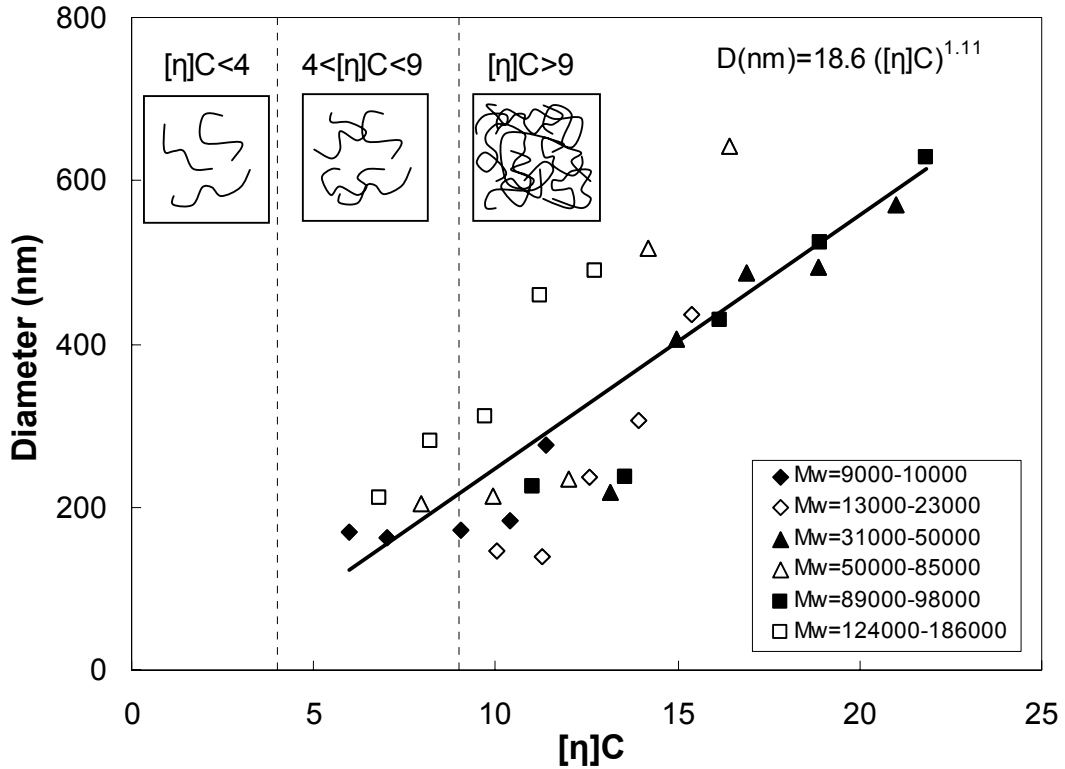
*Fig. 48   Variation of average fiber diameter with dimensionless concentration [η]c.
The critical [η]c values for transition from extremely dilute to dilute to highly
entangled regions are also indicated [62].*

5.5 Fiber distribution and morphology

A variety of distributions were observed in the fiber diameters as shown in Fig. 49 and

51. At low concentration and M_w, a normal distribution was obtained with relatively

narrow distribution. However as the molecular weight and concentration increased,

bimodal or multimodal distributions were observed. Bimodal and multimodal

distributions were observed in electrospinning because of the splitting and splaying of the

fibers that occurs during the transit of the polymer to the collector [63]. The fiber

distribution becomes broader with increasing values of *[η]c* as shown in Fig. 52. This

behavior can be attributed to increased viscoelasticity in the solution at high values of $[\eta]c$.

(a)   (b)
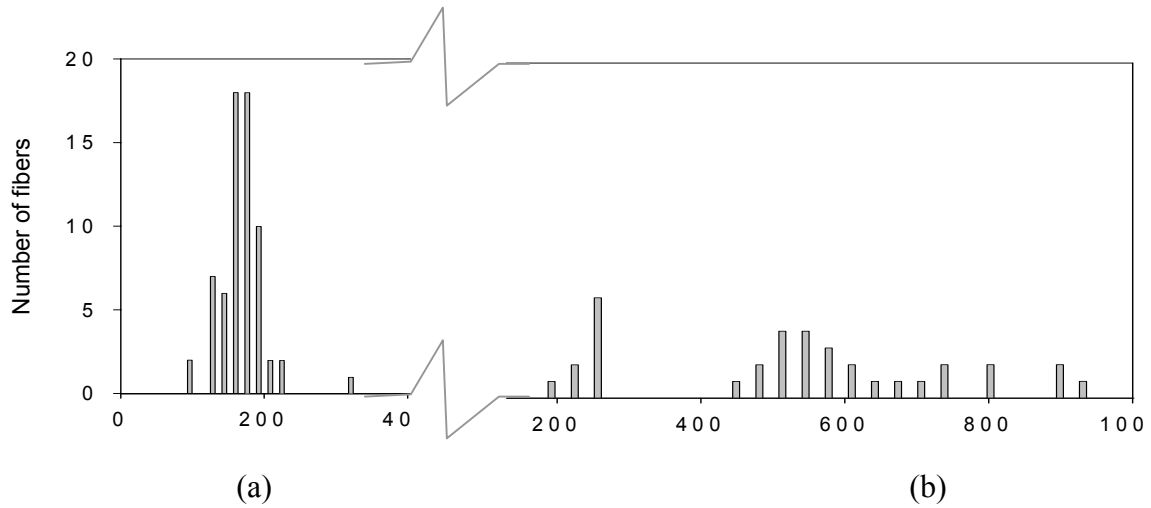
Fig. 49   Fiber distribution of (a) [η]c=4.6 (M$_w$=9000-10000 g/mol, C=22 wt %); (b) [η]c=21.8 (M$_w$=89000-980000 g/mol, c=16 wt%).
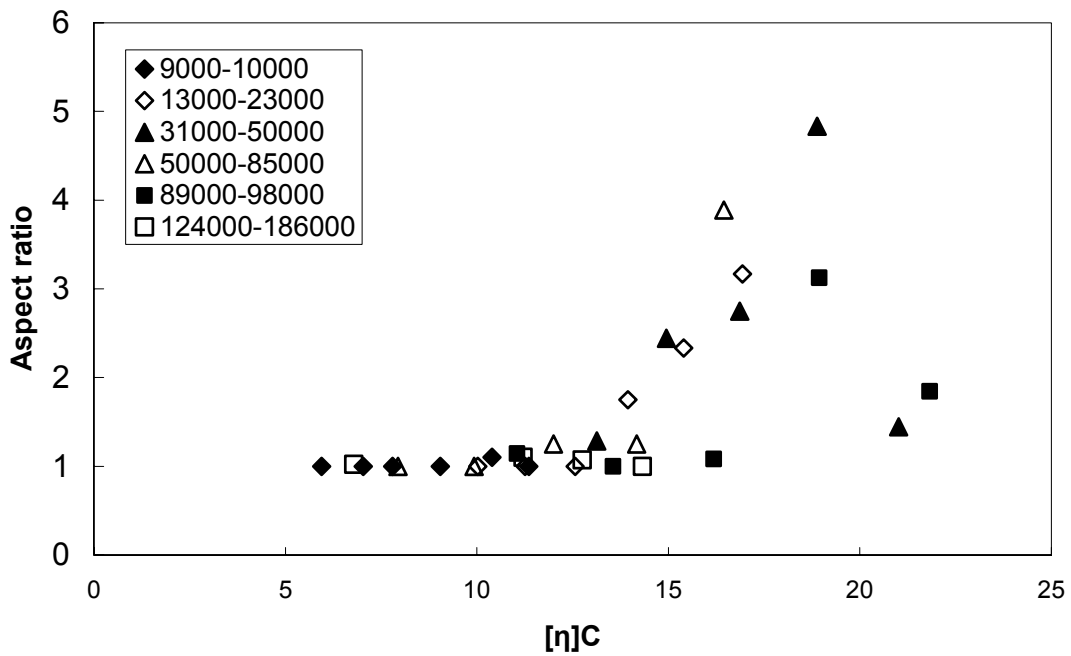
Fig. 50   Variation of the aspect ratio with [η]c for various molecular weights.

It has been shown that at low values of M_w and c, the fibers are generally round while at high concentrations and molecular weights, flat fibers are observed. In order to analyze this transition, the aspect ratio of the fibers was measured. The measured aspect ratios are plotted as a function of $[\eta]c$ in Fig. 50. The transition from round to flat fibers appears to begin at $[\eta]c \sim 12$. At high $[\eta]c$, the extensive entanglements may lead to gelling and trapping of the water. As a result, the rate of water evaporation decreases. The wet fibers can then flatten upon impact at the collector.

5.6 Jet Break up in Polymer Solutions

The dynamics of the breakup of viscous liquids emerging from a capillary have been studied extensively [64]. The volume of a drop emerging from a capillary increases continuously by the addition of liquid. At a critical volume, the drop necks and breaks off from the capillary. In Newtonian fluids, the Weber number, We, is important at low Reynolds number:

$$We = \frac{InertialStress}{InterfacialStress} = \frac{\rho v^2 d}{\gamma} \qquad (11)$$

where ρ is the density, v is the velocity, γ is the surface tension and d is the diameter of the jet. The drop can deform and disintegrate above a critical Weber number, We_{crit}, as shown in Fig. 52.
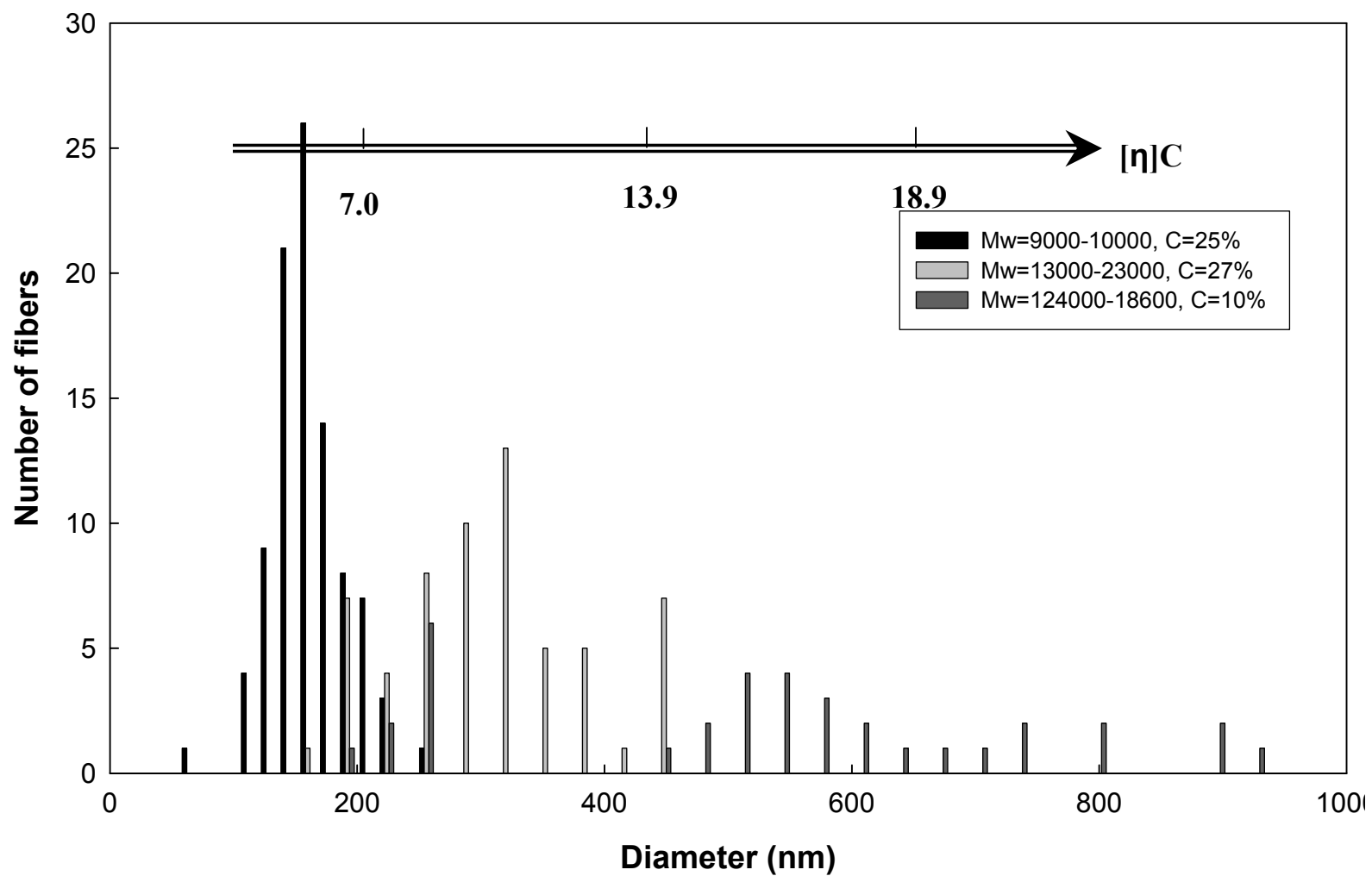
Fig. 51   Types of distributions in the fibers for various molecular weights and concentrations.   The [η]c values are also indicated.

Satellite Drops

Drops

Jet   Rayleigh instability
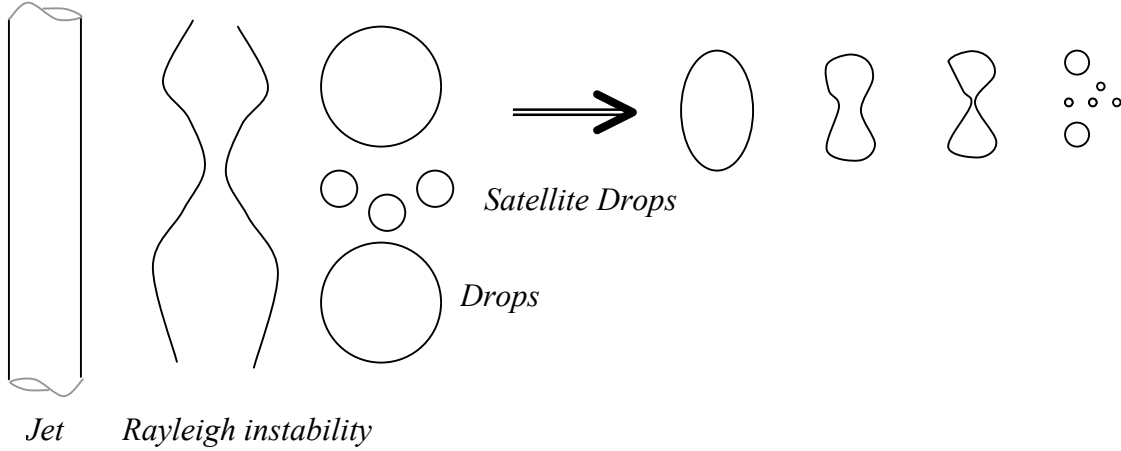
Fig. 52   *Jet breakdown of a Newtonian fluid at low Reynolds number (or low η). Note the formation of drops and satellite drops. Each drop can break down further into smaller drops and satellite drops.*

The breakup of viscous fluid jets occur by the deformation, breakup and coalescence under the action of a stress [64]. In Newtonian fluids, Rayleigh instability plays a major role in the break up of the jet. In this case, inertial forces are important and hence the Weber number is critical.   Two competitive processes determine the breakup of the drops: a) Overall retraction towards a sphere driven the pressure difference b) Growth of capillary waves. At higher Reynolds number, viscous effects become significant. In this case, the Capillary number, *Ca,* becomes important:

$$Ca = \frac{Viscous\ stress}{Interfacial\ stress} = \frac{\tau R}{\gamma} = \frac{\eta v}{\gamma} \tag{12}$$

where τ is the shear stress and R is the radius of the jet. At $Ca > Ca_{crit}$, Rayleigh instability leads to the formation of a long thread that connects drops as shown in Fig. 53.

Ca_{crit}, for many Newtonian fluids has been reported to be around 0.2 [59]. The deformation and breakup of the jet is further illustrated in Fig. 54 [59].

In Non-Newtonian viscoelastic fluids (such as polymer melts and solutions), the Reynolds number is generally large and hence the inertial effects can be neglected. Further, the Bond number is small and so buoyancy forces can also be neglected. In this
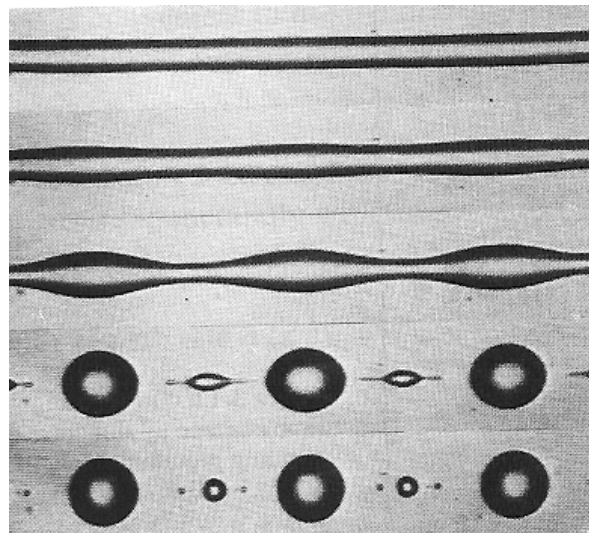
Fig. 53   Jet break-up in a Newtonian fluid at low Reynolds number (or high η) [60].
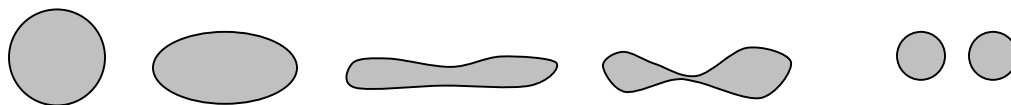
Fig. 54   Deformation, necking and breakup of a highly viscous Newtonian drop of fluid.

case, the Capillary number, Ca, becomes a vital parameter that can be used describe the breakup of the jet. When Ca < Ca_{crit}, the surface tension forces are large and the shape of the jet is preserved. When Ca ~ 1, interfacial disturbances begin to grow, leading to the

breakup of the jet into a series of drops (Fig. 55). Depending on their size, the drops may

be stretched and broken again. When Ca>>Ca$_{critical}$, the effects of viscous shear stresses

become dominant. In this case, the jet may be stretched viscoelastically into long threads

(Fig. 56). Any drops that may form may also be stretched viscoelastically. Viscoelastic

effects important when De > 1 and total strain is large:

$$De = \overset{*}{\varepsilon}\, t = \frac{ElasticStress}{ViscousStress} \qquad (13)$$

The break up of the jet is influenced by the buildup of orientational stress.   Strain

thickening occurs because of the high tensile viscosity then lowers elongational flow.

The effects of strain thickening are especially important in Non-Troutonian fluids.

Another important dimensionless number that describes the breakup of viscoelastic jets is

the Ohnesorge number:

(a)   (b)
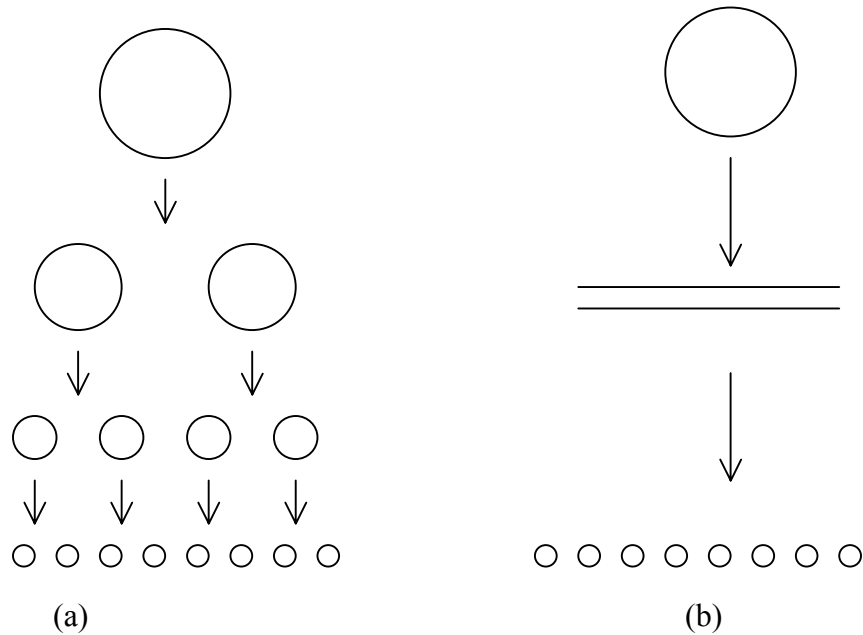
Fig. 55   Schematic illustration of the breakdown of viscoelastic systems. (a) Stepwise repeated breakup at Ca$_{crit.}$ (b) Affine stretching of drop into a thin liquid thread at Ca >> Ca$_{crit}$ and eventual disintegration into droplets.

$$Oh = \frac{\sqrt{We}}{Re} = \frac{\eta}{\sqrt{\rho\gamma D}} \qquad\qquad (14)$$

At constant Oh, axisymmetric waves can develop on the surface depending on Re. A combination of Oh and Re can be used to break up polymer solutions into droplets by the classic Rayleigh breakup.
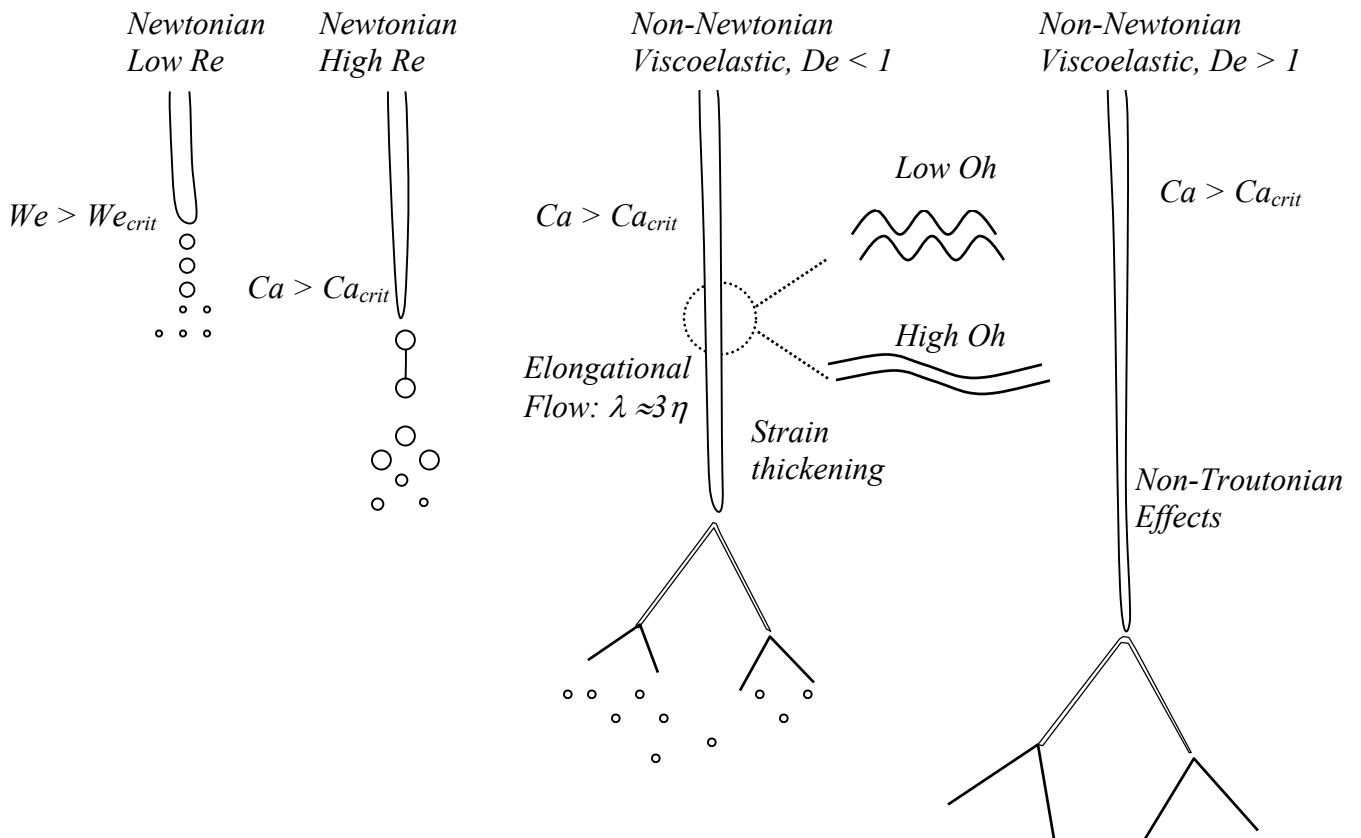
Fig. 56   Schematic illustration of the jet breakup for various types of fluids.   The important dimensionless numbers are also indicated.

The dimensionless numbers described above were used to analyze the data on PVA. The measured Capillary, Reynolds and Ohnesorge numbers are shown in Table XII. The initial Capillary numbers for various conditions ranged from 0.4 to 45.4, while Oh was

between 0.1 and 38.5. It was observed in general that bead on string structures were

observed for Ca about 0.8. This value is close to the Ca_{crit} described previously. The

variation of the average diameter with Oh is plotted in Fig. 57. Clearly, the diameter

*Table XII   Variation of Ca, Re and Oh numbers for various conditions.   The
corresponding distribution of the fiber diameters is also shown.*

Mw	c (wt%)	D (*nm*)	[η]C	Ca	Re	Oh	*Distribution*
A	22	169	6.0	0.4	23.2	0.1	*Unimodal*
	25	163	7.0	0.6	12.4	0.2	*Unimodal*
	27	151	7.8	0.8	8.5	0.3	*Unimodal*
	30	171	9.0	1.2	5.1	0.5	*Unimodal*
	33	183	10.4	1.7	3.2	0.7	*Unimodal*
	35	275	11.4	2.1	2.4	0.9	*Unimodal*
B	21	146	10.0	1.5	3.2	0.7	*Unimodal*
	23	140	11.3	2.0	2.0	1.0	*Unimodal*
	25	237	12.6	2.7	1.3	1.4	*Unimodal*
	27	307	13.9	3.6	0.9	2.0	*Multimodal*
	29	436	15.4	4.6	0.6	2.7	*Bimodal*
	31	373	16.9	5.8	0.5	3.5	*Multimodal*
C	18	219	13.1	6.2	0.5	3.6	*Unimodal*
	20	406	15.0	9.1	0.3	5.7	*Unimodal*
	22	486	16.9	12.8	0.2	8.5	*Bimodal*
	24	493	18.9	17.5	0.1	12.3	*Bimodal*
	26	571	21.0	23.3	0.1	17.3	*Multimodal*
D	9	205	7.9	1.7	2.8	0.8	*Unimodal*
	11	213	9.9	3.5	1.0	1.8	*Unimodal*
	13	235	12.0	6.5	0.5	3.8	*Bimodal*
	15	516	14.2	11.0	0.2	7.0	*Unimodal*
	17	643	16.4	17.4	0.1	12.0	*Multimodal*
E	10	224	11.0	5.3	0.6	3.0	*Unimodal*
	12	237	13.6	10.3	0.2	6.7	*Unimodal*
	16	523	18.9	29.6	0.1	23.2	*Unimodal*
	18	628	21.8	45.4	0.0	38.5	*Multimodal*
	14	429	16.2	18.2	0.1	13.1	*Unimodal*
F	5	210	6.8	1.3	3.6	0.6	*Unimodal*
	6	280	8.2	2.6	1.4	1.4	*Bimodal*
	7	310	9.7	4.6	0.7	2.6	*Multimodal*
	8	458	11.2	7.6	0.3	4.7	*Multimodal*
	9	490	12.7	11.7	0.2	7.9	*Multimodal*
	10	430	14.3	17.2	0.1	12.5	*Multimodal*

increases as Oh increases because of the dominance of viscous effects. There appears to be a Power-law relationship between D and Oh:

$$D(nm) = 224[Oh]^{0.29} \qquad\qquad (15)$$

A similar behavior was observed with Ca, but a better fit was obtained with Oh for the present data. It has been reported that at low Oh numbers, the growth rate of waves in the fibers is large [61]. Therefore, the fibers can neck and undergo splitting, splaying or disintegration dependingon the local conditions. At high Oh, the wavelength of the perturbation increases significantly and the growth rate of the perturbation decreases [61]. Under these conditions, the fibers can undergo viscoelastic stretching and fracture at extreme stresses. The fibers were examined at high magnifications and the photographs of the fiber at high magnification are superimposed on the data in Fig. 57. Wavy fibers can indeed be observed at low Oh, while at high Oh, the fibers appear to be straight. The Oh number changes during the electrospinning process as the diameter of the fiber decreases. The variation of the initial Oh with $[\eta]c$ is plotted in Fig.58 for the conditions under which the fibers were produced in this study. The results show that for each molecular weight, there appears to be a region (or a combination of Oh and $[\eta]c$) below which the jet starts to breakdown. At each $[\eta]c$ there is a critical Oh above which the jet is stable and cannot breakdown easily. In addition, the Oh number changes significantly during the electrospinning process as the diameter of the jet decreases (Fig. 59). As the jet starts to decrease in diameter the surface stresses σ/R become large and the splaying becomes difficult.
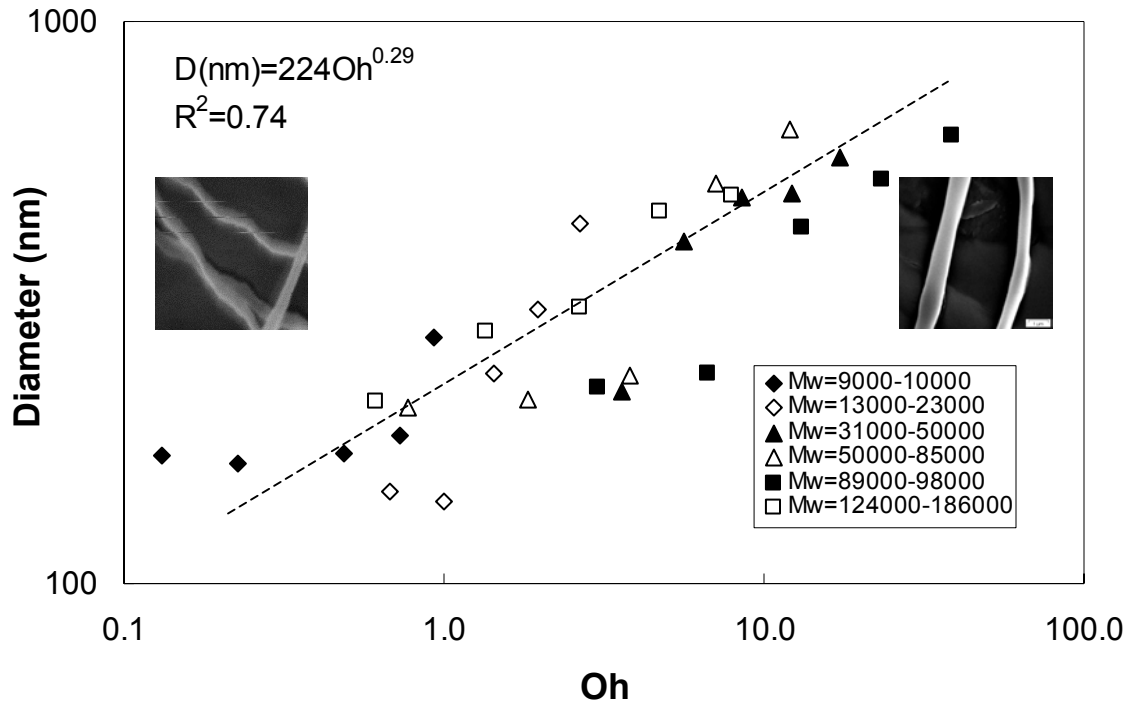
Fig. 57   Variation of average fiber diameter with the Ohnesorge number. The inserts show the wavy fibers at low Oh and straight fibers at high Oh.
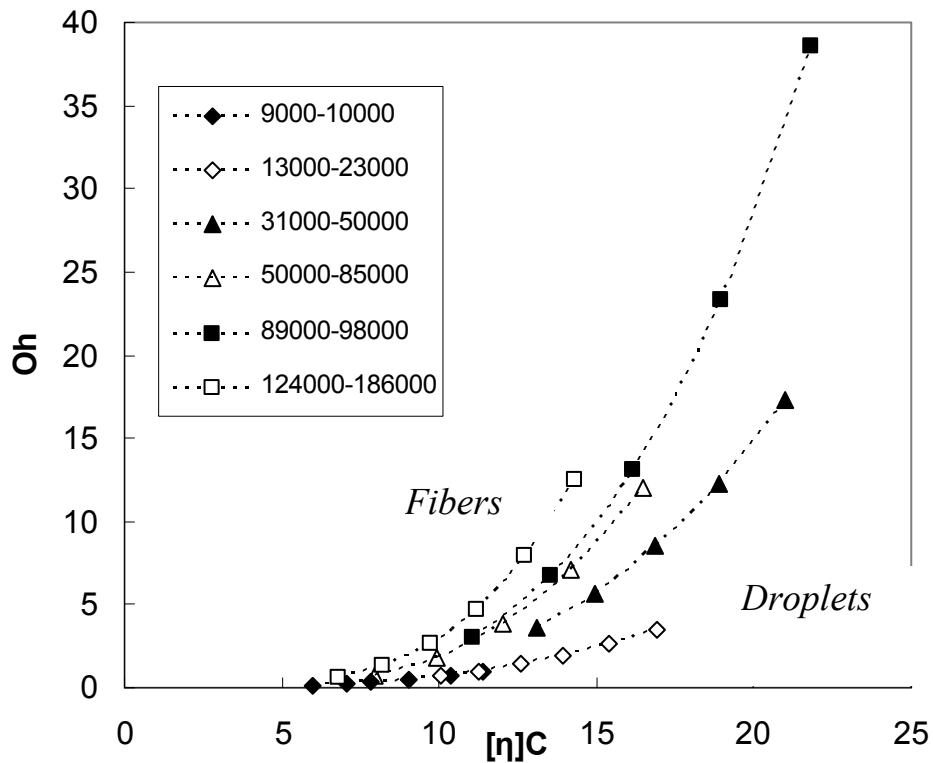
Fig. 58   Variation of initial Oh with [η]c for various molecular weights.
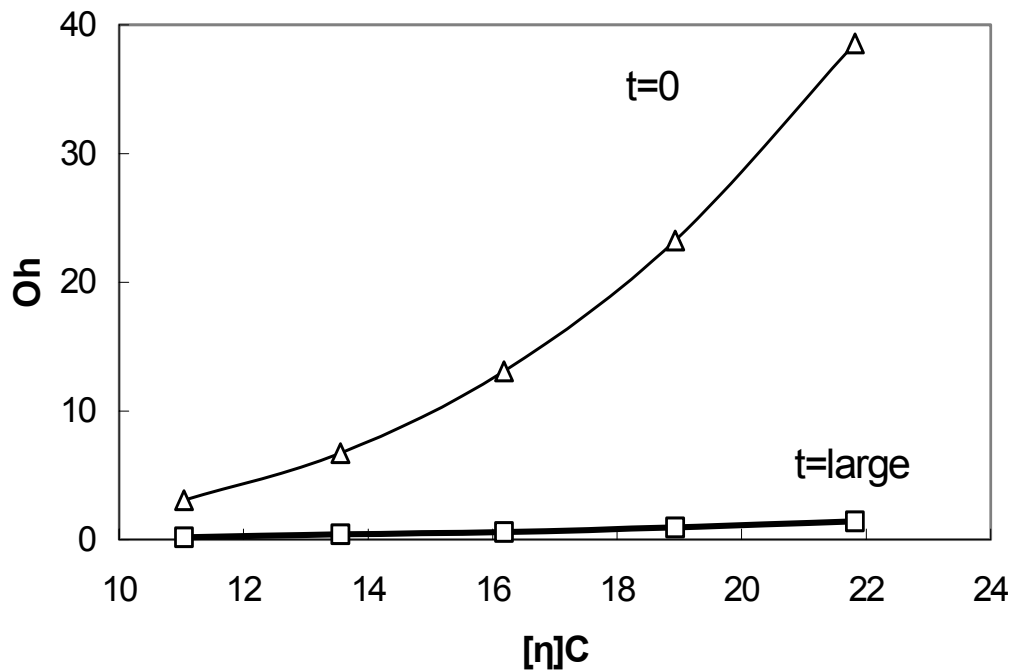
*Fig. 59   Variation of initial (t = 0) and final (t = large) Oh with [η]c. The Oh varies
during the process as the jet diameter decreases.*
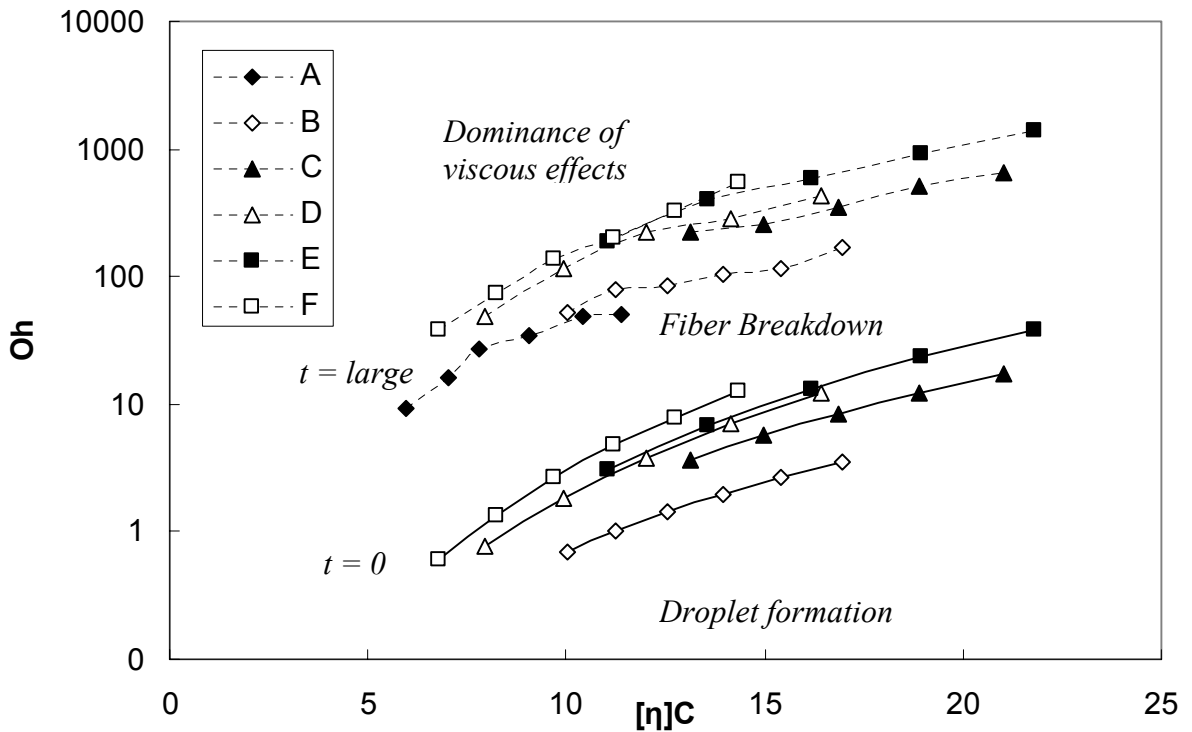
*Fig. 60   Variation of initial (t = 0) and final (t = large) Oh with [η]c for various
molecular weights. The Oh varies during the process as the jet diameter
decreases. The letters in the legend correspond to the data shown in Table IX.*

The large surface stress stabilizes thin filaments and resists further fiber breakdown. The data shown in Fig. 60 indicate that for different values of *[η]c*, at a limiting *Oh* number the surface stresses become so large that splaying essentially stops as the fiber is stabilized.

5.7 Effects of Solvents

A variety of solvents can be used for producing PVA solutions. These include water, DMSO, NMP and ethylene Glycol [20]. Although water has been used extensively as a solvent, it is only a moderately good solvent for PVA [20]. Because of aggregation and micro-gelling, it is difficult to obtain uniformly dispersed molecular solutions. As a result, dissolution of the PVA is rather difficult. The temperature has to be increased to 80°C to achieve dissolution. The solution viscosity and [η] can also change with the type of solvent. In addition, the rate of evaporation can be different for various solvents. All these factors can influence the electrospinning process.

Attempts to produce fibers with other solvents were not very successful. Although a visible jet was detected with all the solvents, the polymer on the collector tended to agglomerate when DMSO, EG or NMP was used as a solvent. This agglomeration was primarily due to the lack of adequate solvent evaporation as shown in Fig. 61. The boiling points and the heats of vaporization of DMSO and EG are much higher than water. EG absorbs twice its weight of water at 100% relative humidity [11]. DMSO is
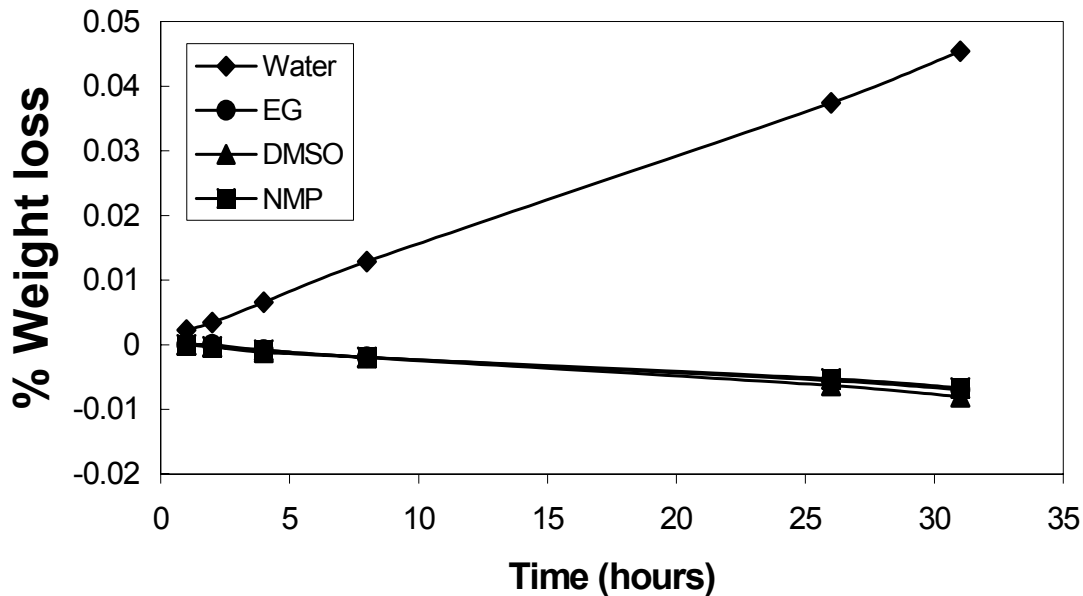
Fig. 61 Weight loss as a function of time under ambient conditions.

also very hygroscopic, readily taking up and retaining moisture. Consequently, additional means of improving the evaporation rate must be incorporated in the set-up in order to use these solvents.

5.8 Effects of Additives

Additives can be used to change the viscosity, surface tension, electrical conductivity, dielectric strength, and viscoelastic properties of the solution. The rheological properties of PVA can be affected significantly by the addition of electrolytes by reducing the intra-molecular hydrogen bonding [12]. NaCl is a common additive to aqueous solutions that may be used to disrupt hydrogen bonding and enhance dissolution. The addition of NaCl increases the solution viscosity and lowers the surface tension [25,12]. There appears to be a maximum concentration of NaCl that can be added before a *salting out* phenomenon is observed. The salting out phenomenon may be a result of the disruption of the solute

and solvent bonding at high NaCl concentrations. The effect of NaCl additions to PVA solutions is shown in Fig. 62. At a low M_w, the addition of NaCl disrupts the fibrous structure. The fibers can start splaying, but break apart after the initial splaying as shown in Fig. 62 (d). This disintegration may be a result of the reduced viscoelastic behavior in the solution. At NaCl concentrations of about 3 wt%, the salting out effect described earlier was also observed as shown in Fig. 63. At a high M_w however, the addition of
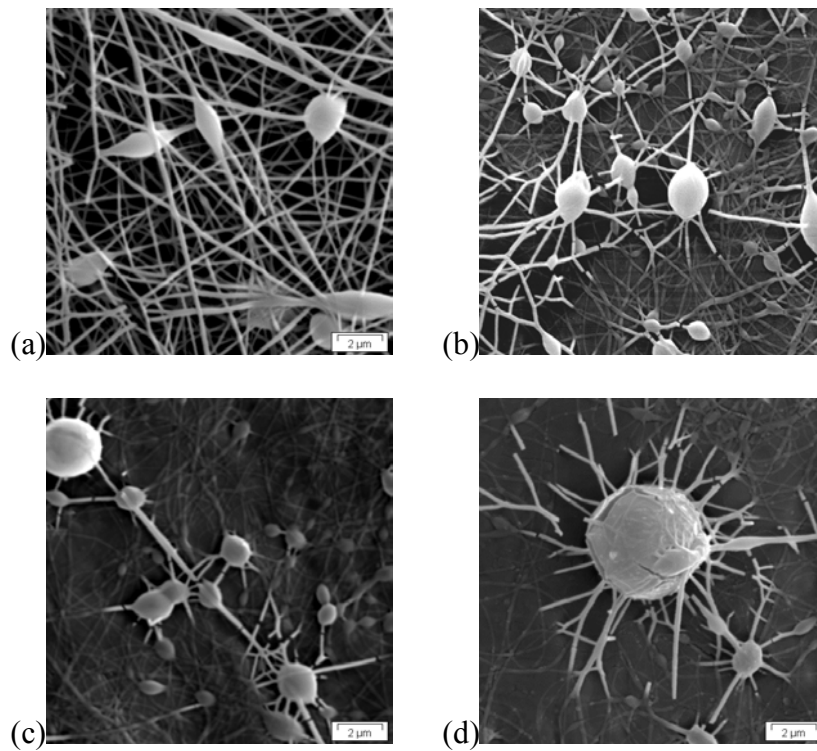
Fig. 62   Photographs showing the effect of NaCl on electrospun PVA (a) 0% (b) 0.5% (c) 1% and (d) 3%. (M_w = 9000-10000 g/mol, c=23 wt %).

NaCl has a beneficial effect on the fibrous structure as shown in Fig. 61. In this case, the fiber diameter decreases upon the addition of NaCl.

The effects of Polyethylene glycol (PEG) additions to PVA are shown in Fig. 65. PEG is

a water soluble polymer that is structurally similar to PVA. PEG additions generally

increase the average fiber diameter. Further, a broader distribution of fibers is observed

as the amount of PEG is increased (Fig. 66). PEG increases the solution viscosity and is

added in many solutions to restrict spraying and droplet formation [64].
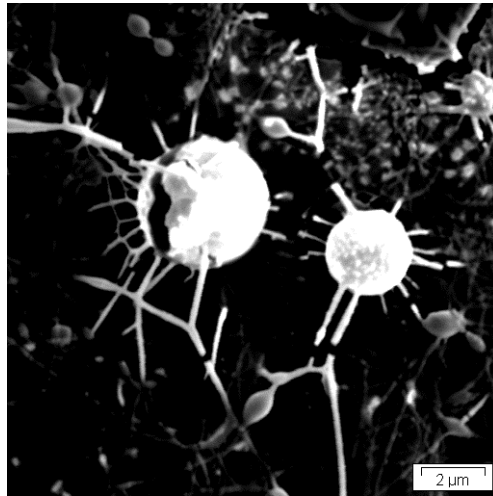
Fig. 63   *Photograph showing the presence of salt crystals on the bead. Such*
             precipitation of salt was observed throughout the sample.

(a)   (b)
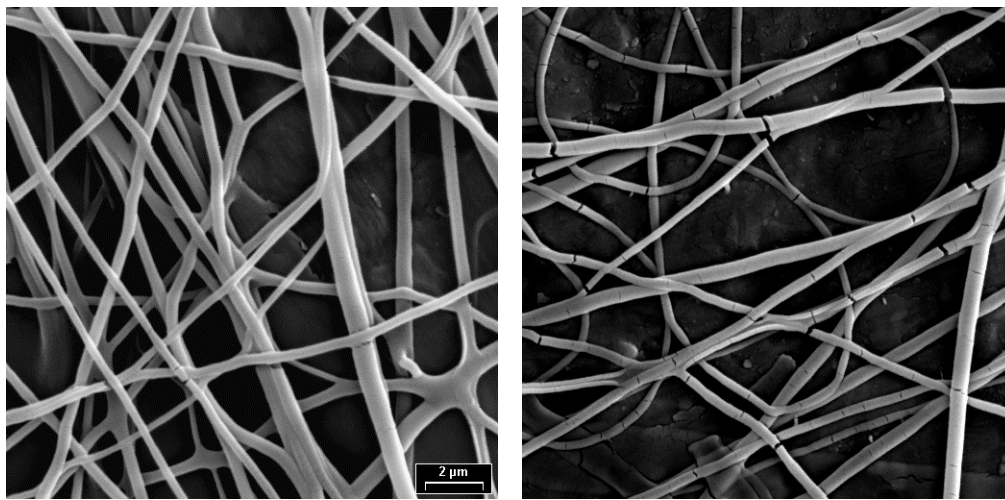
Fig. 64   *Photographs showing the effects of NaCl additions to PVA (a) 0% (b) 1% (M_w*
             = 124000-186000 g/mol, c=7 wt %).

83

0%   5%   10%.
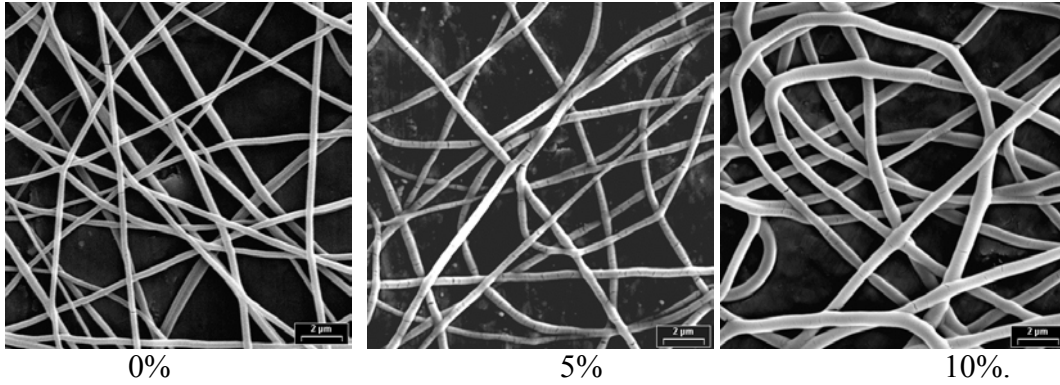
Fig. 65 Photographs showing the effects of polyethylene glycol additions to PVA.
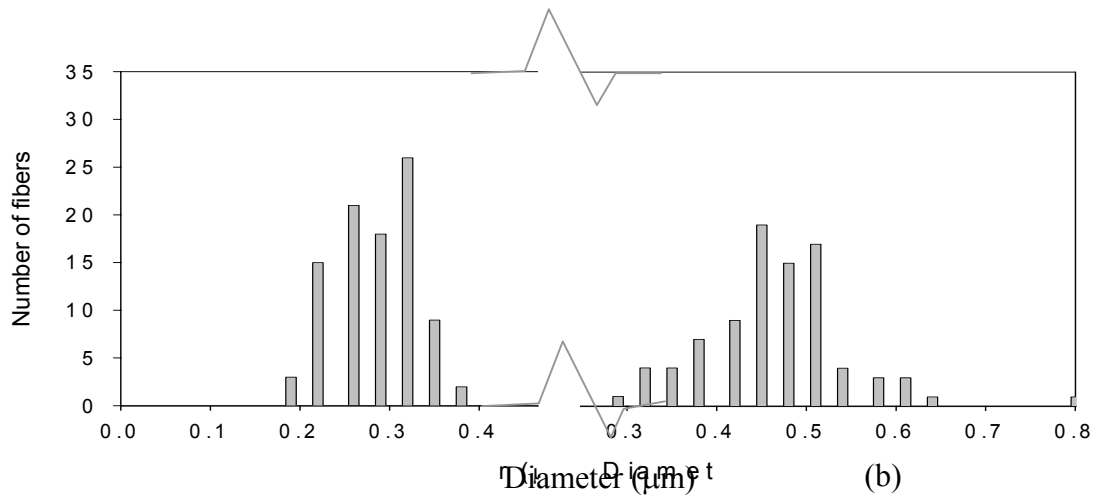
Fig. 66 Distribution of fiber diameters in electrospun PVA with (a) 5 wt% PEG and (b) 10 wt% PEG.

6. CONCLUSIONS

The breakup of polymer jets into droplets and fibers is strongly influenced by rheological properties of the solution. The molecular weight (M_w) and concentration c have significant influence on solution rheology. In particular, M_w plays a vital role in controlling the solution viscosity. A minimum value of the dimensionless concentration *[η]c* is needed to obtain a fibrous structure. At 5 < *[η]c* < 6, the fibrous structure is not completely stable and a bead on string structure is obtained. The stabilization of the fibers from the solution corresponds to Capillary number, *Ca* ~ 0.4 to 0.8. This value of *Ca* is close to the critical capillary number of 0.2 reported in the literature. As M_w or *c* increase, the fiber diameter becomes larger and a broader distribution of fibers may be obtained. The average diameter of the fiber, D, follows a Power law relationship: *D (nm) = 18.6([η]c)$^{1.11}$*. The photographs obtained during the electrospinning process indicate that at low *[η]c*, a drop of solution detaches rapidly from the capillary and starts to split and splay almost instantly. At high *[η]c*, however, it may take up to a second for the drop to detach and elongational flow to begin. Subsequently, the jet may undergo extensive splaying because of the viscoelastic properties of the polymer. The average velocity of the jet decreases from about 0.9 m/s at *[η]c* ~ 7 to 0.5 m/s at *[η]c* ~ 11. At low molecular weights, the fiber diameter increases slightly as the concentration is increased. However, at high M_w, the diameter increases significantly with concentration and also flat fibers are observed even at low concentrations. Round fibers may be obtained at low M_w and *c*, while flat fibers are observed at high M_w and *c*. The transition from round to flat fibers appears to begin at *[η]c* ~ 12. At low concentration and M_w, a

normal distribution of fiber diameters was obtained with relatively narrow distribution. However as the molecular weight and concentration increased, bimodal or multimodal distributions were observed. Bimodal and multimodal distributions are observed in electrospinning because of the splitting and splaying of the fibers that occurs during the transit of the polymer to the collector. The fiber distribution becomes broader with increasing values of *[η]c*. The initial Capillary numbers for various conditions ranged from 0.4 to 45.4, while the Ohnesorge number, Oh, was between 0.1 and 38.5. The average fiber diameter increases with *Oh* and a power law relationship between *D* and *Oh* was observed: $D(nm) = 224[Oh]^{0.29}$. Wavy fibers were observed at low *Oh*, while at high *Oh*, the fibers appear to be straight. Both *Ca* and *Oh* number change significantly during electrospinning as the diameter of the jet decreases. For different values of *[η]c*, at a limiting *Oh* number, the surface stresses become so large that splaying essentially stops as the fiber is stabilized. Hence, at any [η]c, there is a minimum Capillary and Ohnesorge numbers at which fibers are stabilized and a maximum at which viscous effects become dominant. Because of the low evaporation rate of DMSO, NMP and EG, the splayed fibers which are wet when they reach the collector, tend to agglomerate and merge. Consequently, a blend of solvents may be suitable for lowering the diameter of the fibers further. At a low M_w, the addition of NaCl disrupts the fibrous structure. The jet can start splaying, but break apart after the initial burst. At high M_w, however, the addition of NaCl lowers the average fiber diameter. A salting out effect, where the NaCl precipitates out was observed at about 3 wt%. Therefore optimum additions of NaCl are between 0.5 and 3 wt%. The average fiber diameter can be increased by the addition of

polyethylene glycol. Electrospinning can be used a processing technique to produce porous PVA structures with various pore architectures assembled from nano-sized fibers.

7. APPENDICES

Appendix I Major Physical Properties of Poly Vinyl Alcohol

Table A 1   Major Physical Properties of PVA

Property	Value	Remarks
Appearance	White to ivory white granular powder	
Specific gravity	1.27–1.31	Increases with degree of crystallinity
Tensile strength, MPa[a](98–99% hydrolyzed)	67–110	Increases with degree of crystallinity (heat treatment), and molecular weight, decreases with increasing humidity
Tensile strength, MPa (87–89% hydrolyzed)	24–79	Increases with molecular weight and decreases with increasing humidity
Elongation, %	0–300	Increases with increasing humidity
Thermal coefficient of expansion per °C	$7–12 \times 10^{-5}$	
Specific heat, J/(g·K)[b]	1.67	
Thermal conductivity, W/(m·K)	0.2	
Glass-transition temperature, K	358	98–99% hydrolyzed
	331	87–89% hydrolyzed
Melting point, K	503	98–99% hydrolyzed
	453	87–89% hydrolyzed
Electrical resistivity, Ω·cm	$(3.1–3.8) \times 10^{7}$	
Thermal stability	Gradual discoloration above 100°C; darkens rapidly above 150°C; rapid decomposition above 200°C	
Refractive index n_D(20°C)	1.55	
Degree of crystallinity	0–0.54	Increases with heat treatment and degree of hydrolysis

Storage stability (solid)	Indefinite when protected from moisture
Flammability	Burns similarly to paper
Stability in sunlight	Excellent

Appendix II   Fabrication Techniques to Produce Porous Scaffolds

Fiber bonding technique involves dissolving one polymerA in its solvent and adding the solution to a nonwoven mesh of another polymerB, which does not dissolve in this solvent. After the evaporation of the solvent, the heat treatment is applied to stabilize the matrix before the nonwoven mesh polymerB was removed using another solvent, which is nonsolvent for the other. This process is effective to produce highly porous and perfectly interconnected structure as show in Fig. A1. But the limitation of it includes undesirable stipulations of heating and the choice of solvent, immiscibility of the two polymers and their relative melting temperatures
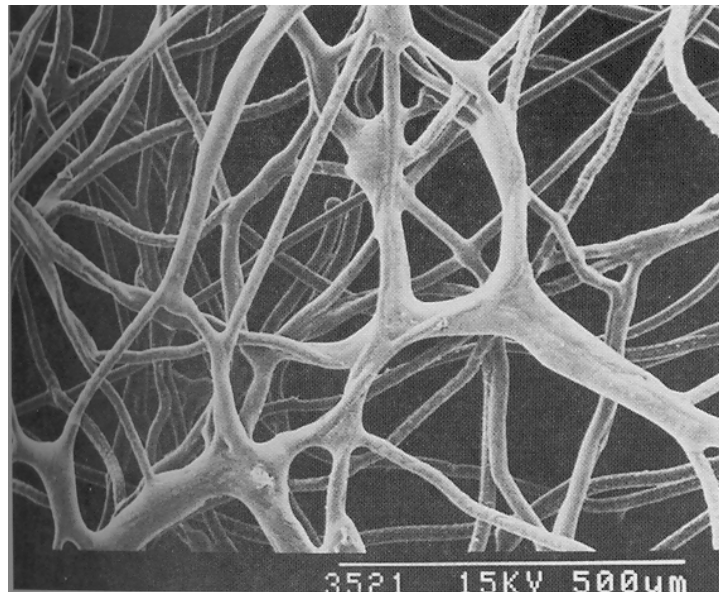
Fig. A 1   Porous structure produced by fiber bonding

In this *Solvent casting and particulate leaching*, a polymer solution dispersed with small insoluble particles is cast onto a specific container to produce desired shape of scaffold. The solvent is allowed to evaporate and the porogen can be removed by dissolving the

structure into water. The typically size of sodium chloride used in here is 300-500um. This process can produce structures of controllable crystallinity and controllable pore size. The major disadvantage of this process is that it can only be used to produce thin wafers or membranes. Three-dimensional structures can be produced by membrane lamination or melting molding, but these also involve high temperatures or pressures in the process.

Membrane Lamination is to construct three dimensional structures by laminating porous membranes of polymers prepared by other processes. It is not applicable for some polymers like PGA, which dissolves only in highly toxic solvent.

Gel casting is similar to that of solvent casting in the first stage, i.e., casing a polymer solution in a mold to produce a specific structure. The solution is then allowed to stand a room temperature until ti forms a gel. The major difference between them is that gel casting technique produce micro-porous structure by processed the initial gel through several stages of solvent exchanges in mixtures of acetone, ethanol, and water. The advantage of this technique is that it uses low heat(,45C) so the probability of denaturing the bioactive agents is low. But protein release from the scaffolds has been found to be non-uniform.

Extrusion is developed to produce porous, biodegradable tubular conduits, as shown below, for the purpose of peripheral nerve regeneration by combining this process with the aforementioned solvent casting technique. Extrusion usually needs high temperature

to initiate extrusion at lower pressure. However, at the high temperatures, a decrease in molecular weight is most likely caused by thermal degradation of the polymer. Pore diameter is also reduced at very high extrusion temperatures due to the increase in polymer viscosity.

Three-dimensional printing is a solid free-form fabrication process that produces components by inkjet printing a binder into sequential powder layers. This process can produces complex-shaped scaffolds in a well controlled fashion. But its drawback lies in the relatively complex device and procedures.
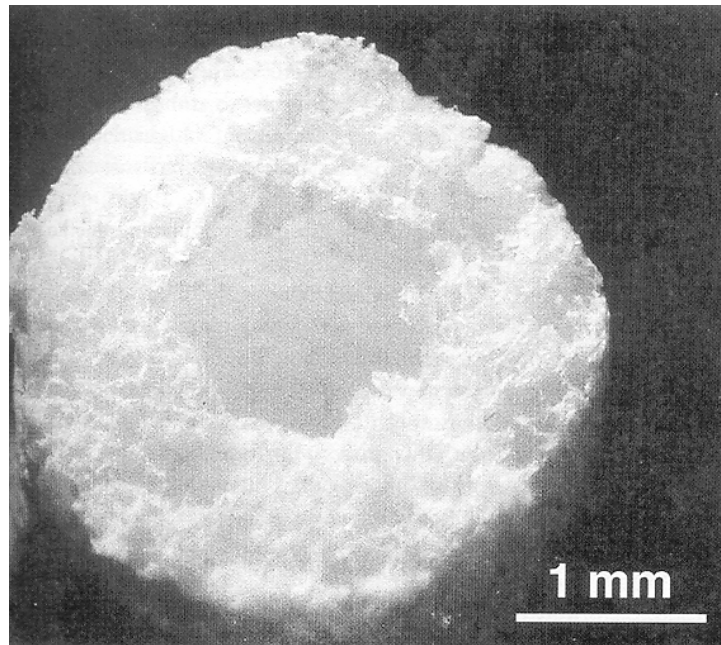
Fig. A 2   Porous structure produced by Extrusion

Gas foaming avoids the drawback of the use of organic solvent found in the process of solvent casting and particulate leaching. the matrices formed have a closed pore

morphology, which may be undesirable for tissue engineering applications. In this method polymer pellets are compression molded into solid disks, and then the disks are exposed to high pressure gas, e.g., CO_2 to saturate the polymer. Then the pressure is decreased to cause the nucleation and formation of pores in the polymer matrix. However the closed pore morphology produced is undesirable for tissue engineering applications.

Phase separation is a process primarily to address the problem of drug delivery. To incorporate bioactive molecules into the scaffolds requires to prevent any loss of drug activity due to exposure to harsh chemical or thermal environments. The polymer is dissolved in a solvent at a low temperature, and the bioactive molecules. The solution is then cooled until liquid-liquid phase separation is induced. The resulting structure is then quenched to produce a solid and the solvent component is removed by sublimation and leave behind a porous structure. This process is useful as a means of incorporating small molecules into polymer scaffolds but not incorporate large protein structures.

8. REFERENCES

1.   Robert C. Thomson, Albert K. Shung, Michael J. Yasemski, and Antonios G. Mikos, Principles of Tissue engineering, 2nd edition, Academic Press, Boston, 2000.

2.   C. Mauli Agrawal, Robert B. Ray: in *Encyclopedic Handbook of Biomaterials and Bioengineering*, Part A, Materials , Volume 2, Marcel Dekker, Inc, New York, 1995.

3.   L. Poole-Warren, D.J. Martin, K. Schindhelm, G.F. Meijs, *Materials Forum* **21** (1997) 241-256

4.   John C. Middleton, Arthur J. Tipton, *Biomaterials* **21** (2000) 2335-2346

5.   O. Pillai and R. Panchagnula, *Current Opinion in Chemical Biology* **5** (2001) 447-451

6.   *Biomaterials Science Ed:* Buddy D. Ratner et al, *Academic Press, Boston,* (1996)

7.   L. Griffith, *Acta Materialia* **48** (2000) 263-277

8.   C.M. Agrawal, G. G. Niederauer, D. MA Micallef, and K. A. Athanasiou, *Biomaterials,* **21** (2000) 2333-2335

9.   Yale L. Meltzer, *Water-soluble polymers*, Noyes Data Corporation, Park Ridge, NJ (1981) 1-3

10.   E. A. Bekturov, Z. Kh. Bakauova, *Synthetic water-soluble polymers in solution*, Basel, New York, NY (1986) 9-11

11.   Wensheng Cai, Ram B. Gupta, "Hydrogels", *Kirk-Othmer Encyclopedia of Chemical Technology2002*

12.   B. Briscoe; Luckham, P.; Zhu, S., *Polymer* **41** (2000) 3851-3860

13.   Vinyl Alcohol Polymers, *Encyclopedia of Polymer Science and Technology*, John Wiley & Sons, New York, NY, **14** (1971) 149-207

14.   J. Feng, F. Dogan, *Materials Science and Engineering A: Structural Materials: Properties, Microstructure and Processing* **283** (2000) 56-64

15.   Philip Molyneux, *Water-soluble synthetic polymers*, CRC, Boca Raton, FL, **1** (1983) 119-186

16.   Darlene M. Back, Elke M. Clark, Ramesh Ramachandran, Polyethers, Ethylene Oxide Polymers *Kirk-Othmer Encyclopedia of Chemical Technology, Wiley, New York, NY 2002 Online*

17.   F. L. Marten, Vinyl Alcohol Polymers**,** *Kirk-Othmer Encyclopedia of Chemical Technology2002 Wiley, New York, NY 2002 Online*

18.   J. Brandrup, E.H. Immergut, and E.A. Grulke, Crystallographic data and melting points for various polymers, Polymer handbook, 4th ed., Wiley, New York, NY, (1999) VI/14,

19.   Po-Da Hong and Keizo Miyasaka, *Polymer* **35** (1994) 1369-1374

20.   J. C. J. F. Tacx, H. M. Schoffeleers, A. G. M. Brands and L. Teuwen, *Polymer* **41** (2000) 947-957

21.   A. Hebeish, N.A. Ibrahim, M.H. Abo Shosha, H.M. Fahmy, H.M, *Polymer-Plastics Technology and Engineering* **35** (1996) 517-543

22.   B. Wang , S. Mukataka , E. Kokufuta , M. Ogiso , M. Kodama, *Journal of Polymer Science Part B: Polymer Physics* **38** (2000) 214-221

23. Katarzyna Lewandowska, Danuta U. Staszewska and Miloslav Bohdanecký, *European Polymer Journal* **37** (2001) 25-32

24. E. Levanen, T. Mantyla, P. Mikkola and J. Rosenholm, *J. of Colloid and Interface Science* **234** (2001) 28-34

25. Garba O. Yahya, S. K. Asrof Ali and Esam Z. Hamad, *Polymer* **37** (1996) 1183-1188

26. M. Suzuki, T. Yoshida, T. Koyama, S. Kobayashi, M. Kimura, K. Hanabusa and H. Shirai, *Polymer* **41** (2000) 4531-4536

27. K. Yamaura and M. Naitoh, *J. of Materials Science*, **37** (2002) 705-708

28. B. C. Shekar, V. Veeravazhuthi, S. Sakthivel, D. Mangalaraj, and Sa. K. Narayandass, *Thin Solid Films* **348** (1999) 122-129

29. K. F. Leong, C. M. Cheah, C. K. Chua, *Biomaterials* **24** (2003) 2363-2378J M Deitzel, J. D. Kleinmeyer, J. K. Hirvonen, N. C. Beck Tan, *Polymer* **42** (2001) 8163-8170

30. J M Deitzel, J. D. Kleinmeyer, D. Harris, N. C. Beck Tan, *Polymer* **42** (2001) 261-272

31. Jayesh Doshi and Darrell H. Reneker, *Journal of Electrostatics* **35** (1995) 151-160

32. D. H. Reneker, Alexander L. Yarin, Hao Fong ,and S. Koombhongse, *Jounal of Applied Physics* **87** (2000) 4531-4547

33. El-Refaie Kenawy, J. M. Layman, J. R. Watkins, Gary L. Bowlin, J. A. Matthews, D. G. Simpson, and Gary E. Wnek, *Biomaterials* **24** (2003) 907-913

34. P. Gibson, H. Schreuder-Gibson and D. Rivin, *Colloids and Surfaces A: Physicochemical and Engineering Aspects*, **187-188**, (2001) 469-481

35. J. A. Matthews, Gary E. Wnek, D. G. Simpson, and G. L. Bowlin, *Biomacromolecules* **3** (2002) 232-238

36. C. J. Buchko, L.C. Chen, Y. Shen and D. C. Martin, *Polymer* **40** (1999) 7397-7407

37. H. Fong, W. Liu, C. Wang, R. A. Vaia, *Polymer* **43** (2002) 775-780

38. K. H. Lee, H. Y. Kim, M. S. Khil, Y. M. Ra, and D. R. Lee, *Polymer* **44** (2003) 1287-1294

39. Geoffrey Taylor, *Proceedings of the Royal Society of London. Series A, Mathematical and Physical Sciences* **313** (1969) 453-457

40. C. D. Hendricks, R.S. Carson, J. J. Hogan and J. M. Schneider, AIAA J 2 (1964) 733-737

41. Geoffrey Taylor*, Proceedings of the Royal Society of London. Series A, Mathematical and Physical* **280** (1969) 383-397

42. Chen-Ming Hsu, "Electrospinning of PCL" M.S. thesis, Worcester Polytechnic Institute, Worcester, MA, 2003.

43. Y.M Shin, M. M. Hohman, M. P. Brenner, G. C Rutledge, *Polymer* **42** (2001) 9955-9967

44. Moses M. Hohman, Michael Shin, *Gregory Rutledge and Michael P. Brenner, Physics of Fluids* **13** (2001) 2201-2220

45. Moses M. Hohman, Michael Shin, Gregory Rutledge and Michael P. Brenner, *Physics of Fluids* **13** (2001) 2221-2236

46. Sureeporn Koombhongse, Wenxia Liu, Darrell H. Reneker, *Journal of Polymer Science: Part B: Polymer Physics* **39** (2001) 2598-2606

47. H. Fong, I. Chun, and D.H. Reneker, *Polymer* **40** (1999) 4585-4592

48. Hao Fong, Rarrell H Reneker, *Journal of Polymer Science: Part B: Polymer Physics* **37** (1999) 3488-4393

49. Xinhua Zhong, Kwangsok Kim, Dufei Fang, Shaofeng Ran, Benjamin S. Hsiao, Bemjamin Chu, *Polymer* **43** (2002) 4403-4412

50. Changlu Shao, Hak-Yong Kim, Jian Gong, Bin Ding, Douk-Rae Lee, Soo-Jin Park, *Materials Letters* **57** (2002) 1579-1584

51. *CRC Handbook of Chemistry and Physics*, (2002) 6-106, 6-148, 6-153, 6-184;

52. *Polymer Handbook* (1999) III-60,

53. *The Merck index : an encyclopedia of chemicals, drugs, and biologicals* (2001) 573, 675, 1090, 1791

54. X. Zhang, *Chemical Engineering Science*, **54** (1999) 1759-1774

55. B. Ku and S. Kim, *Aerosol Science* **33** (2002) 1361-1378

56. L.H. Sperling, *Introduction to Physical Polymer Science, 2nd edition, John Wiley and Sons, Inc., New York, 1992.*

57. E. A. Bekturov, *Synthetic water-soluble polymers in solution*, Heidelberg, New York, NY, 1981, 147-162

58. Po-Da Hong, C. M. Chou, and C. H. He, *Polymer* **42** (2001) 6105-6112

59. R. P. A. Hartman, D. J. Brunner, D. M. A. Camelot, J. C. M. Marijnissen, and B. Scarlett, *Journal of Aerosol Science* **31** (2000) 65-95

60. Materials Science and Technology: Volume 18, Ed. R.W. Cahn, P. Haasen and E.J. Kramer, Wiley-CCH, New York, 1997.

61. B. Ambravaneswaran, E. Wilkes and O. Basaran, *Physics of Fluids*, **14**(8) (2002) 2606-2621

62. K. Yamamura and M. Naitoh, *Journal of Materials Science* **37** (2002) 705-708

63. El-Refaie Kenawy, Gary L. Bowlin, Kevin Mansfield, John Layman, David G. Simpson, Elliot H. Sanders and Gary E. Wnek, *Journal of Controlled Release* **81** (2002) 57-64

64. A. L. Yarin, Sureeporn Koombhongse and D. H. Reneker, *Journal of Applied Physics* **90** (2001) 4836-4846